KONINKLIJK NEDERLANDS METEOROLOGISCH INSTITUUT

On the theory and application of simple climate models to the problem of long range weather prediction.

Collected papers presented at the KNMI Workshop
De Bilt, 1-3 March, 1981

Edited by R. Mureau
C.J. Kok
R.J. Haarsma

De Bilt, 1982

KONINKLIJK NEDERLANDS METEOROLOGISCH INSTITUUT

On the theory and application of simple climate models to the problem of long range weather prediction.

Collected papers presented at the KNMI Workshop
De Bilt, 1-3 March, 1981

Edited by R. Mureau
C.J. Kok
R.J. Haarsma

De Bilt, 1982

K.N.M.I. publikatie no. 163

Koninklijk Nederlands Meteorologisch Instituut,
Postbus 201,
3730 AE De Bilt,
Nederland.

U.D.C.: 551.58 :
551.513.1 :
551.509.33

Contents

Introduction

At many places in the world long-range weather predictions (LRWP) have been produced (and sometimes issued) for a great number of years. The skill of these forecasts has never been very convincing, especially not in the mid-latitudes. In spite of all efforts significant improvement in the skill of operational LRWP has been virtually absent even though the understanding of the physics of the problem is much better than 50 years ago. So, how do we proceed?

It makes sense to mention briefly the methods used to produce LRWP.
(i) Statistical methods: previous values of meteorological parameters are used to inform us about future values. This method relies on the reproducibility of statistical relationships that are known to exist in earlier data sets.
(ii) Dynamical methods: we integrate the equations governing the instantaneous atmosphere over an extended period of time. Because we do not believe the details of the atmospheric flow after x days we will usually apply an average (in time and for space) to arrive at a forecast of the y-days averaged atmospheric circulation z days ahead.
(iii) Statistical-Dynamical methods: the aim is to compute directly the average of the atmospheric circulation over a certain period of time and to treat the transient details of the flow at best statistically.

So far most of the, admittedly low, skill of LRWP has come from the statistical methods. It is clear, however, that the statistical methods cannot eternally be improved, certainly not if we are not guided by physical understanding of cause and effect. Therefore physical models should be developed (or improved), first of all to clarify the nature of the statistical relationships used in LRWP (such as teleconnections, persistence), then to guide the improvement of the statistical methods, and finally the physical models can be used to, possibly, surpass the level of skill reached by statistical methods.

The best physical model of method ii we can think of is an ideal version of a General Circulation Model. GCM's so far have had difficulties to reproduce the relations that are known to exist between, for example, the external boundaries (state of the sea) and the time-mean atmosphere. One way to improve our understanding of GCM-results (including its deficiences) is to do similar experiments with one or more increasingly

simpler models. The KNMI-workshop was devoted to models that are simpler than GCM's but sufficiently realistic to have some potential in LRWP and also to be used along with GCM's.
The main objective of the workshop was to investigate the usefulnes of simple climate models in studying and eventually predicting climate variations on time scales of a month to a year. Scientists were invited to present a paper on observational and model aspects of climate variations on these time scales.
The topics of the workshop can roughly be divided into four parts:

1. What do observations tell us about predictability?
   (Van den Dool, Wallace, Schuurmans).
   Van den Dool showed that there is some skill in long range weather forecasting in The Netherlands, due to persistence. This persistence can be interpreted as a boundary layer effect controlled by the near presence of the North Sea. In contrast to this small scale phenomenon Wallace discussed atmospheric motion on planetary scales. He discussed the nature of teleconnection patterns and showed that atmospheric blocking has a preference for certain areas. Schuurmans demonstrated that the occurrence of blocking also depends on the period of the year.

2. Linear, steady state models.
   (Simmons, Opsteegh, Haarsma).
   Model simulations with linear steady state models (Opsteegh and Van den Dool, 1980; Hoskins and Karoly, 1981; Simmons, 1981; Webster, 1981) agree remarkably well with observational evidence as presented by Wallace. Simmons showed the importance of a zonally varying basic state. His results suggest that the phase of the standing eddies in the basic state determines the areas where teleconnection patterns are most pronounced and not so much the exact location of the forcing. Opsteegh emphasized the importance of the Hadley cell for the cross equatorial propagation of wave energy through a region of easterlies. Haarsma investigated the potential predictability of atmospheric forcing by developing a model for the prediction of SSTA's.

3. Multiple steady states in simple models.
(Källen, Egger, Hantel).
Since the pioneering work of Charney and De Vore (1979) in which they showed the existence of multiple stable equilibria in a barotropic flow on a beta-plane, there has been a renewed interest in the possible explanation of the so-called blockings. A natural next step is the extension to a sphere. Källen showed the existence of multiple stable equilibria for a barotropic flow on a sphere. He also discussed the effects of baroclinic eddies in connection with orographic forcing. Egger parameterized the baroclinic eddies as a stochasting forcing term in the equations for barotropic flow. He computed the probability density distribution in phase space of his three component system by using the Fokker-Planck equation.
Hantel analysed the behaviour of a climate point in phase space by examining the properties of Riccati's differential equation.

4. Analysis of atmospheric eddies.
(Hoskins, Alestalo).
Hoskins discussed the influence of the transient eddies on the time mean flow. He pointed at the consequence of different eddy shapes for the eddy flux convergence of vorticity, which he expressed in terms of an anisotropy vector. He showed the importance of the transients in maintaining a block in December 1981 and 1982.
Alestalo presented budget calculations on the relation between the mean flow and transient eddy flux divergence.

We would like to thank the participants and all others who contributed to the workshop. Together they made it interesting and fruitful days. Also we thank Anja de Bree, Marlie Collet and Karin Haaken who devoted so much effort to typing the manuscript.

References

1. Charney, J.G., J.G. De Vore, 1979: Multiple flow equilibria in the atmosphere and blocking. J. atm. sc., 36, 1205-1216.
2. Hoskins, B.J., D.J. Karoly, 1981: The steady linear response of a spherical atmosphere to thermal and orographic forcing. J. atm. sc., 38, 1179-1196.

3. Opsteegh, J.D., H.M. van den Dool, 1980: Seasonal differences in the stationary response of a linearized primitive equation model: prospects for long-range weather forecasting? J. Atm. Sci., 37, 2169-2185.
4. Simmons, A.J., 1981: Tropical influences on stationary wave motion in middle and high latitudes. Technical Report of ECMWF, No. 26.
5. Wallace, J.M., D.S. Gutzler, 1981: Teleconnections in the geopotential height field during the Northern Hemisphere Winter. Mon. Wea. Rev., 109, 784-812.
6. Webster, P.J., 1981: Mechanisms determining the atmospheric response to sea surface temperature anomalies. J. Atm. Sci., 38, 554-571.

List of Participants

M. Alestalo
Department of Meteorology
University of Helsinki
Helsinki, Finland

H.M. van den Dool
Royal Netherlands Meteorological Institute
De Bilt, The Netherlands

J. Egger
Meteorologisches Institut der Universität München
München, Federal Republic of Germany

R.J. Haarsma
Royal Netherlands Meteorological Institute
De Bilt, The Netherlands

M. Hantel
Meteorologisches Institut der Universität Bonn
Bonn, Federal Republic of Germany

B.J. Hoskins
U.K. Universities' Atmospheric Modelling Group
University of Reading
Reading, England

E. Källen
European Centre for Medium Range Weather Forecasts
(ECMWF)
Reading, England
Present affiliation:
Institute for Meteorology and Oceanography
State University of Utrecht
Utrecht, The Netherlands

J.D. Opsteegh
Royal Netherlands Meteorological Institute
De Bilt, The Netherlands

C.J.E. Schuurmans
Institute for Meteorology and Oceanography
State University of Utrecht
Utrecht, The Netherlands

A.J. Simmons
European Centre for Medium Range Weather Forecasts
(ECMWF)
Reading, England

J.M. Wallace
Department of Atmospheric Sciences
University of Washington
Seattle, USA
Present affiliation:
University of Reading
Reading, England

WHAT DO OBSERVATIONS TELL ABOUT LONG-RANGE PREDICTABILITY?

H.M. van den Dool

1. Introduction

Observational evidence of long-range weather predictability must appear from relations of the form: Fact A (t,x,y,z) is followed by Fact B $(t+\Delta t, x',y',z')$, where Facts A and B are weather events. The number of relations you can imagine is infinite and therefore we are in the position of someone pushing a stick into the ground to find gold. In fact, very few reproducible relations are found and only a fraction of them is of practical value.

A generally useful, reliable and reproducible sort of relation is autocorrelation. Lorenz (1973) computed the autocorrelation, $\rho(\tau)$, of instantaneous height fields τ days apart (τ=1...15). His result is essentially a space- and time-averaged autocorrelation based on five years of data covering three quarters of the northern hemisphere. At lag one day $\rho(1)$ amounts to about 0.75. Up to six days $\rho(\tau)$ obeys the law $\rho(\tau) = \rho(1)^{\tau}$, which follows directly from a first order linear Markov process. However, for $\tau > 6$ days the observed $\rho(\tau)$ is larger than $\rho(1)^{\tau}$; this indicates that there is some extra predictability in the long range.

2. Long-term correlations

Because day-to-day predictions beyond a certain range do not seem to be possible (Lorenz, 1969), it has become customary to study monthly or seasonal mean values. (Even if we were able to forecast monthly means perfectly, this would mean a considerable loss of information as compared to a day-to-day forecast). Based on the typical day-to-day correlation of 0.75, one would expect $\rho(\overline{x}_i, \overline{x}_{i+1})$ to be 0.05 to 0.1 (Van den Dool, 1981); the bar indicates a 30-day mean and i is the number of the month. In the following, two examples are given where month-to-month correlations of monthly means turn out to be much higher than 0.1.

Example 1. Wright (1979) showed that monthly mean rainfall ($\overline{R}$) in the Central Pacific has a month-to-month correlation (= $\rho(\overline{R}_i, \overline{R}_{i+1})$) of about 0.8. This positive correlation, or persistence of anomalies, decreases only very slowly with increasing time lag. This means that the atmosphere does not just show resistance against change, but moreover there must be a positive feedback to keep $\rho(\overline{R}_i, \overline{R}_{i+\tau})$ large for large τ.

Example 2. In Fig. 1 the month-to-month correlation of (a) monthly mean temperature at De Bilt, and (b) area-mean precipitation in the Netherlands is given. The results are based on records of 125 years of measurements.

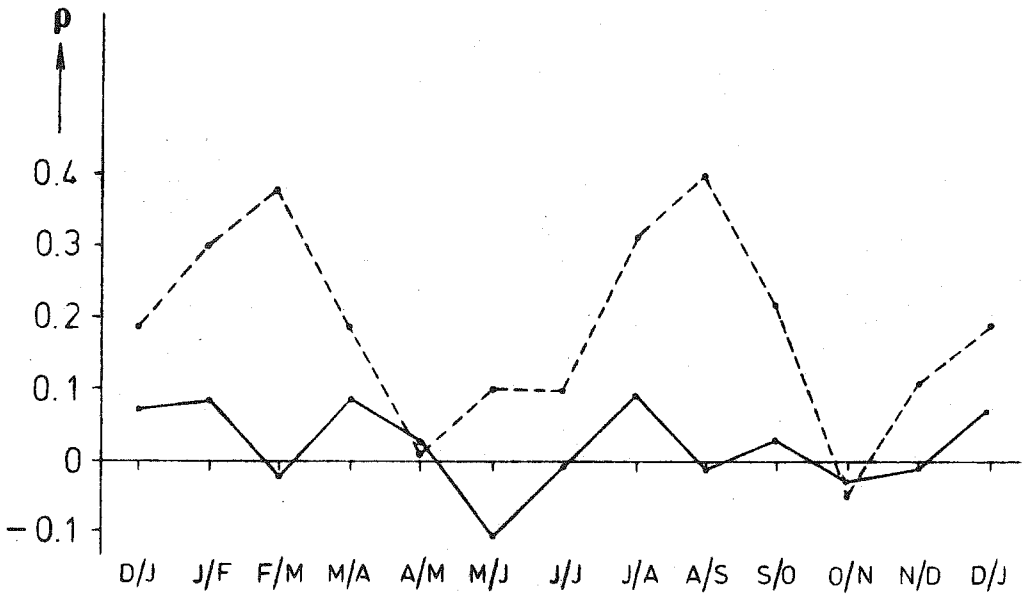

Fig. 1. The temporal correlation coefficient of (a) monthly mean air temperature in adjacent months at De Bilt (1849-1975, the dashed line), and (b) monthly mean rainfall averaged over the Netherlands in adjacent months (1849-1980, full line). Correlations larger than 0.18 differ from zero at the 95% confidence level.

There is virtually no persistence in rainfall anomalies in this mid-latitude area, but the surface temperature shows some month-to-month correlation with two peaks at the end of summer and winter. In these periods of the year damped persistence would be of marginal use in forecasting $\overline{T}$ at De Bilt.

3. An explanation of persistence

A natural question that arises is: Why do we find in a given area some persistence in $\overline{T}$ and none in $\overline{R}$. The answer may be deduced from the fact that $\rho(\overline{T}_i, \overline{T}_{i+1})$ is high over the North Sea (yearly average ~ 0.45) and decreases rapidly over the land with increasing distance from the coast down to a yearly averaged value of about 0.15 (Van den Dool and Nap, 1981). This was found by studying the records of about 15 stations in the Netherlands, all within 200 km from the coast-line. Obviously, this points to a local effect due to the presence of the sea. In Fig. 2 the skill score of damped persistence (full

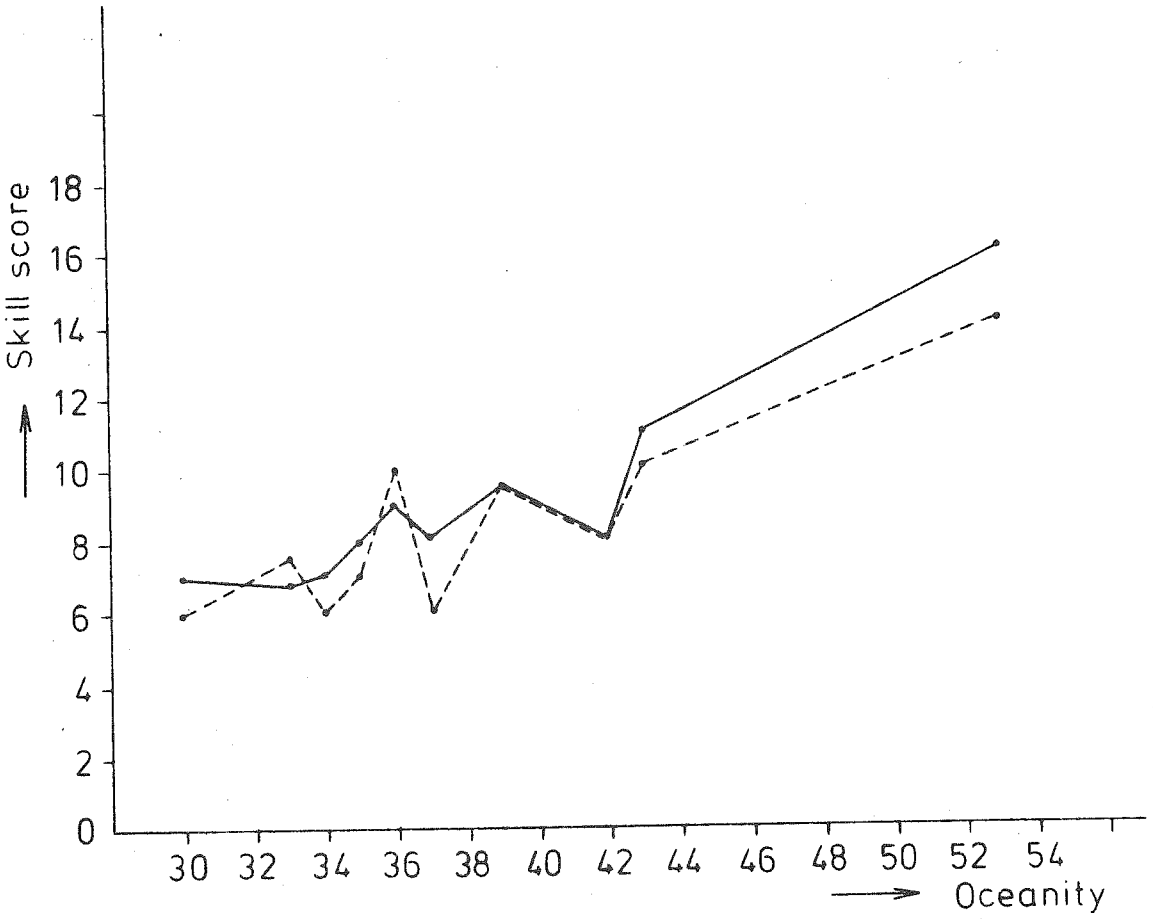

Fig. 2. The skill score, expressed in per cent better than climatology, of damped persistence (full line) of the monthly mean air temperatures for various stations in the Netherlands as a function of their oceanity. The dashed line represents the skill obtained by taking the sign of the sea surface temperature anomaly on the last day of month i at lightvessel Texel as a forecast of monthly mean air temperature in month i+1 at any station in the Netherlands.

line) is plotted against an oceanity index. (Defined in Van den Dool and Nap, 1981). The score is defined here as per cent better than climatology. Right on the beach (oceanity ≈ 50) damped persistence reached 15% more hits than climatology. To ascertain that this effect is due to the sea we also used the sign of the anomaly of the sea surface temperature at lightvessel Texel (25 km off the coast) on the last day of month i as a forecast of the sign of the anomaly of the monthly mean air temperature in month i+1. The results, shown by the dashed curve, confirm the role of local effects of the North Sea.

The conclusion at this point is that persistence in $\overline{T}$ in this region is mainly a local small-scale effect, and apparently, persistence in $\overline{T}$ at the surface is not strongly determined by persistence in the larger-scale circulation aloft. It is certainly worth noting that such small spatial scales appear to be relevant to low-frequency variability in the atmosphere. Because rainfall is more strongly determined by the circulation and less by boundary layer effects, persistency in monthly mean rainfall in this area is small.

4. Persistence of large-scale circulation anomalies

In an implicit way we have derived in the foregoing paragraph that the large-scale atmospheric circulation anomalies are not very persistent. This can be checked in a more direct way, of course. Based on data provided by the German Met. Office in Offenbach, we calculated the month-to-month pattern correlation coefficient of anomalies in observed monthly mean fields of 500 mbar height, surface pressure and 500-1000 mbar thickness. The pattern correlation coefficient expresses the similarity of two maps in one number (representative of the whole area north of about 25^{o} N in this case). For the pair January/February, for example, we obtained 29 coefficients for the years 1949-1977. In Fig. 3 the averages of the 29 individual estimates are shown. It turns out that, indeed, the circulation shows very little persistence, at least much less than found in the surface air temperature over the North

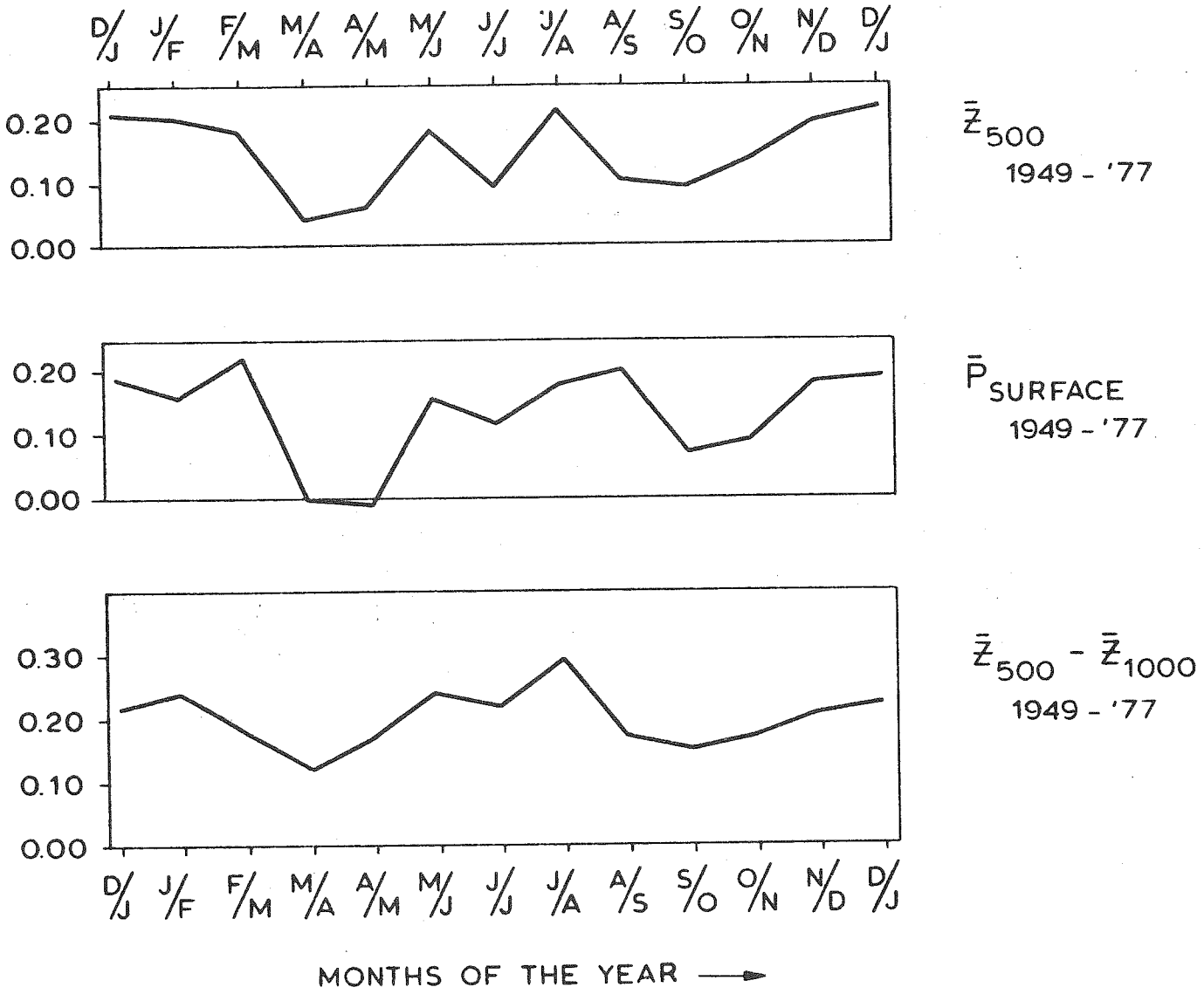

Fig. 3. Month-to-month pattern correlation coefficients of anomalies in observed monthly mean fields of 500 mbar height, surface pressure and 500-1000 mbar thickness. The observations, analyzed at Offenbach, cover most of the area North of 25° N. The graphs represent averages over 29 individual estimates for the years 1949-1977.

Sea. We speculate that the graphs in Fig. 3 show essentially a small background persistence to which local effects have to be added. In the eastern part of the Netherlands (low oceanity index) the persistence in surface air temperature does not exceed the background persistence provided by the circulation aloft.

The Offenbach data set covers the area north of 25° N. So we cannot check whether the large persistence of rainfall anomalies in the Central Pacific (Wright, 1979) is consistent with a similar degree of persistence in circulation anomalies. In fact, the graphs in Fig. 3 do not discriminate at all between low and high latitudes. In principle we can as well determine a temporal correlation coefficient in each grid point of the Offenbach data and map the results. Because only about 30 pairs of observations (= monthly means in adjacent months) are involved, the results are very uncertain and sensitive to trends in the data. All we dare to conclude from such calculations is that there is a substantial increase in persistence from high to low latitude, that is from virtually zero at 60° N to about 0.6 at 30° N. This confirms earlier work by Namias (1959) for seasonal mean 700 mbar heights.

5. Space-time lags

In all foregoing sections we have dealt with lags in time only. In some recent studies (Barnett, 1981; Horel and Wallace, 1981, etc. etc.) also lags in space were allowed. Barnett, for example, tried (with some success) to link Pacific sea surface temperatures with seasonal mean surface air temperature in the USA a season later by employing a linear statistical model.

6. Potential predictability

A completely different approach to the long-range prediction problem is to estimate first the unpredictable part of a time-mean of a weather element. A time-mean will always exhibit some variance solely due to day-to-day variations in the weather. This unavoidable feature is called natural variability or climate noise. It has been investigated by Madden for surface

pressure (Madden, 1976) and for surface air temperature (Madden, 1981). About 40-80% of the interannual variability in winter-mean surface air temperature in the USA can be attributed to day-to-day variability; this leaves 20-60% of the variance as "potentially predictable". (Although we do not know yet how to predict!). The largest potential predictability is found near the coasts and it seems reasonable to believe that also in the USA area local inertia effects enhance the potential predictability near coasts and lakes. The situation for surface pressure in the mid-latitudes is much worse. Madden (1976) reports only 10-20% potential predictability in monthly mean sea level pressure.

A conclusion to be drawn from Madden's work is that daily weather events make the prediction of time means very difficult. This argument is of a purely statistical nature.

7. Model simulations

One can use almost the same words to describe daily weather (or transient eddies) as a "problem" in dynamically modelling the time-mean atmosphere. Consider, for example, the equations of time-mean momentum (where the bar is a time average, and the prime a deviation, all other symbols as usual).

$$\frac{\partial \bar{u}}{\partial t} = - \bar{u} \frac{\partial \bar{u}}{\partial x} - \bar{v} \frac{\partial \bar{u}}{\partial y} - \bar{\omega} \frac{\partial \bar{u}}{\partial p} - \frac{\partial \bar{\Phi}}{\partial x} - f \bar{v} + \bar{F}_E$$

where $\bar{F}_E = \partial \overline{u'^2}/\partial x + \partial \overline{u'v'}/\partial y + \partial \overline{u'\omega'}/\partial p$.

The extra $\bar{F}_E$-term represents the forcing of the time-mean by transient eddies. This eddy-term is known to be large and therefore we have to deal with it in one way or another. One can try either to parameterize, prognose or prescribe the eddy forcing. The first two possibilities being extremely difficult, we have done experiments with precomputed fields of eddy forcing. The fields were obtained empirically from NMC-analyses for eight consecutive Januaries. The anomalous part of the horizontal eddy terms were used to drive the two-layer stationary anomaly model of Opsteegh and Van den Dool

(1980). No other forces (or driving mechanisms) were used. The driving eddy force was applied both to the momentum and thermodynamic equations. In Fig. 4a/b we can compare the computed and observed anomalies of the time mean height of an upper tropospheric level in January 1972. There is some agreement: pattern correlation coefficient = 0.70. The agreement means that (in January 1972) the eddy forcing, which we did not know beforehand, determined to a large extent the anomalies in the time mean atmosphere. It would be a bad thing, in terms of long-range predictability, if this would happen all the time. On the other hand, a good agreement can only be found if the dynamics of the model are all right. Averaged over eight cases (Jan. 1972-78) the agreement expressed in the pattern correlation coefficient was 0.21. In all cases the response to the eddy forcing was large, that is 10-20 decameter height anomalies at 400 mbar. The response to dynamical forcing by the eddies appears to be much larger than to thermodynamical forcing by the eddies.

8. Conclusions

Observations suggest that there is an interesting amount of potential predictability in the time-mean surface air temperature ($\overline{T}$) in the coastal areas of the mid-latitudes. Away from the coasts there is much less potential predictability of $\overline{T}$. For most other weather elements, rainfall, pressure, the situation seems to be worse. The major problem of long-range weather predictions is (and will be) the large effect of daily weather disturbances on the time mean. Even if we were in the ideal situation that we could parameterize transient eddies, at least half of the variance of monthly means would remain unpredictable.

-o-o-o-

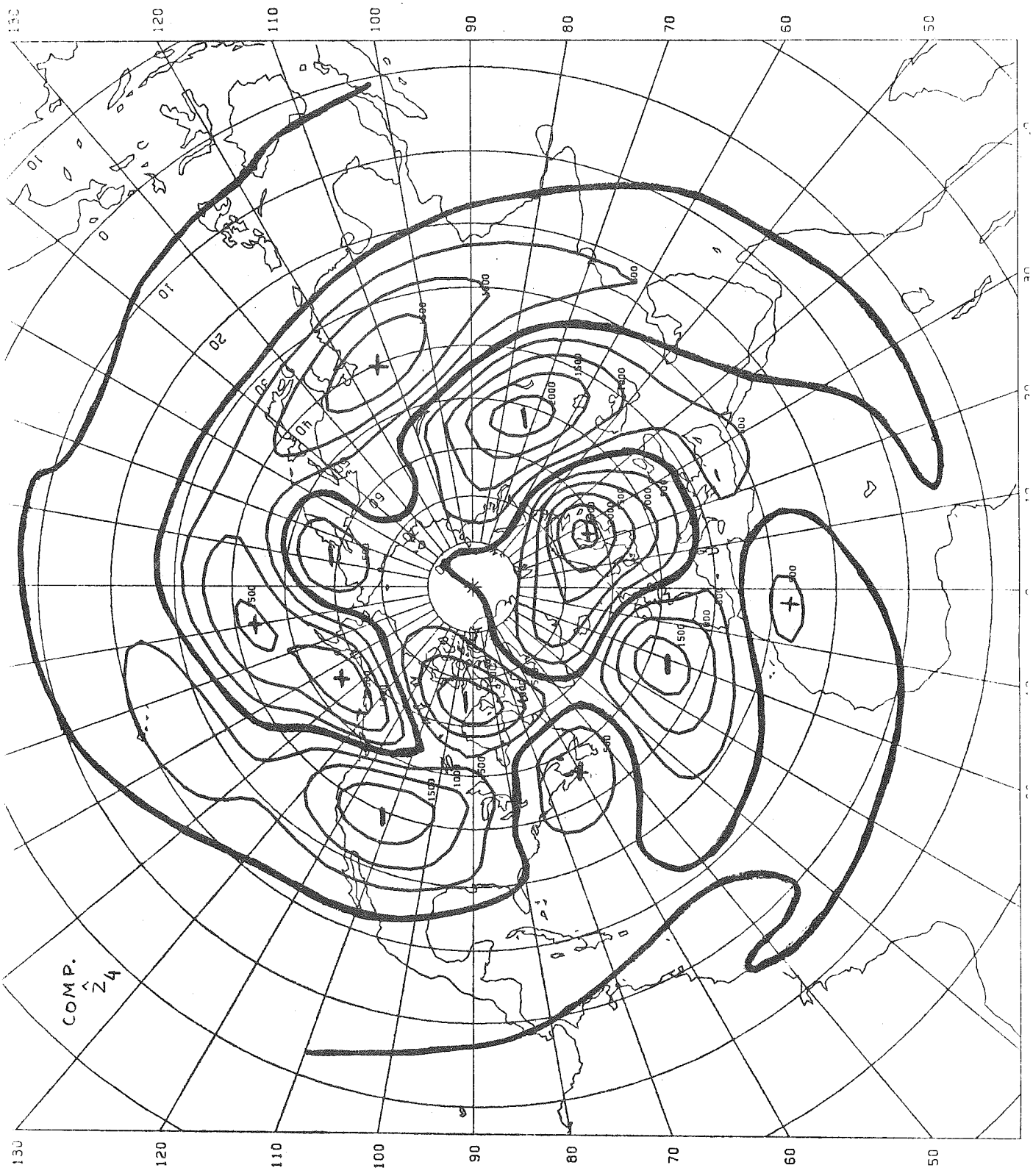

Fig. 4a. Geopotential height anomalies at 400 mbar in response to forcing the thermodynamic and momentum equations by observed anomalous horizontal eddy forcing during January 1972. Contours every 5 gpdam.

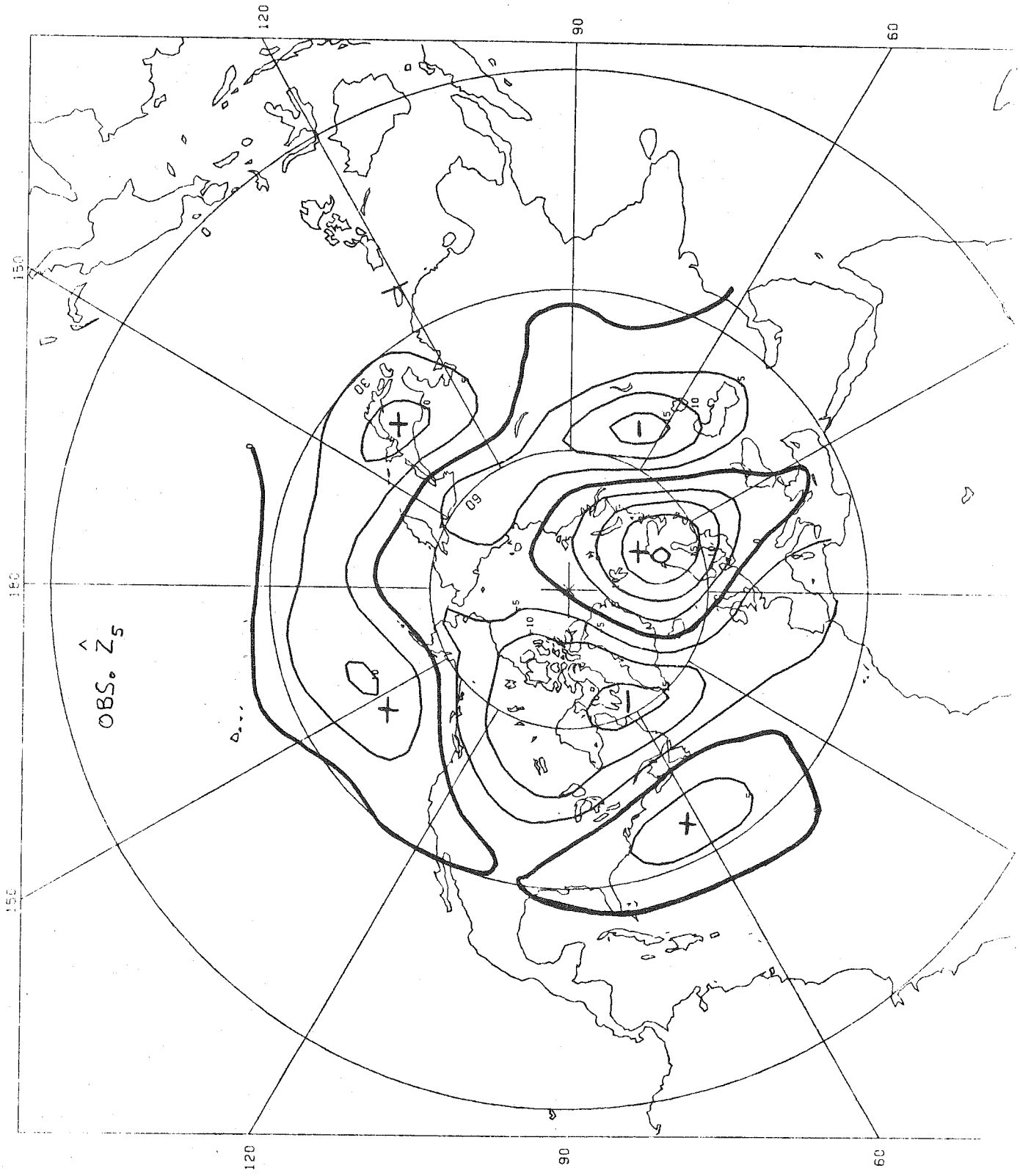

Fig. 4b. Observed anomalies in the monthly mean 500 mbar height during January 1972. Contours every 5 gpdam.

References

T.P. Barnett, 1981, Mon. Wea. Rev., 109, 1021-1041

H.M. van den Dool, 1981, Scientific Report KNMI 81-6

H.M. van den Dool and J.L. Nap, 1981, Tellus, 33, 123-131

J.D. Horel and J.M. Wallace, 1981, Mon. Wea. Rev. 109, 813-829

E.N. Lorenz, 1969, Bull. Am. Met. Soc., 50, 345-349

E.N. Lorenz, 1973, Journ. Appl. Met., 12, 543-546

R.A. Madden, 1976, Mon. Wea. Rev., 104, 942-952

R.A. Madden, 1981, Journ. Geoph. Res., 86, 9817-9825

J. Namias, 1959, Rossby Memorial Volume, p. 240-248

J.D. Opsteegh and H.M. van den Dool, 1980, Journ. Atm. Sc., 37, 2169-2185

P.B. Wright, 1979, Nature, 277, 371-374

-o-o-o-

ON THE NATURE AND CAUSES OF LOW FREQUENCY VARIABILITY

John M. Wallace

1. Distinctions between low and high frequency fluctuations

For purposes of this discussion it is convenient to divide the frequency spectrum of atmospheric motions into two broad ranges: the high frequencies which encompass fluctuations with periods shorter than about 10 days and the low frequencies which encompass fluctuations with periods longer than about 15 days. (The gap between the two frequency ranges is intentional). It will also be useful to divide the low frequency range into three subranges: one for 15-30 day periods, which is well resolved by 5 day or weekly mean data; a second encompassing periods between 60 days and a year, which is well resolved by monthly mean data; and a third encompassing periods of a few years or longer, which is manifested in the interannual variability of seasonal mean data. I will refer to these subranges in terms of week-to-week, month-to-month and interannual time scales, respectively.

The review paper by Wallace and Blackmon (1982), hereafter referred to as WB discusses the distinction between the structure and time evolution of fluctuations in the high and low frequency ranges. The main points in that discussion can be summarized as follows:

(a) The high frequency variability appears to be organized in terms of elongated "storm tracks" along 40°N in the Pacific and western Atlantic sectors, whereas the low frequency variability is largest in regions of frequent blocking near 50°-60°N over the eastern oceans.

(b) The high frequency variability shows a well defined, wavelike structure near the stormtracks, with a characteristic zonal wavelength of 4000 km and a rather long meridional scale; the wind fluctuations are highly anisotropic, with $\overline{v'^2} >> \overline{u'^2}$. *

* The structure of these high frequency disturbances and their feedback upon the background, low frequency flow will be elaborated on in the workshop contribution of B.J. Hoskins.

The low frequency variability is organized in terms of two dimensional Rossby wavetrains with a characteristic "great circle route" orientation. Near their turning points the zonal wavelength of these patterns is on the order of 8000 km. The wind field associated with these patterns tends to be anisotropic in the opposite sense with $\overline{u'^2} > \overline{v'^2}$, particularly at low latitudes.

(c) The time evolution of the high frequency fluctuations is dominated by simple phase propagation, at a rate suggestive of a "steering flow" which resembles the 700 mb wind field. The low frequency fluctuations evolve by energy dispersion through what appear to be standing wave patterns, with geographically fixed nodes and antinodes. Energy dispersion along the great circle ray paths, from west to east, is clearly evident in lag correlation statistics on the week-to-week time scale, but no well defined pattern of time evolution is evident on longer time scales.

(d) The spatial correlation structure of unfiltered daily geopotential height data tends to be dominated by the low frequency fluctuations, which account for most of the variance.

2. Spectral characteristics of the low frequency fluctuations

Evidence presented in WB based on simultaneous and time lagged spatial correlation patterns indicates that at tropospheric levels the two dimensional Rossby wavetrains described above have a more clearly defined structure and time evolution than ultra-long waves propagating along latitude circles. These results support the view that low frequency phenomena such as blocking are inherently local in the longitude domain.

3. Causes of low frequency variability

Numerical experiments to be described by A.J. Simmons at the workshop indicate that the observed spatial correlation structure of the low frequency fluctuations is largely a consequence of the existence of stationary waves in the climatological mean wind field.
In fact, it seems plausible that, in the presence of the observed stationary wave pattern, even stochastic forcing by high frequency fluc-

tuations would be capable of producing correlation structures much like the observed. Hence, the observed correlation patterns do not, in and of themselves, provide much information concerning the causes of low frequency variability. In order to extract such information from the observations, it is going to be necessary to apply dynamical insights derived from theoretical studies of specific causal mechanisms.

Observational results concerning two possible causal mechanisms are presented in WB.

(a) 500 and 1000 mb height maps from the 1980-81 winter were composited on the basis of the position of the 500 mb ridge relative to the Rockies. In one composite, based on a continuous 24 day period, the ridge was centered over the Rockies whereas in the other composite, based on three separate but shorter episodes, the ridge was centered about one quarter wavelength upstream, over the Gulf of Alaska. The ridge configurations at the two levels and the related thermal pattern bear certain intriguing similarities to multiple equilibria in the model of Reinhold and Pierrehumbert, discussed in E. Källén's workshop contribution.

(b) Index cycle fluctuations were analyzed in order to determine whether the 500 mb flow takes on any preferred configuration during periods of low zonal index (vigorous eddies). It was found, rather unexpectedly that such periods are characterized by a strong enhancement of the stationary waves. Hence it appears that index cycle type fluctuations in the Northern Hemisphere are primarily a consequence of alternating constructive and destructive interference between the stationary waves and the low frequency transients. If vacillation phenomena are involved, they are not directly analogous to those that occur in azimuthally symmetric rotating annuli.

Returning now to the general question of causal mechanisms, it seems likely that much of the variability on the week-to-week time scales is simply due to the formation of long-lived circulation features which usually involve closed circulations with an equivalent-barotropic structure, such that the horizontal advections of heat, vorticity and potential vorticity are small. Isolated cyclonic or anticyclonic gyres are common at high latitudes where their presence is reflected in the high 1 and 2 day autocorrelations for 500 mb height. In middle latitudes where the westerlies are stronger, long-lived features often assume the form of dipole patterns

which resemble analytic functions associated with modons or solitons. These features can remain stationary for long periods, even in the presence of a mean westerly current. Along the west coasts of the continents long-lived cutoff lows are often observed.
As one moves toward lower frequencies it seems likely that the relative importance of such special flow patterns should diminish in relation to external forcing associated with anomalies in tropical sea-surface temperature and soil moisture. However it is only on the interannual time scale that external forcing accounts for a substantial fraction of the total variance.
The mechanisms responsible for atmospheric variability on the month-to-month time scale are the least well understood of low-frequency dynamical processes. This scale is longer than the typical lifetime of gyres and ordinary blocking patterns and it is shorter than the characteristic time scale of tropical sea-surface temperature fluctuations. Hence it seems likely that month-to-month variability is due to other causes. In view of the geographically localized zonal structure of low frequency fluctuations, it would appear that the most likely mechanisms are transitions between discrete "weather regimes" related to multiple equilibria of the stationary wave patterns, and maintenance of long-lived features such as blocks by the eddy fluxes of potential vorticity.

4. Prospects for long range forecasting

Deterministic numerical weather prediction models such as the one in use at ECMWF are already producing quite accurate simulations of high frequency variability. Such models exhibit modest, but significant skill on the week-to-week time frame. Important low frequency events such as the development or breakdown of blocks or shifts in the positions of the jetstreams can often be anticipated out to 5 or 6 days in advance. The cutoff lows mentioned above are not yet forecast very well, but there are good prospects for improvements within the next few years. Therefore, it seems unlikely that simplified models will be able to compete with deterministic NWP models on the week-to-week time-scale.

On the interannual time scale there is hope that the use of simple models which yield steady state solutions can be used to increase the

skill of seasonal forecasts, relative to the level presently attainable through the use of statistical methods alone. However, they face some stiff competition* from GCM's, which offer the hope of simulating not only the seasonal mean anomalies, but also the distribution of weather regimes that might be expected to occur within the season. Pitcher, Geisler and Blackmon are already performing multiple 1000 day "perpetual winter" simulations of the effects of an equatorial sea-surface-temperature anomaly with the NCAR Community Climate Model and generating statistics on the frequency of blocks and cutoff lows in various regions for the "control" and "anomaly" experiments. A distinct advantage of the GCM's over the simpler models is the explicit treatment of the higher frequency transients.

The month-to-month time scale is perhaps the most difficult problem for long range prediction. There is little question that events on this scale are meteorologically and societally important.

The 40 day episode of cold weather in Europe this winter is but one example. It would appear that neither determinstic numerical weather prediction models nor simplified models of the atmospheric response to external forcing are likely to be effective for this time scale: the former are limited by predictability constraints to the week-to-week time scale, and the latter are effective only for the seasonal time scale, where the climatic signal associated with external forcing is strong enough to be detectable. Nor do the observations offer any clues as to the pattern of time evolution on this scale (as they do for the week-to-week time scale, where one sees two dimensional Rossby wave dispersion).

Similar considerations have led the long range prediction group at NMC to downplay their monthly forecasts and to put more emphasis upon sea-

---

*) Perhaps it is best to think of the GCM's and the simpler models, not as being in competition with one another in seasonal climate prediction, but as complementary tools designed to advance the understanding of low frequency variability. The simplified models play an interpretive role, elucidating processes which take place within the atmosphere and presumably within the GCM's as well.

sonal forecasting during the past few years.

If transitions between weather regimes prove to be a major source of variability on the month-to-month time scale, then the annual cycle might play an important role in determining the timing of the transitions. The frequency distribution of the various ridge-trough configurations relative to mountain ranges such as the Rockies is likely to be highly dependent upon the mean zonal wind speed which, in turn, is modulated by the annual cycle. This is a recurrent theme in the works of J. Namias, who believes that the onset and breakdown of anomalous circulation patterns tends to take place within certain rather narrow ranges of calendar dates. The use of simplified models such as highly truncated GCM's could perhaps shed some light on this question. More observational work is needed in order to determine whether the concept of multiple weather regmies is useful for climate prediction.

Reference

Wallace, J.M. and M.L. Blackmon, 1982: Observational Evidence of Low Frequency Variability. Published in Large-Scale Dynamical Processes in the Atmosphere, B.J. Hoskins and R.P. Pearce, ed., Academic Press, London.

SOME REMARKABLE ASPECTS OF THE ATMOSPHERIC CIRCULATION, WITH BEARING ON LONG RANGE FORECASTING

C.J.E.Schuurmans

Introduction

A most relevant and still extremely simple short term climate model is the atmospheric analogue. In this paper I present some facts and ideas, which mainly result from a 5-year experiment in using circulation analogues in monthly weather forecasting. The experiment was conducted at KNMI in the early seventies. The items to be treated are:

. régime changes
. month-to-month persistence
. secular variations
. blocking

In order to appreciate some of the results I briefly summarize the analogue selection method used. The data consisted of daily values of sea level pressure for the period 1 January 1881 to present. The area covered is the eastern North-Atlantic and Western-Europe, between 40°N and 60°N and between 20°W to 20°E. The selection procedure makes use of the daily values in such a way that values of the last 30 days (or any other series of 30 days for which analogues are sought) are systematically compared with each 30-day period of the historical record and a score for each comparison is noted. In order to avoid out of season analogues, the comparisons are restricted however to those parts of the record which differ less than 15 days with the dates of our 30 day series. The output of the procedure may consist then of a list which for each year (1881 - present year minus one) specifies the maximum score found in that particular year and the shift (in days, maximum 14) at which the maximum score occurs.
By definition the highest scores are the best analogues. Usually a gradual change from high to lower scores is found, which makes the number of years to be chosen as analogues for forecasting rather arbitrary.
A rather essential point in the final selection of analogue years was the additional requirement of persistence in analogy. When possible only those years were chosen as analogues which had shown high scores also in the previous month(s). Such analogues were called long-running analogues and the idea behind it was that analogy in the sequences of pressure patterns over a long enough period of time somehow must be indicative of a similarity in external conditions between the present and the analogue year.

Régime changes

We distinguish atmospheric circulation states and atmospheric circulation régimes. While there is an infinite number of instantaneous atmospheric states the number of régimes for all practical purposes is finite. As a definiton this is still rather unsatisfactorily, but we know from experience that day after day the atmospheric state changes within certain bounds - a régime - and then suddenly the atmosphere acquires a state which allows it to pass a boundary and enter into a new régime. Lorenz (1965) has shown that such régime changes may have nothing to do with changes in external forcing, but simply may be the result of the non-linear behaviour of the atmospheric system. He illustrated this with the following cubic difference equation

Table 1. Particular solution X of Equation (1), and mean $\bar{X}$ and standard deviation σ of ensemble of solutions of Equation (1), for twenty iterations.

n	X	$\bar{X}$	σ
00	.800	.800	.000
01	.308	.308	.001
02	.706	.706	.004
03	.621	.621	.010
04	.792	.791	.014
05	.340	.341	.057
06	.756	.745	.079
07	.474	.461	.243
08	.871	.586	.231
09	-.028	.520	.305
10	-.075	.418	.345
11	-.194	.333	.364
12	-.484	.276	.435
13	-.874	.194	.498
14	.041	.137	.527
15	.108	.100	.532
16	.278	.054	.519
17	.655	.053	.535
18	.737	.016	.544
19	.534	-.010	.538
20	.869	-.018	.528

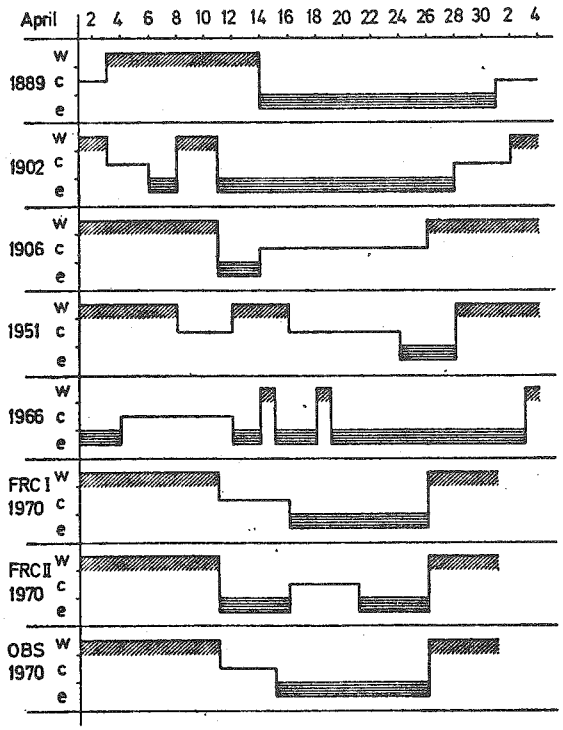

Fig. 1 Phase of the long waves (west, near or east of the 0^{o}-meridian) in April 1970 as inferred from the circulation sequels of the analogoues years for March 1970 (1889, 1902, 1906, 1951 and 1966): FRC I and FRC II are composite curves based upon the curves for the individual years: OBS is the curve for the observed circulation in April 1970.

$$X_{n+1} = 0.875\ (3X_n - 4X_n^3) \qquad (1)$$

Given the initial "observed" value $X_o = 0.800$ a series X_o, X_1 ... X_{20} may be generated by this equation (see second column of table 1). Slightly different initial values produce series which are nearly identical for some time, but then start to deviate from each other. They enter different régimes. In order to prove the real existence of such régimes Lorenz defined a set of initial values all being in the range of 0.799 to 0.801. With these initial values he generated a number of ensembles of forecasts. It is to be expected that for the first few iterations all states within an ensemble will be nearly the same, while for some later iterations, two states within an ensemble will be as different as two randomly chosen states. If however régimes exist one might expect that in the intermediate range of iterations the states within an ensemble, although being different, have some features in common. In Lorenz case such common features are apparent from a consideration of ensemble means and standard deviations (see columns 3 and 4 in table 1). For iterations 1 to 6 ensemble means do not differ very much from an individual realisation and standard deviations are nearly zero. For iterations 14 to 20 ensemble means are nearly zero and standard deviations approach their maximum value. In between however, for iterations 7 to 13 ensembles seem to pass through a set of states which show some similarity, since their ensemble means differ from zero and their standard deviation is much less than the maximum value. While Lorenz' case does not prove the existence of régimes in the real atmosphere, our experience with long-range prediction using circulation analogues strongly points in that direction. Let 1,2,...5 be the best analogues for a particular month and let us consider their circulation sequels for some 30 days into the future. Let us further concentrate on one aspect of the future circulation, namely the phase of the long waves (with respect to the 0^o-meridian). From the 1,2,...5 phase sequels we can construct an ensemble phase sequel. Instead of doing this many times and starting each time with 5 different analogues (a procedure used in Lorenz' case, and customary also in numerical weather prediction) we did it only two times, starting each time with the same set of analogues (since normally only 4 - 5 good analogues are available) but using a different averaging technique. The result for April 1970, taken from Schuurmans (1973) is reproduced in Fig. 1. It is clear from this diagram that the mid-month change of régime which occurred in April 1970, could be inferred from the available circulation analogues well in advance. From our 5-year experience we can show that examples like this are not uncommon. It appears that régime changes are real phenomena, at least as far as the atmospheric circulation over a restricted region is concerned. From our experience in applying circulation analogues, however limited, such régime changes appear to be predictable, probably out to several weeks in advance. However, in view of the non-linearities involved it does not seem that other, more simple approaches than the ensemble averaging techniques of GCM's are capable of predicting such régime changes.

Month-to-month persistence

"Persistence is hard to beat", long-range forecasters sometimes complain. On the other hand persistence may be the sole factor which positively contributes to the low, but significantly positive results of existing long-range forecasting methods. Month-to-month persistence of large-scale temperature anomalies has its underlying cause in month-to-month persistence of large-scale atmospheric circulation anomalies. The latter, as well as the former, exhibit a well-known annual variation, with minima in spring and autumn and maxima in late winter and late summer. See Fig. 2.a

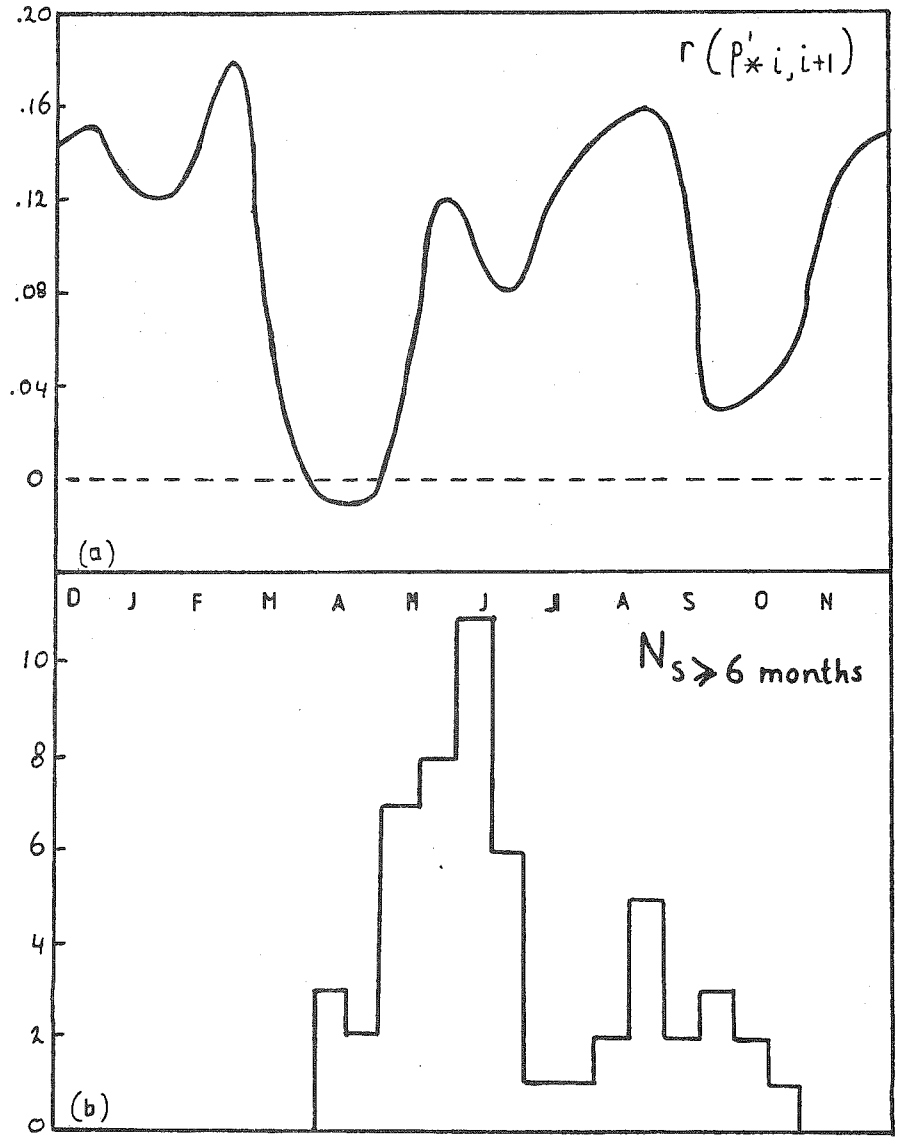

Fig. 2(a) Annual variation of month-to-month persistence of anomalies of sea-level pressure over the Northern Hemisphere, based on data for the period 1881 - 1975.
(b) Annual distribution of the starting dates of long-running circulation analogues (for definition see text).

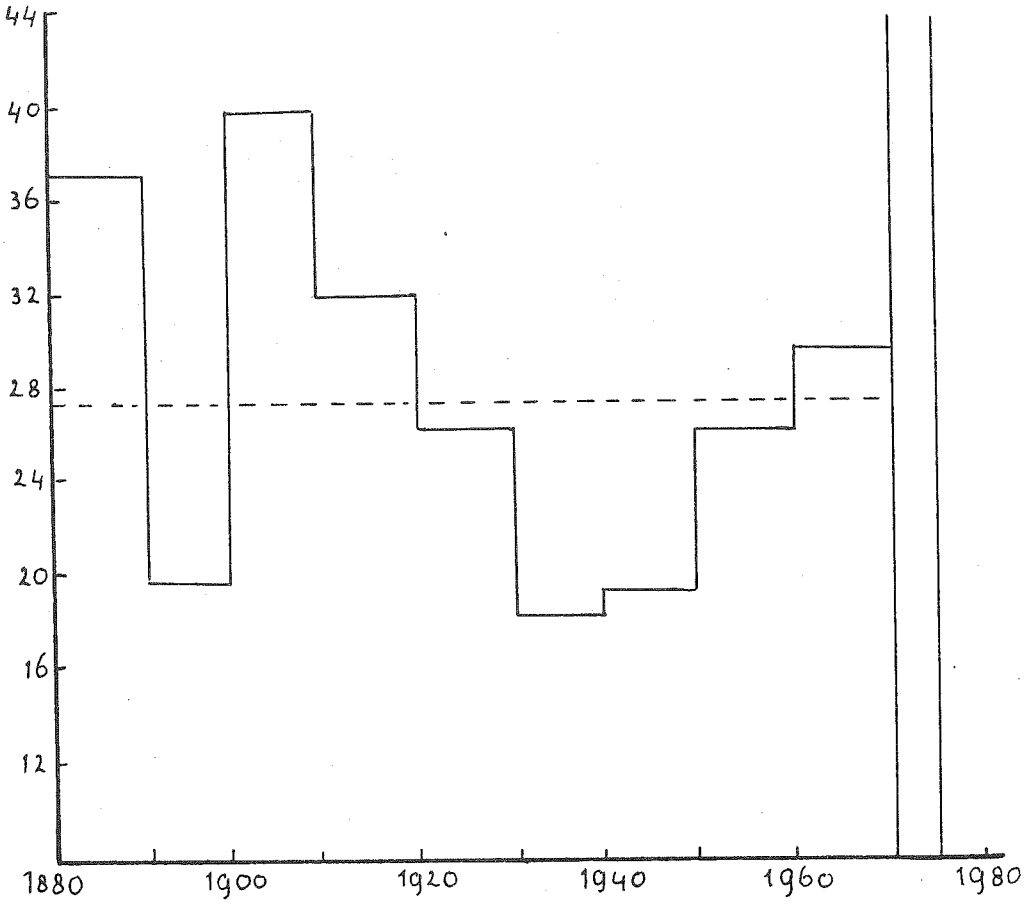

Fig. 3 Distribution of long-running circulation analogues, selected for individual months of the years 1970 - 1975. The total number of cases is approx. 250.

According to some people persistence is to be considered as a kind of sluggishness of an atmosphere, which is forced at irregular intervals. Within such a framework one would explain the observed annual variation of month-to-month persistence as an indication that strong forcing occurs especially in spring and autumn, at least at the epochs of minimum persistence. It has been shown however, for instance by Opsteegh and Van den Dool (1980) that seasonal differences exist in the atmospheric response to a constant anomalous forcing. In fact it was shown that the shape of the annual variation of the month-to-month persistence of the atmospheric response to a constant anomalous heating in the tropics is exactly the same as the curve shown in Fig. 2.a. From this observation it would seem that some properties of the atmosphere, rather than those of the forcing are responsible for the annual variation of month-to-month persistence. Such a conclusion could be supported by the following experimental result.

In our forecasting experiment using circulation analogues we emphasized the possible importance of long-running analogy. The underlying assumption was that similarity in the sequence of circulation types over a certain area during a relatively long time interval can be taken as an indication of similarity in the anomalous forcing (being constant or slowly varying in time) over very large areas and perhaps the whole hemispheric domain. So we might consider our records of long-running analogues as cases (years) of rather similar behaviour of the anomalous forcing fields.
Looking then for cases (analogues years) with a parallel behaviour with the "present" year over at least 6 months and classifying them according to the half-month in which the similarity started we found a rather peculiar annual variation, which is shown in Fig. 2.b. The variation does say for instance that none of the cases started later in the year than the 15th of October. Why not? Simply because long-running analogues started e.g. in November did not survive the following spring period and so none of them could meet the requirement of "at least 6 month duration". So according to the graph the best time to start a long series of persistence is just after the spring time. The autumn dip seems to be less harmful. Results discussed in this section seem to indicate that the atmospheric factors which determine the atmospheric response to external forcing are much more variable in spring than in any other part of the year. This will make prediction by simple climate models for spring rather more dubious than for other seasons.
On the other hand, since we know that the spring period is the period of maximum occurrence of blocking, a better understanding of the latter phenomenon, may perhaps improve our forecasting abilities for spring.

Secular variations

Long-term variations are a well-known feature of the atmospheric circulation, although our upper-air observational records are too short to document such variations in enough detail. Mainly from surface observations we know that the first half of this century was a period of prevailing westerlies, at least over the North-Atlantic (Lamb, 1970, 1972).
The atmospheric circulation since the 1950 's, for which extensive observational statistics have been analysed and studied (e.g. Oort and Rasmusson, 1971) seems to behave like in the pre-westerly epoch, around the turn of the century.

Analogue selection for the sixty months in 1970-1974 verifies this description quite well. See Fig. 3. The figure shows the distribution of analogue years per decade from 1881-1890 to 1961-1970. As a mere demonstration of the existence of secular variations the result is unimportant.

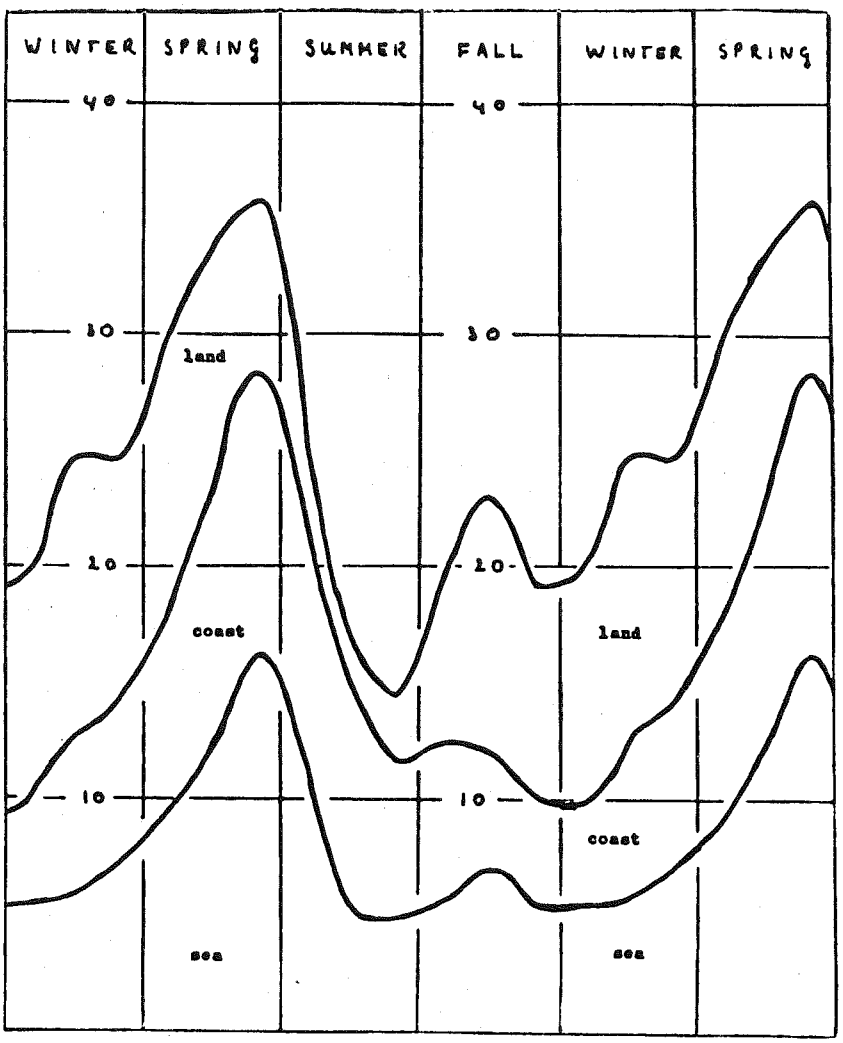

Fig. 4 Annual variation of the frequency of occurrence (percentage of tot. number of days per month) of blocking anticyclones in the Iceland-Scandinavian area, subdivided according to the exact location of the anticyclone at the surface (over sea, coast or land).

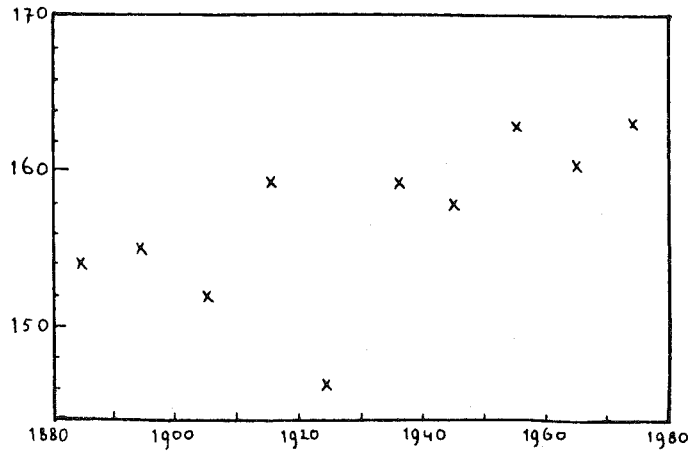

Fig. 5. Long-term variation of the number of days per year with blocking anticyclones in the Atlantic-European area.

However in view of the fact that the analogues take into account a day-by-day similarity over periods of a month or longer, they probably say something about similarity in eddying motion of the atmospheric circulation. For instance, as regards the preference in time and space scales of the eddies in the area concerned. In this respect the curve in Fig. 3 may perhaps indicate that a ten, or 20-year period is not long enough to produce atmospheric circulation statistics which have a universal validity in all detail. Which should be borne in mind when comparing results of numerical simulations with data of the real atmosphere.

Blocking

It may just be a coïncidence that the maximum of blocking frequency is found in spring, exactly at the time that the atmospheric response to persistent anomalous forcing changes most rapidly. Apart from that the blocking phenomenon merits an investigation on its own for several reasons. One of the reasons is that the blocking régime is an example of a circulation régime which most probably is not caused by non-linear interaction of atmospheric modes of circulation alone. It can be shown that forcing from below (conditions at the earth's surface) as well as from above (conditions in the stratosphere) may be of importance.
First however I will discuss a few observational results in regard to blocking in the Atlantic-European sector. (with the Pacific-Alaskan sector the most prominent location of blocking occurrence on the Northern hemisphere). In Fig. 4 the annual variation of blocking occurrence is shown. Blocking is defined here as the occurrence of a blocking anticyclone at sea level north of 55°N in the indicated sector. The data used are daily Grosswetterlagen (see Hess and Brezowsky, 1969) from 1-1-1881 to 31-12-1980. The ordinate gives the percentage of days with blocking for each month. In addition the diagram shows the contributions of the land, coastal and sea-areas to the total frequency of blocking occurrence. It is clear that the relative contributions vary strongly in the course of the year. In winter when the land is much colder than the sea the frequency of blockings over the continent is much larger than over the sea, while in summer just the opposite occurs. Apart from other, more large scale factors it does seem that temperatures of the underlying surface do have a strong influence on the location of the blocking anticyclone. Differences as shown in Fig. 4 have already been observed by Flohn et al. (1951). It must be stressed however that such results strongly depend on the definition of blocking used. For instance, in a recent study, Austin (1980) using a less restricted definition of blocking comes to the conclusion that "a blocking anticyclone is most likely to occur on the coast or in the Mid-Atlantic in winter, but over Western Europe in summer"! In view of these contradictory results it is clearly of importance to know exactly before one starts to explain, what feature has to be explained.
In Fig. 5 some information is given on the year-to-year and long-term variation of blocking occurrence. The data base is the same as used in Fig. 4. On average over the last century 157 days of the year (43%) had a blocked circulation type. In the year with the lowest frequency of occurrence of blocking (1948) only 96 days (26%) with blocking were counted; the highest frequence observed was 58% (212 days) in 1972. So from year-to-year the number of blocking days may vary by at least a factor of two. As is to be expected ten-year averages also vary considerably. Apparently the last 50 years of the period were more blocking-productive than the first 50 years.

As to the explanation of the blocking phenomenon a number of theories have been developed, especially in recent years. See e.g. Green (1976), who also summerizes some of the older theories, Egger (1978), Mc Williams (1980) and Källén (1981).

Notwithstanding the progress made, we are far from a complete understanding of the phenomenon. Forcing from below is certainly of importance as has been shown by many authors. A direct relation with the amplitudes of the forced long waves has recently been advanced by Austin (1980). According to his analysis the relation is as follows:

	wavenumber one	wavenumber two	wavenumber three
Atlantic blocking	large	large	small
Pacific blocking	small	large	large
Double blocking	large	large	large

Concentrating on the occurrence of Atlantic or Scandinavian blockings we see that an increase of the amplitude of wavenumber one is necessary. Apart from possible sources for such an increase at the earth's surface I will show that especially wavenumber one might also be triggered by auroral heating in the stratosphere. The idea of auroral heating of the stratosphere was put forward many years ago by Riehl (1956). It has been studied later on by Berkowsky and Shapiro (1964) using a (too) simple numerical model of the atmosphere. The approach I followed (Schuurmans, 1965) is also quite simple, but I do not have to specify the vertical distribution of the heat source. I only prescribe a heating Q in the auroral zone (a nearly circular belt around the geomagnetic pole, which is located at 78^{o},30'N, 70^{o}W), which in geomagnetic coordinates (x,y) has the form

$$Q(x,y,z) = F(z) \exp\left(-\frac{(y-y_m)^2}{b^2}\right)$$

The heating will cause a disturbance of the pressure distribution which subsequently will give rise to an isallobaric wind $\vec{V}_i$. The divergence of the isallobaric wind $\nabla . \vec{V}_i$ then becomes

$$\nabla . \vec{V}_i = \text{const.} \; \frac{1}{f^2} \frac{\partial^2}{\partial y^2} \left\{ Q(y) \right\}$$

Here $f = 2\,\Omega \sin\phi$ and we have to transform this also to geomagnetic coordinates by using from spherical geometry

$$\sin\phi = \cos\partial \sin y + \sin\partial \cos y \cos x$$

with $\partial = 11^{o}30'$, being the distance between the geographic and the geomagnetic poles.
The final result is

$$\nabla . \vec{V}_i = \text{const.} \times \left\{ \frac{\exp\left(-\frac{(y-y_m)^2}{b^2}\right) \left\{ 2\,\frac{(y-y_m)^2}{b^2} - 1 \right\}}{\sin^2 y \cos^2\partial + \cos^2 y \sin^2\partial \cos^2 x + \tfrac{1}{2} \sin 2y \sin 2\partial \cos x} \right\}$$

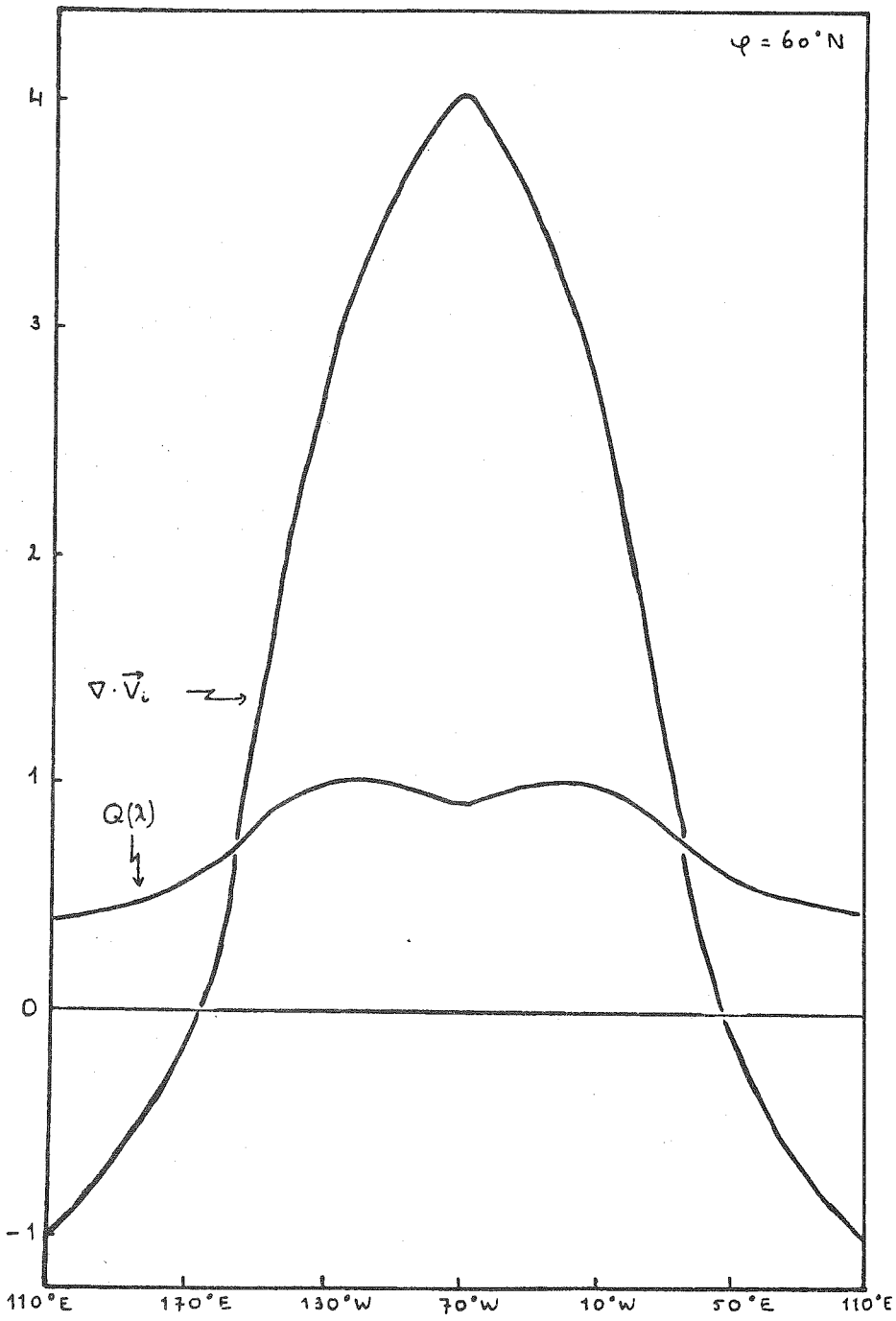

Fig. 6. Amplitude of the assumed stratospheric heat source and the corresponding tropospheric response, both along 60°N.

When portrayed in geographic coordinates the divergence pattern turns out to be ring-shaped but strongly asymmetric with respect to the geomagnetic pole (because of $\frac{1}{f^2}$).

This means that along a certain geographical latitude circle the pattern is mainly characterized by a wavenumber one variation. In Fig. 6 the forcing function Q and the response function $\nabla.\vec{V}_i$ are shown for $\phi = 60^0$ N. Since we do not specify the amplitude of the heating, units are arbitrary. Further investigations of the possible triggering of wavenumber one by this effect must make use of a more complete dynamical model.

References

Austin, J.F., 1980: The blocking of middle latitude westerly winds by planetary waves, Quart. J. Roy. Meteor. Soc., 106, 327 - 351.

Berkofsky, L. and R. Shapiro, 1964: Some numerical results of a model investigation of the atmospheric response to upper level heating, Plan. Space Sci., 12, 219.

Brezowsky, H., H. Flohn and P. Hess, 1951: Some remarks on the climatology of blocking action, Tellus, 3, 191 - 194.

Egger, J., 1978: Dynamics of blocking highs, J. Atmos. Sci.,35, 1788 - 1801.

Green, J., 1977: The weather during July 1976: Some dynamical considerations of the drought. Weather, 32, 120 -126.

Hess, P. and H Brezowsky, 1969: Katalog der Grosswetterlagen Europas. Ber. d. Deutschen Wetterd., no. 113.

Källén, E., 1981: The non-linear effects of orographic and momentum forcing in a low-order barotropic model. J. Atmos. Sci., 38, 2150 - 2163.

Lamb, H.H., 1970, 1972: Climate: Present, Past and Future, Vol. I and II, Methuen, London.

Lorenz, E.N., 1965: On the possible reasons for long-period fluctuations of the general circulation. WMO Tech. Note, no. 66, 203 - 212.

Mc Williams, J., 1980: An application of equivalent modons to atmospheric blocking. Dyn. Atmos. Ocean., 5, 43 - 66.

Oort, A.H. and E.M. Rasmusson, 1971: Atmospheric Circulation Statistics, NOAA Prof. Paper, no. 5.

Opsteegh, J.D. and H.M. van den Dool, 1980: Seasonal differences in the stationary response of a linearized primitive equation model: Prospects for longe-range weather forecasting? J. Atmos. Sci., 37, 2169 - 2185.

Riehl, H., 1956: On the atmospheric circulation in the auroral belt at 500 mb. J. Geophys. Res., 61, 525.

Schuurmans, C.J.E., 1965: Influence of solar flare particles on the general circulation of the atmosphere. Nature, 205, 167 - 168.

Schuurmans, C.J.E., 1973: A 4-year experiment in long-range weather forecasting using circulation analogues. Meteorol. Rdsch. 26, 2 - 4.

TROPICAL INFLUENCES ON STATIONARY WAVE MOTION IN MIDDLE AND HIGH LATITUDES

A.J. Simmons

ABSTRACT

Idealized models of stationary wave motion are examined. Attention is concentrated on the influence of the tropics on middle and high latitude.

A steady, linear, primitive-equation model illustrates the sensitivity of extratropically-forced wave motion to tropical boundary conditions, and indicates the extratropical response to tropical forcing. In the latter case an isolated tropical region of diabatic heating may excite a wavetrain with a substantial poleward direction of propagation. The sensitivity of this response is discussed. Specifying the tropical forcing by means of a relaxation towards climatology results in a large extratropical response.

Barotropic experiments have been performed in which an isolated tropical forcing is superimposed on a constant forcing which maintains a climatological basic flow with zonal variation. In these cases a large response is found in the North Pacific region, and to a lesser extent the North Atlantic region, particulcrly when the forcing is located to the south of the region of strongest flow. Nonlinearity amplifies or damps this response depending on the sign of the forcing. Maintenance of a region of tropical westerly wind of limited zonal extent results in a substantial cross-equatorial propagation.

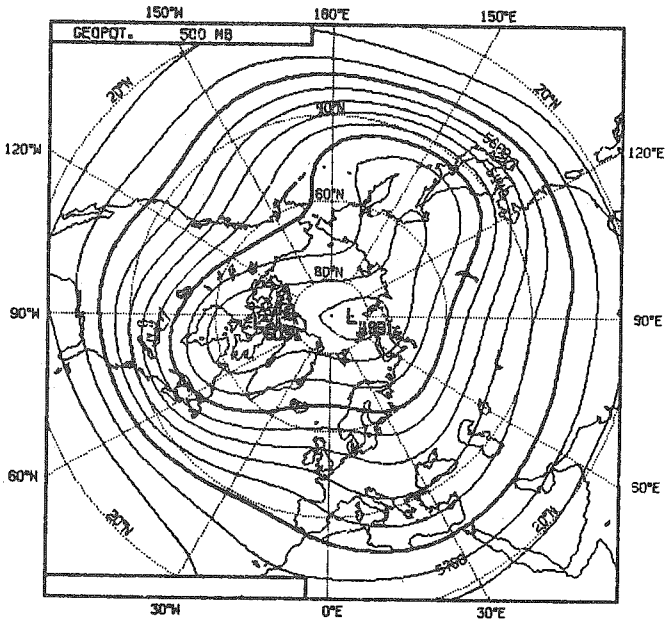

January climate

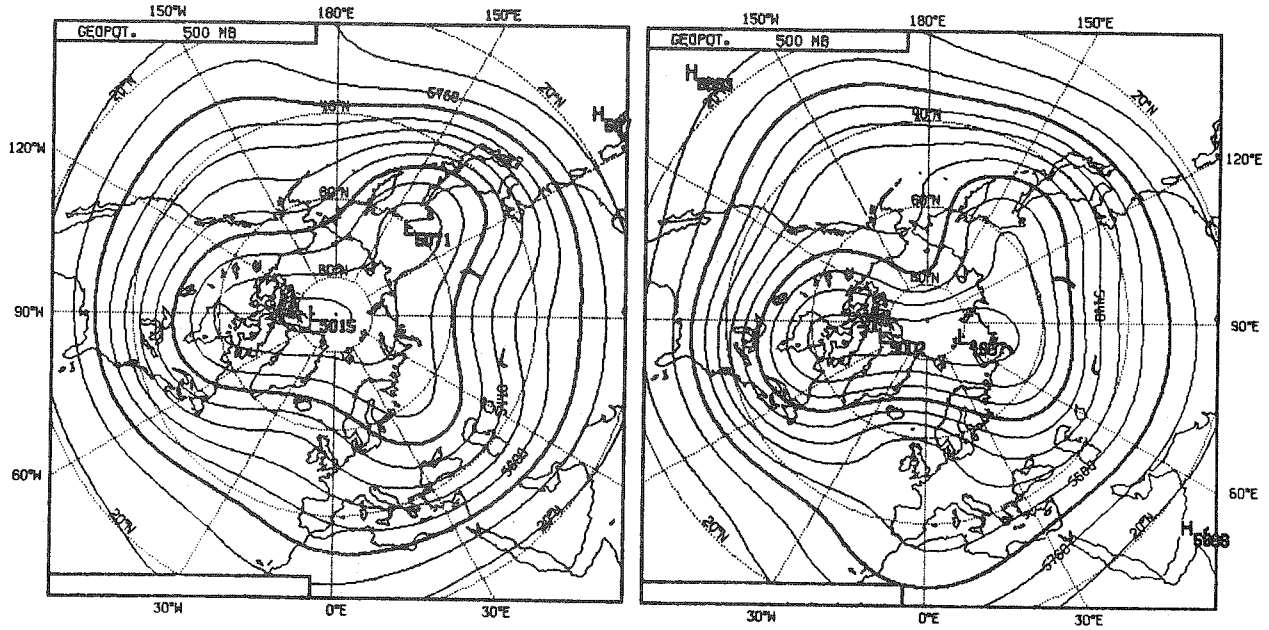

Global model

v = 0 at 15°N

Fig. 1 The climatological mean 500 mb geopotential for January (upper) and calculations using a global model (lower left) and a model with a reflecting boundary condition close to 15°N (lower right). The contour interval is 8 dam.

1. INTRODUCTION

Some of the evidence that the tropics may exert a marked influence on stationary wave motion in middle and high latitudes will be discussed in this paper, which is a shortened version of an account published by Simmons (1982). The immediate motivation for this study was a major systematic error of the ECMWF forecast model (and, moreover, of other forecast and general circulation models), namely a tendency to weaken the major standing-wave pattern in the middle and upper troposphere (Hollingsworth, et al., 1980). This error becomes evident, in the mean, before the limit of useful predictability has been reached, and determination of its origin is thus clearly of importance. More generally, interest in the subject of the impact of the tropics on middle latitudes has been stimulated by a growing body of evidence that regions of anomalous heating of the tropical atmosphere, associated with sea-surface temperature anomalies, may influence the extratropical standing wave, and thus the seasonal climate.

Attention in this paper will be concentrated on results from idealized models. The first of two such models examined in detail computes the steady linear primitive-equation response to a steady forcing. For an isolated region of tropical diabatic heating, the extratropical response is largely in agreement with results obtained (using lower model resolution) by a number of authors (Egger, 1977; Opsteegh and Van den Dool, 1980; Hoskins and Karoly, 1981; Webster, 1981). In addition, a calculation is presented in which the forcing of the extratropical wave motion is given not by an explicit heating, but rather by a relaxation of the steady tropical wave motion towards its climatological distribution.

The second idealized model is a time-dependent, non-linear barotropic vorticity equation model, and forcing is provided by an isolated, steady source of vorticity. Linear results for an extratropical forcing, and a related theoretical examination of wave propagation in a slowly-varying medium, are included in the paper by Hoskins and Karoly (1981). These results are extended here to include the response to an isolated tropical forcing for a basic climatological circulation in which a zonal variation is maintained by a second steady forcing. It is found that the zonal asymmetry of the basic state results in an enhanced perturbation over the North-East Pacific, an especially large response being found when the forcing is located to the south of the strong Western Pacific jet. An enhanced cross-equatorial propagation is also found.

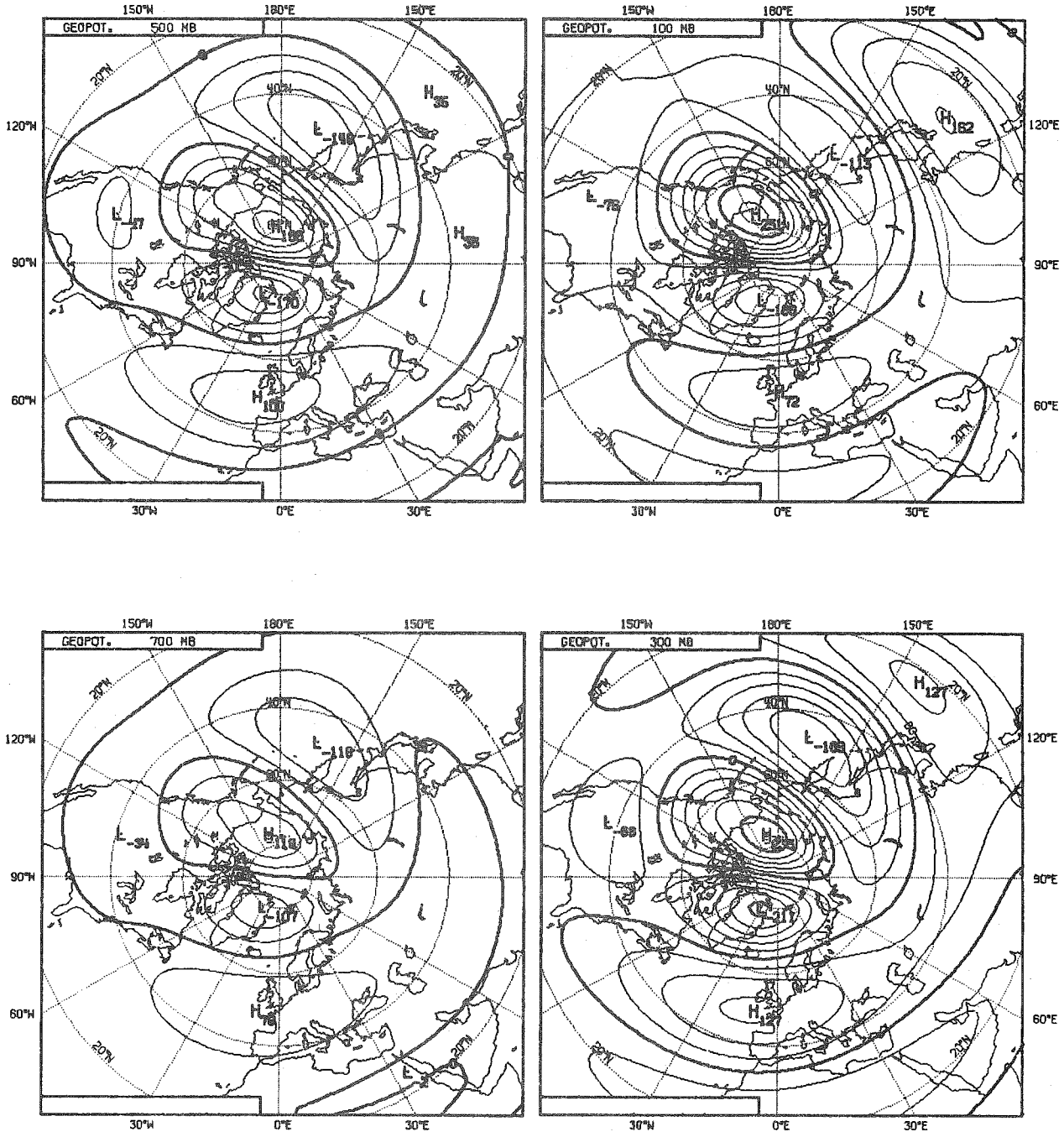

Fig. 2 The response to a heating centred at 15°N, 135°E with a meridional extent of some 20° latitude and a zonal extent of 60° longitude. The perturbation geopotential is shown at 700 mb (lower left), 500 mb (upper left), 300 mb (lower right) and 100 mb (upper right). The amplitude is arbitrary since the calculation is linear, but for a heating maximum of 5°C/day at 400 mb, the contour interval is 4 dam.

2. MIDDLE-LATITUDE FORCING

A linearized steady-state version of the ECMWF, adiabatic gridpoint model has been developed. Stationary wave solutions are determined from a set of linearized equations with forcing by a prescribed distribution of orography and/or diabatic heating, or by relaxation of a limited area of the atmosphere towards a prescribed state. The model includes a simple boundary-layer dissipation and Newtonian damping, together with a friction near critical latitudes (singular lines), where the zonal-mean flow vanishes. The latter is necessary in order to ensure well-behaved solutions. Fixed climatological zonal-mean flows are used. The resolution employed is that of the operational ECMWF model.

One experiment performed with this model was designed to illustrate the role of the tropics as the boundary condition on wave motion forced from extra-tropical latitudes. Figure 1 compares the climatological 500 mb height field for January with model results showing the response to a realistic extratropical forcing for two cases. In the first the model is global, and there is a dissipative critical latitude at all levels in the tropics. In the second the reflecting boundary condition $v = 0$ is applied close to $15^{\circ}N$. The differences in the extratropical response suggest that an accurate representation of the tropics is important for an accurate simulation of the middle latitude circulation, even in the absence of explicit tropical forcing. They also provide further evidence for the importance of acquiring an improved theoretical understanding of a singular-line effects, since the extent to which singular lines act to dissipate or nonlinearly reflect is currently far from clear.

3. THE STEADY, LINEARIZED RESPONSE TO TROPICAL FORCING

The same model as used in Section 2 has been employed, with forcing here provided solely by an isolated source of tropical heating. In agreement with a number of recent studies by others, notably that by Hoskins and Karoly (1981), a significant extratropical response is found. For the January climatology, the response is largest for a forcing at $15^{\circ}N$, and appears as an approximately barotropic train of waves with a substantially poleward direction of propagation (Fig. 2). The amplitude of the response is halved for forcing at $5^{\circ}N$ or $25^{\circ}N$, as shown in Fig. 3, and phase differences are also evident. A very weak steady Northern Hemispheric response is seen for a forcing at $15^{\circ}S$ on account of wave trapping in the equatorial region of easterly winds. Figure 4 shows a weak response due to forcing at $15^{\circ}N$ for a July flow, for similar reasons.

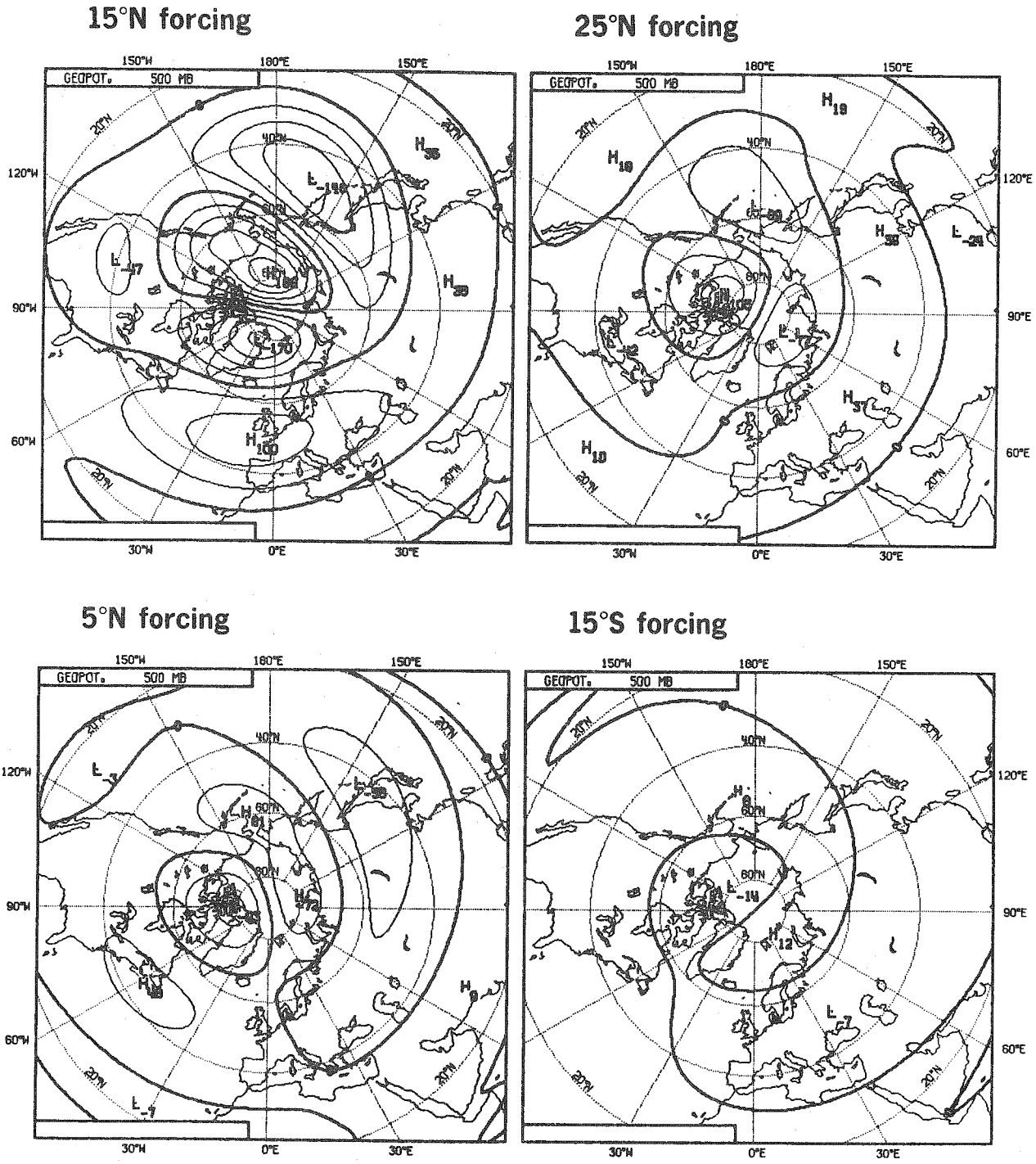

Fig. 3 The 500 mb response to an isolated heating centred at 135°E and 15°N (upper left), 25°N (upper right), 5°N (lower left) and 15°S (lower right).

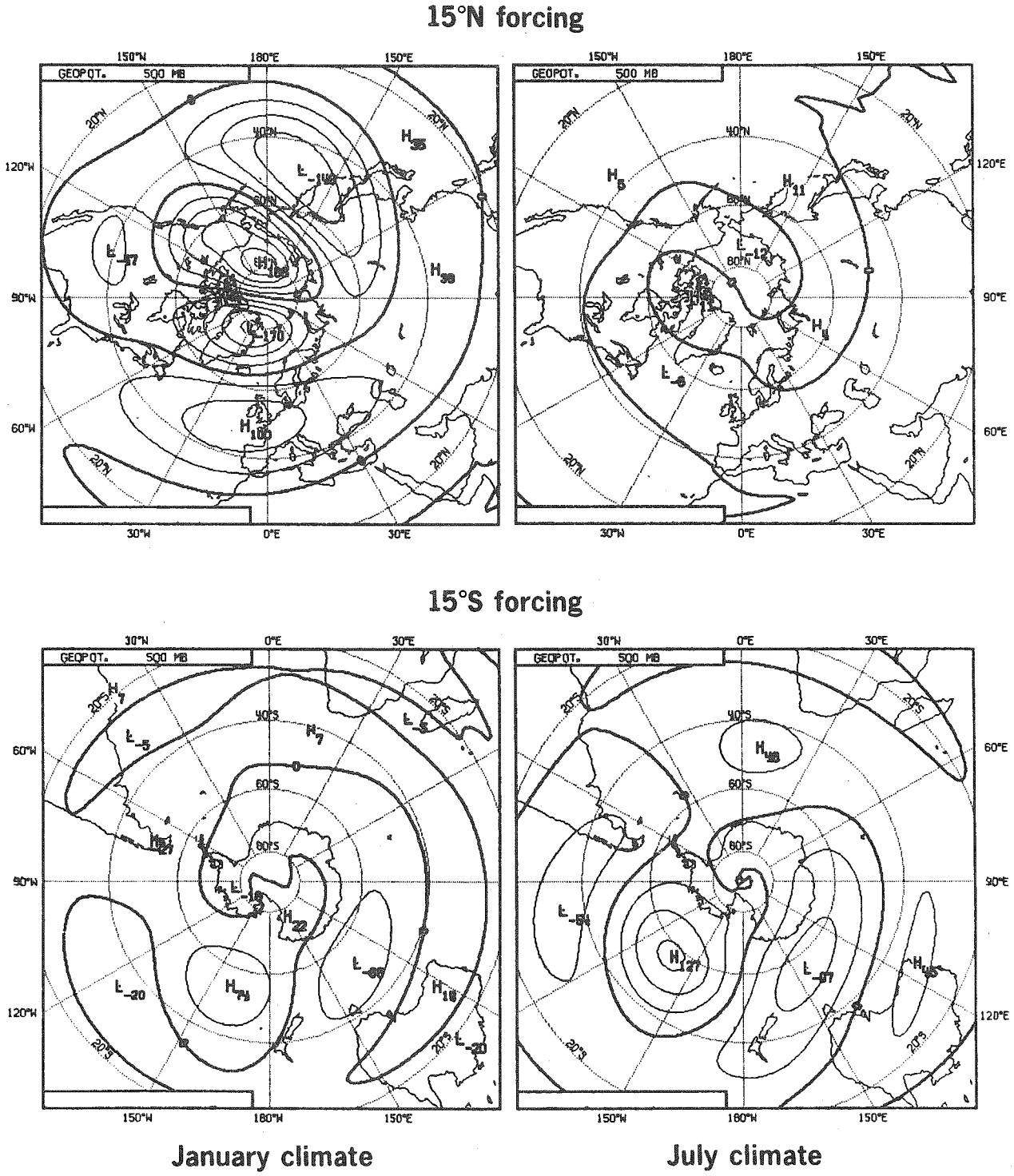

Fig. 4 The 500 mb response for the Northern Hemisphere (upper, isolated heating at 15°N) and the Southern Hemisphere (lower, isolated heating at 15°S). Results are presented for the January (left) and July (right) climatological mean flows.

Figure 4 also illustrates a marked difference for the Southern Hemisphere response to a forcing at 15°S. In this case there is an inhibition of poleward propagation south of the jet maximum, with a clear zonal and then equatorward direction of propagation. This is consistent with the theory of latitudinal planetary wave propagation which shows waves in westerly flow to be reflected by a region of negative poleward gradient of absolute vorticity. Such a gradient occurs on the poleward flank of the climatological jet in the Southern Hemisphere. Since climatological vorticity gradients are inevitably smoother than day to day values, it is likely that similar results may commonly hold for actual propagation in the Northern Hemisphere.

Additional calculations show that results are not particularly sensitive to the detailed vertical structure of the tropical diabatic heating, a result of some significance from the viewpoint of the parameterization of convection. Little sensitivity to the meridional scale of the forcing is also found, while the high latitude (low wavenumber) response increases with the longitudinal scale of the forcing region.

In a second set of experiments the forcing has been specified, not as a direct diabatic heating, but rather as a relaxation towards tropical climatology. If this relaxation is applied south of about 25°N, with no explicit extra-tropical forcing, a substantial extratropical response is found. In particular, a pronounced (and surprisingly realistic) North American trough is evident, as shown in Fig. 5. Uncertainties over the level of dissipation and parameterization of transient wave activity makes it difficult to make quantitative assessment of results such as these, but it is clear that the possible importance of an accurate representation of the tropics must be borne in mind when developing and diagnosing the performance of forecast or general circulation models.

4. EFFECTS OF TRANSIENCE, ZONALLY NON-UNIFORM BASIC FLOWS AND NONLINEARITY

For these studies a spectral, nonlinear barotropic vorticity equation model originally developed at Reading University has been used. Initial conditions comprise either a zonal mean or a zonally-varying climatological basic flow, and in the latter case a vorticity forcing is included to keep the basic flow constant in time. An additional vorticity forcing is initiated over an isolated tropical region at t=0.

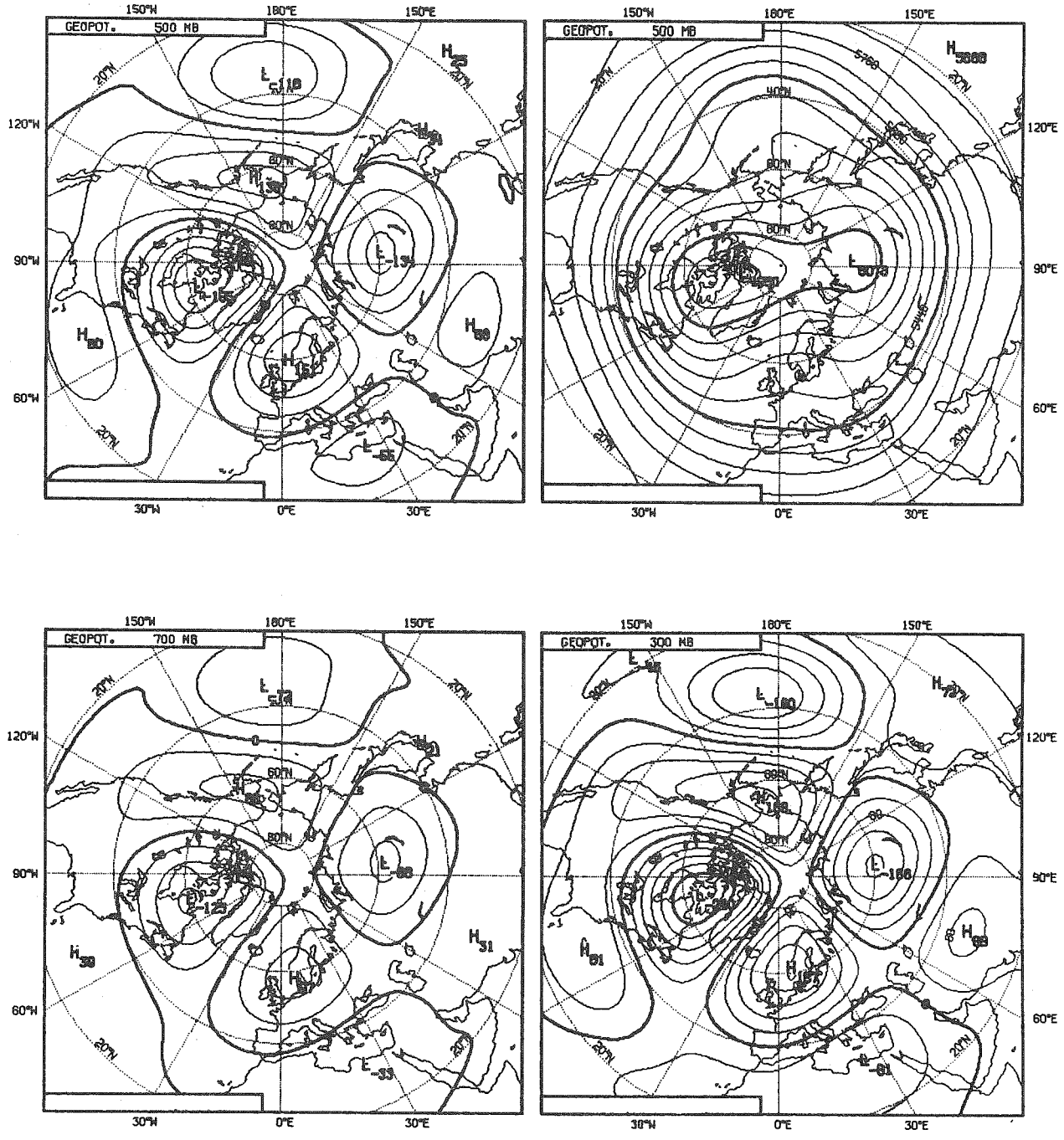

Fig. 5 The extratropical response forced by a relaxation towards tropical climatology. Perturbation geopotentials are plotted with a contour interval of 4 dam at 700 mb (lower left), 500 mb (upper left) and 300 mb (lower right) The total 500 mb field (contour interval 8 dam) is also shown.

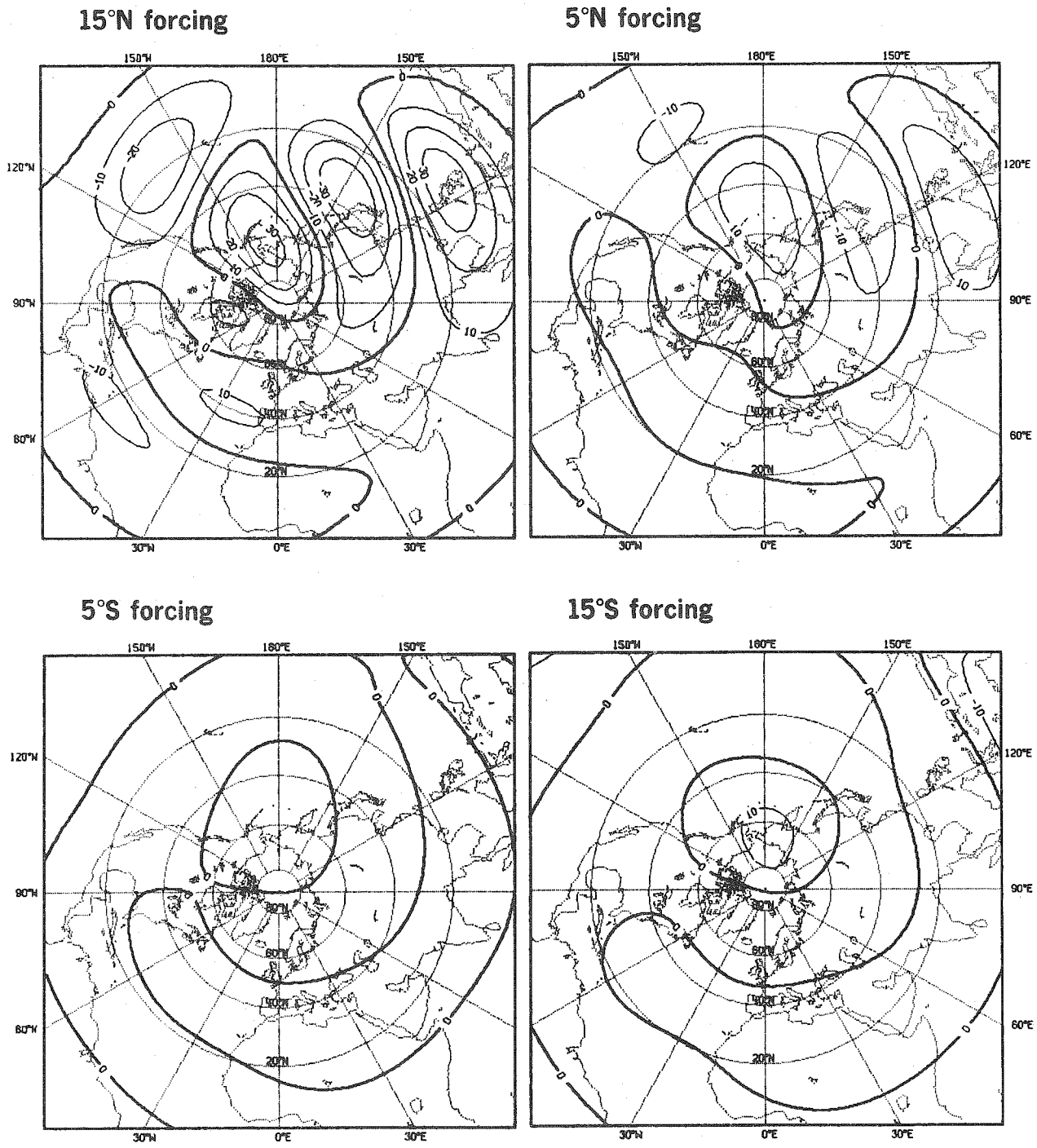

Fig. 6 The barotropic response of the stream function at day 10 to an isolated forcing centred at 135°E and 15°N (upper left), 5°N (upper right), 5°S (lower left) and 15°S (lower right). The January zonal-mean flow at 300 mb is used. The forcing corresponds to a maximum divergence of $2 \times 10^{-6}\,s^{-1}$. The stream function is non-dimensionalized by a factor $10^{-4} a^2 \Omega$, where a is the radius of the earth and Ω its angular rotation. The contour interval of 10 corresponds approximately to a height interval of 4 dam in polar latitudes.

Results shown in Fig. 6 for a zonal-mean basic flow are in broad agreement with those of the steady, linear, three-dimensional model, pronounced wave trains being set up over the first 5 to 10 days, although a larger propagation across equatorial easterlies is found. This latter result is in agreement with similar calculations by Hoskins, Simmons and Andrews (1977) for time-dependent motion and mid-latitude sources.

Introduction of a zonally-varying basic flow gives rise to a marked sensitivity of the response to the longitude of maximum forcing (Fig. 7). In particular, an especially large response is found when the forcing is located to the south of the strong climatological jet in the western Pacific. The nature of the response suggests that an isolated, very weakly dispersive, Rossby wave may exist in a region of decelerating basic flow. Although the wave amplitude varies significantly with the longitude of the forcing, in all four cases shown in Fig. 7 the largest response is found in the same region of the Pacific. For a forcing centred at $80^{\circ}W$, south of the North American jet maximum, the largest response occurs over the North-East Atlantic, although it is not as large as in the corresponding Pacific case shown for the $135^{\circ}E$ forcing.

Nonlinearity can also play an interesting, and easily understood, role in this case. Figure 8 compares the linear and nonlinear response to cyclonic and anticyclonic vorticity forcing centred near $15^{\circ}N$, $135^{\circ}E$. The linear response is identical for the two forcings, apart from a change of sign, while nonlinearity results in a substantial weakening of the response in the case of cyclonic forcing, and a marginal strengthening for anticyclonic forcing. In the latter case, the large anticyclonic response in the North Eastern Pacific reinforces the climatological ridge, which is itself responsible for the anomalous response in the first place. A positive feedback thus occurs. Conversely, for cyclonic forcing the cyclonic response tends to reduce the climatological ridge, and thus damp itself.

Another important effect of introducing a zonally-varying basic flow is a marked influence on the degree of cross-equatorial propagation. For the zonal-mean climatology, winds are easterly at the equator. The Northern Hemisphere response to a forcing at $15^{\circ}S$ has been shown for day 10 in Fig. 6, and beyond this time its amplitude weakens to give the particularly small long-term response indicated by the steady-state calculations.

A quite different result is shown in Fig. 9 for the zonally-varying January flow and a forcing at $15^{\circ}S$, $135^{\circ}W$. At day 10 the maximum amplitude of the

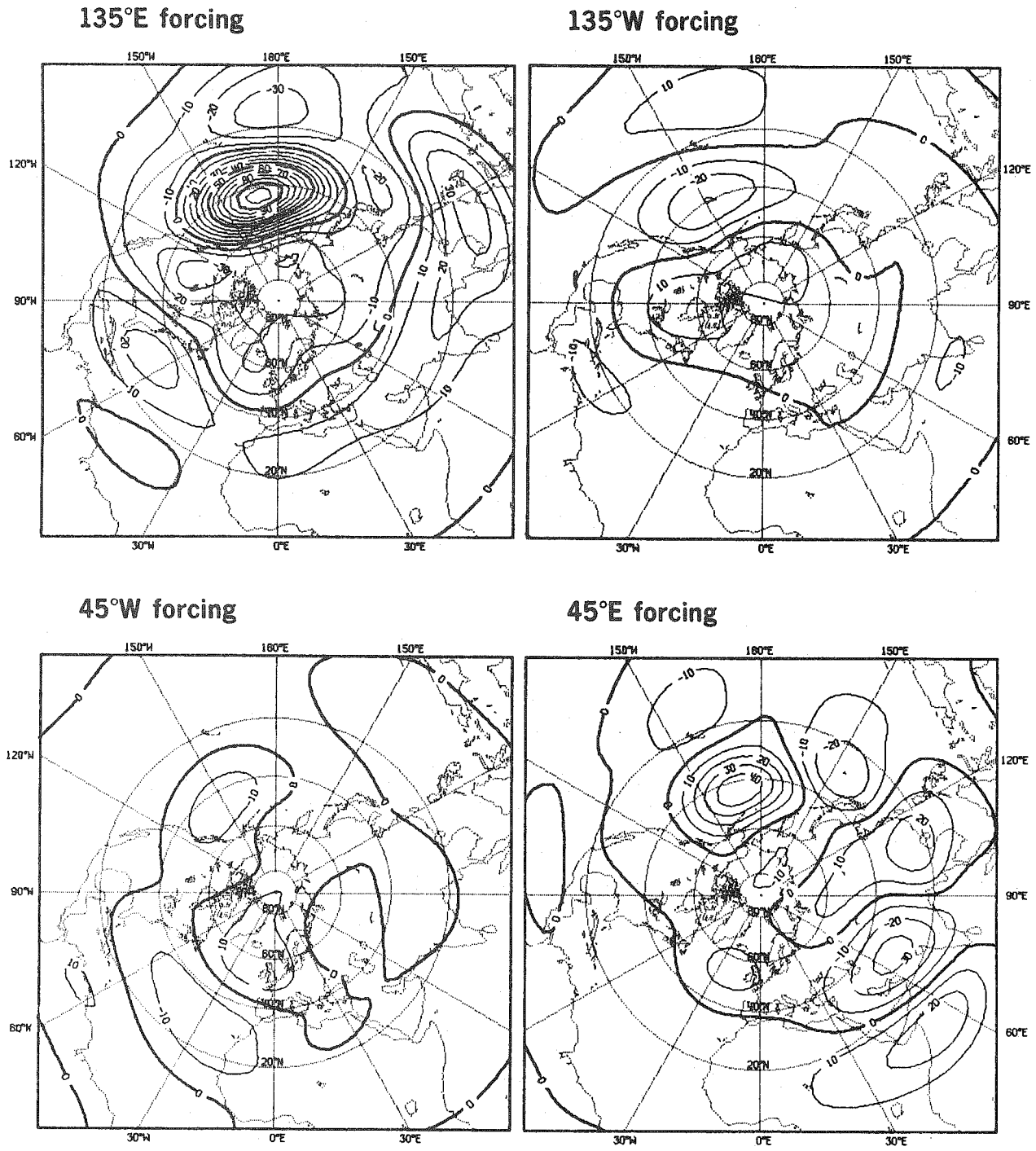

Fig. 7 The day 10 response for a basic flow derived from the zonally varying January climatology. The forcing is centred at 5°N and 135°E (upper left), 135°W (upper right), 45°W (lower left) and 45°E (lower right). Other details are as in Fig. 6.

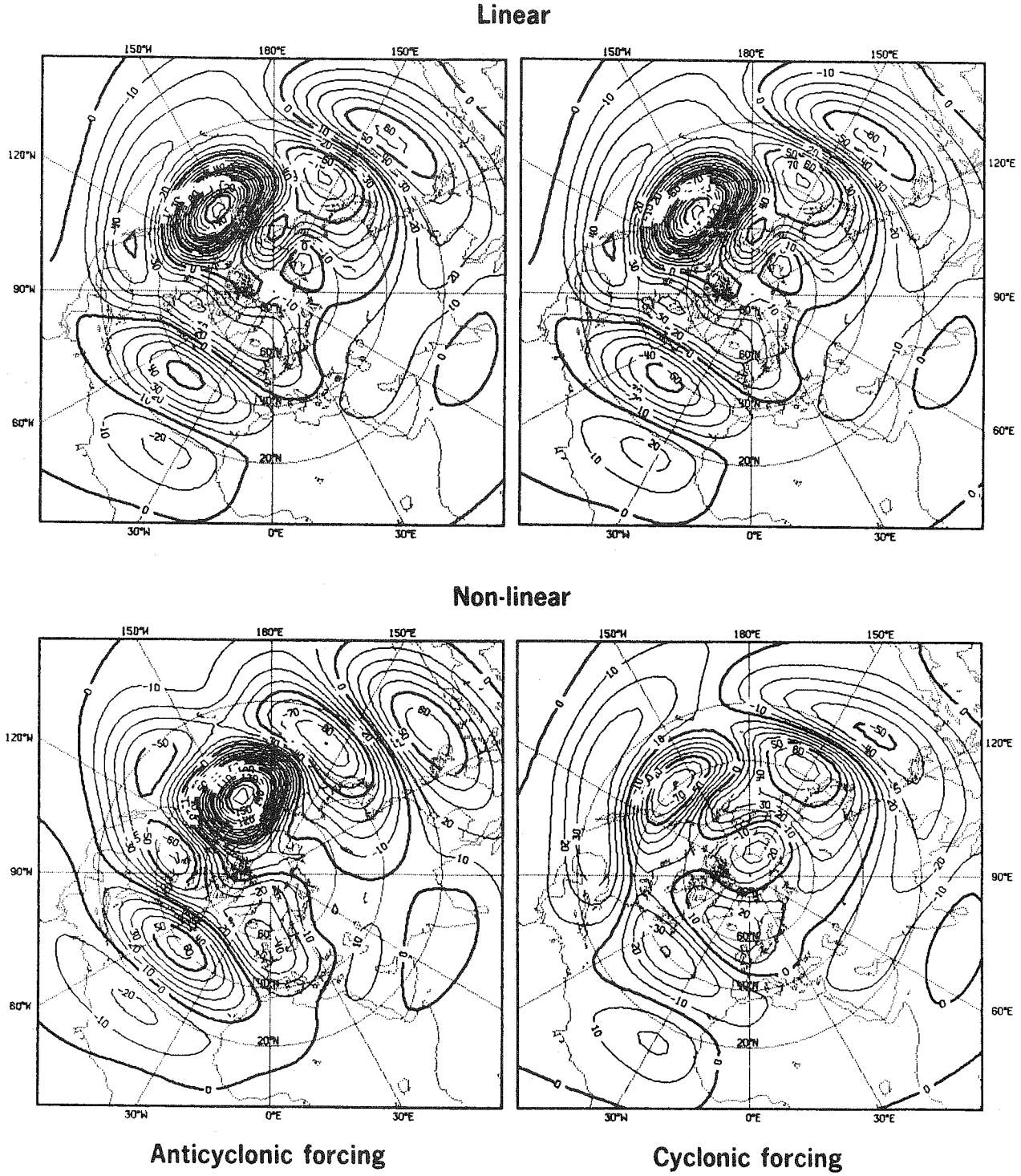

Fig. 8 The linear (upper) and non-linear (lower) day 10 response to anticyclonic (left) and cyclonic (right) vorticity forcing centred at 15^{o}N and 135^{o}E for the zonally varying January climatological flow. Other details are as in Fig. 6.

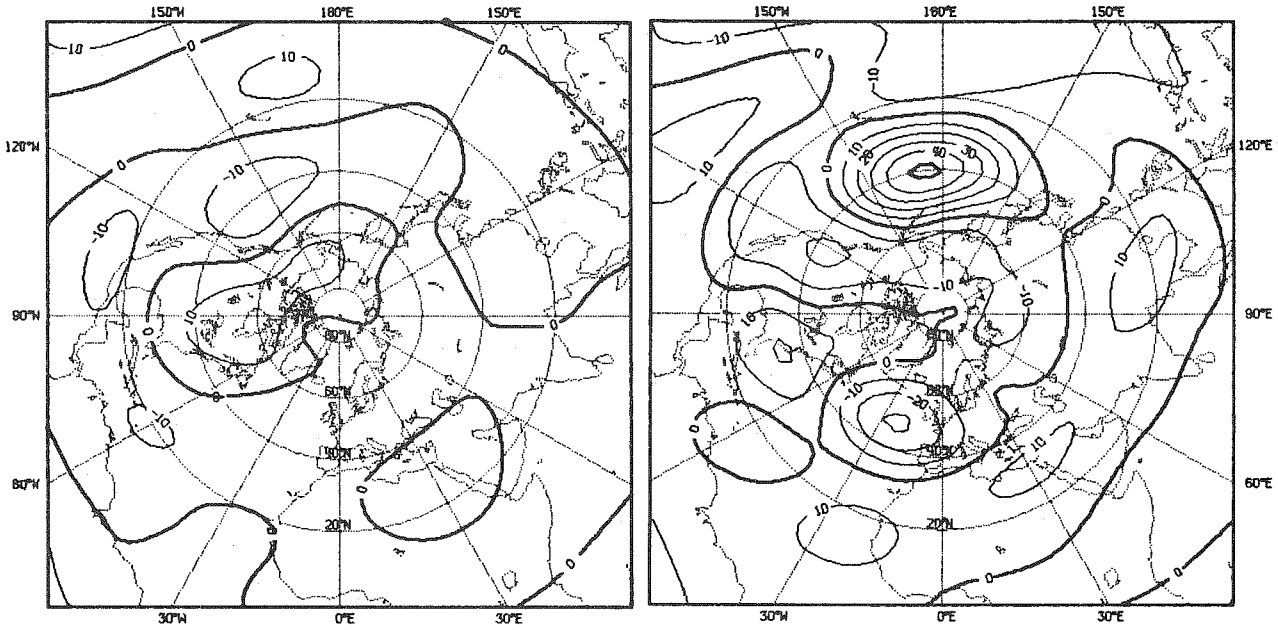

Fig. 9 The Northern Hemisphere response at days 10 (left) and 30 (right) for a forcing centred at 15°S, 135°W for the zonally-varying basic flow.

Northern Hemisphere response differs little from that in the case of the zonal-mean flow, but beyond this time the amplitude increases, rather than decays. Thus, by day 30 a substantial wave amplitude is found, particularly in the North Pacific region which we have already seen to be a favourable region for a large-amplitude response.

This result confirms a speculation by Webster (1981) that cross-equatorial propagation may occur through regions of westerly flow of limited longitudinal extent which appear in seasonal-means. Such westerly flow occurs over the East Pacific for the 300 mb level used for the calculations shown in Fig. 9.

5. CONCLUDING REMARKS

It is difficult to assess quantitative aspects of the simple model results summarized here for a number of reasons, in particular because of the presence in reality of significant interactions between standing and transient waves and perhaps also because of the lack of any direct vorticity forcing or dissipation to accompany the imposed diabatic heating which was chosen to model the effect of an area of tropical convection. There is, however, substantial observational evidence, both from case studies (e.g. Bjerknes, 1966, 1969) and from objective studies of many winters (e.g. Horel and Wallace, 1981; Wallace and Gutzler, 1981), and also some evidence from general circulation models (Rowntree, 1972, 1976; Julian and Chervin, 1978) which, together with theoretical and idealized model studies, leads to a reasonably coherent picture which shows a significant influence of the tropics on the standing wave pattern in the middle and high latitudes of at least the winter hemisphere.

From the idealized model studies it may be seen that it is important to simulate accurately the geographical distribution, the magnitude, and the temporal variability of the tropical convective heating in order to represent accurately its effect on stationary motion in middle latitudes. A particularly accurate vertical profile of heating does not appear to be as important in this respect. It is also important to represent the detailed structure of the mid-latitude jet in order to obtain the correct extratropical response to tropical forcing.

The tropical response to an isolated region of heating has not been discussed here, but details are given by Simmons (1982). This response possesses a vertical structure in good agreement with the analytical solution for zero zonal-mean wind. This structure is more sensitive to the vertical profile of diabatic heating than is the extratropical response, and it also depends sensitively on the mean temperature profile through a vertical derivative of

the associated static stability. Although climatological zonal-mean winds have little qualitative influence on the response in the immediate vicinity of the equator, a pronounced asymmetry about the equator at 200 mb may be associated with the latitudinal variation of the meridional gradient of absolute vorticity. Calculations of this type may provide a useful complement to observational and general circulation model studies of particular atmospheric phenomena, as is illustrated by a recent study of drought in North East Brazil by Moura and Shukla (1982). They may also help clarify relationships between erroneous diabatic heating and erroneous tropical circulations encountered in the diagnosis of the performance of forecast or general circulation models.

The barotropic solutions for a zonally-varying basic flow show that in favourable circumstances there can be a significant interaction between a pre-existing forced stationary wave and wave motion forced from an isolated tropical region. The largest response occurs downstream of the main climatological jet streams at locations close to those of maximum observed variance (Blackmon et al, 1979), and close to those of maximum amplitude of the Eastern Atlantic and Pacific/North American teleconnection patterns analyzed by Wallace and Gutzler (1982). It is important to note, however, that the large, localized response found for these calculations may also be excited by extratropical forcing, and the qualitative agreement with observation does not imply a predominant role of tropical forcing in the maintenance of extratropical anomalies.

A consequence of these results is the possibility that experiments with a general circulation model may substantially underestimate the effect of anomalous boundary conditions, for example sea surface temperature anomalies, if the model used underestimates the climatological standing wave pattern. A further result worthy of note is that substantial cross-equatorial propagation may occur in the presence of an equatorial region of westerly flow of limited longitudinal extent.

REFERENCES

Bjerknes, J., 1966A Possible response of the atmospheric Hadley circulation to equatorial anomalies of ocean temperature. Tellus, 18, 820-829.

Bjerknes, J. 1969 Atmospheric teleconnections from the equatorial Pacific. Mon. Wea. Rev., 97, 163-172.

Blackmon, M.L., R.A. Madden, J.M. Wallace and D.S. Gutzler, 1979 Geographical variations in the vertical structure of geopotential height fluctuations. J. Atmos. Sci., 36, 2450-2466.

Egger, J., 1977 On the linear theory of the atmospheric response to sea surface temperature anomalies. J. Atmos. Sci., 34, 603-614.

Hollingsworth, A., K. Arpe, M. Tiedtke, M. Capaldo and H. Savijärvi, 1980 The performance of a medium range forecast model in winter - Impact of physical parameterizations. Mon. Wea. Rev., 108, 1736-1773.

Horel, J.D. and J.M. Wallace, 1981 Planetary scale atmospheric phenomena associated with the interannual variability of sea-surface temperature in the equatorial Pacific. Mon. Wea. Rev., 109, 813-829.

Hoskins, B.J., A.J. Simmons and D.G. Andrews, 1977 Energy dispersion in a barotropic atmosphere. Quart.J.Roy.Met.Soc., 103, 553-567.

Hoskins, B.J. and D.J. Karoly, 1981 The steady linear response of a spherical atmosphere to thermal and orographic forcing. J. Atmos. Sci., 38, 1179-1196.

Julian, P.R. and R.M. Chervin, 1978 A study of the southern oscillation and Walker circulation phenomena. Mon.Wea.Rev., 106, 1433-1451.

Moura, A.D. and J. Shukla, 1982 On the dynamics of droughts in Northeast Brazil: Observations, theory, and numerical experiments with a general circulation model. Submitted to J. Atmos. Sci.

Opsteegh, J.D. and H.M. van den Dool, 1980 Seasonal differences in the stationary response of a linearised primitive equation model: prospects for long range weather forecasting? J. Atmos. Sci., 37,

Rowntree, P.E., 1972 The influence of tropical east Pacific Ocean temperatures on the atmosphere. Quart.J.Roy.Met.Soc., 98,290-321.

Rowntree, P.E., 1976 Response of the atmosphere to a tropical Atlantic ocean temperature anomaly. Quart.J.Roy.Met.Soc., 102, 607-626.

Simmons, A.J., 1982 The forcing of stationary wave motion by tropical diabatic heating. Quart.J.Roy.Met.Soc., 108, in press.

Wallace, J.K. and D.S. Gutzler, 1982 Teleconnections in the geopotential height field during the Northern Hemisphere winter. Mon.Wea.Rev., 109, 784-812.

Webster, P.J., 1981 Mechanisms determining the atmospheric response to sea surface temperature anomalies. J.Atmos.Sci., 38, 554-571.

ON THE IMPORTANCE OF THE HADLEY CIRCULATION FOR CROSS EQUATORIAL PROPAGATION OF STATIONARY ROSSBY WAVES.

J.D. Opsteegh

1. Introduction

In a number of recent papers several aspects of horizontal energy propagation in Rossby waves on a sphere are studied. With barotropic models Hoskins et al (1977) investigated the propagation of the energy of a local initial disturbance, whereas in Grose and Hoskins (1979) the steady spherical response to local mountain forcing is studied. In both papers significant meridional propagation of wave energy is found. Grose and Hoskins (1979) show that for a basic zonal flow in super rotation the stationary wave train crosses the equator, but for observed zonal mean conditions with equatorial easterlies cross equatorial propagation is negligible. Webster (1981) mentions the possibility of cross equatorial propagation in a zonally-varying basic flow, which partly consists of a region of equatorial westerlies. Simmons (1981) has shown this to be true.

In the present paper we will investigate the ability of stationary Rossby waves to cross a region of equatorial easterlies, assuming that they are linear perturbations of a non-zonally varying basic flow. The basic flow consists of zonal-mean, zonal, meridional and vertical winds, temperature and static stability. We will concentrate on the importance of the Hadley circulation for the spherical response to a local heat source.

2. The Idea

The reason for doing model experiments to study the effect of a weak mean meridional circulation (MMC) on the ability of stationary Rossby waves to cross the equatorial easterlies is illustrated with the help of the linearized barotropic vorticity equation. The equation is

linearized around a basic wind which has a zonal as well as a weak meridional component. For the moment we do not consider any dependence of the basic state on latitude and height.

The equation for this case is:

$$\frac{\partial \hat{\zeta}}{\partial t} + U_n \frac{\partial \hat{\zeta}}{\partial x} + V_n \frac{\partial \hat{\zeta}}{\partial y} + \beta \hat{v} = 0 \qquad (1)$$

U_n and V_n are the zonal and meridional components of the basic flow. $\hat{\zeta}$ and $\hat{v}$ are relative vorticity and meridional velocity assocated with the perturbations. $\hat{\zeta}$ and $\hat{v}$ are expressed in a streamfunction $\hat{\Psi}$ as follows:

$$\hat{\zeta} = \nabla^2 \hat{\Psi} \qquad (2)$$

$$\hat{v} = \frac{\partial \hat{\Psi}}{\partial x}$$

Looking for wavelike solutions for $\hat{\Psi}$ of the form:

$$\hat{\Psi} = Ae^{i(mx + ny - \nu t)} \qquad (3)$$

leads to the following relation for the frequency ν

$$\nu = U_n.m + V_n.n - \frac{\beta m}{K^2} \qquad (4)$$

with $K^2 = m^2 + n^2$.

For particular values of U_n the wave (m,n) becomes stationary. This value depends on V_n, m and n as follows:

$$U_{n_s} = \frac{\beta}{K^2} - V_n\left(\frac{n}{m}\right) . \qquad (5)$$

It is easy to see from (5) that with zero meridional velocity Un_s must be positive for all waves. However, if V_n is nonzero Rossby waves solutions do exist which are stationary perturbations of an easterly mean flow. To illustrate this I have computed Un_s for various combinations of zonal and meridional wavenumbers. For V_n a value of 1 m sec^{-1} is assumed, while for β a low latitude value (at 5 degrees) is used m and n satisfy the following relations

$$m = \frac{2\Pi}{L} m^* \qquad (6)$$

$$n = \frac{2\Pi}{D} n^*$$

L and D are the length and width of the basin. L is taken 40.000 km and D is 20.000 km. The wavenumber m^* and n^* run from 1 to 10. The results for Un_s are given in table 1. For small values of n^*, Un_s is always positive independent of the value for m^*. For large values of n stationary Rossby wave solutions exist in the presence of a negative value for Un_s. For large values of m^*, Un_s is only marginally negative, but for zonal wavenumber 1 and meridional wavenumber 5 to 6 Un_s has negative values which are approximately in agreement with the observed strength of the tropical easterlies.

For a strong easterly basis flow the stationary wave solutions have very high meridional wavenumbers. Therefore it can be expected that the ability of the waves to cross the equatorial easterlies will decrease with increasing strength of the easterlies.

The direction of the energy flow is computed from the group velocity of the stationary wave:

$$Cg_x = \left(\frac{\partial \nu}{\partial x}\right)_{\nu = 0} = - V_n \frac{n}{m} + \frac{2\beta m^2}{(K^2)^2}$$

$$Cg_x = \left(\frac{\partial \nu}{\partial y}\right)_{\nu = 0} = V_n + \frac{2\beta m n}{(K^2)^2} \qquad (7)$$

with $K^2 = m^2 + n^2 = \dfrac{\beta m}{U_n . m + V_n . n}$

In order for a stationary Rossby wave to exist, K^2 must be positive. If m is taken positive and U_n is negative then the product of V_n and n must be positive. So V_n and n must have equal sign. The direction of the energy flow in meridional direction is given by Cg_y. From (7) it is clear now that Cg_y and V_n must have equal sign. The energy can thus only be transported in the direction of V_n. In the Hadley cell of the NH winter V_n is positive in the upper part of the troposphere and negative in the lower part. So wave energy is transported from SH to NH in the upper troposphere and from NH to SH in the lower part.

As the strength and width of the easterlies decreases with height it can be anticipated that in the NH winter it is much easier to transport wave energy from SH to NH than vice versa.

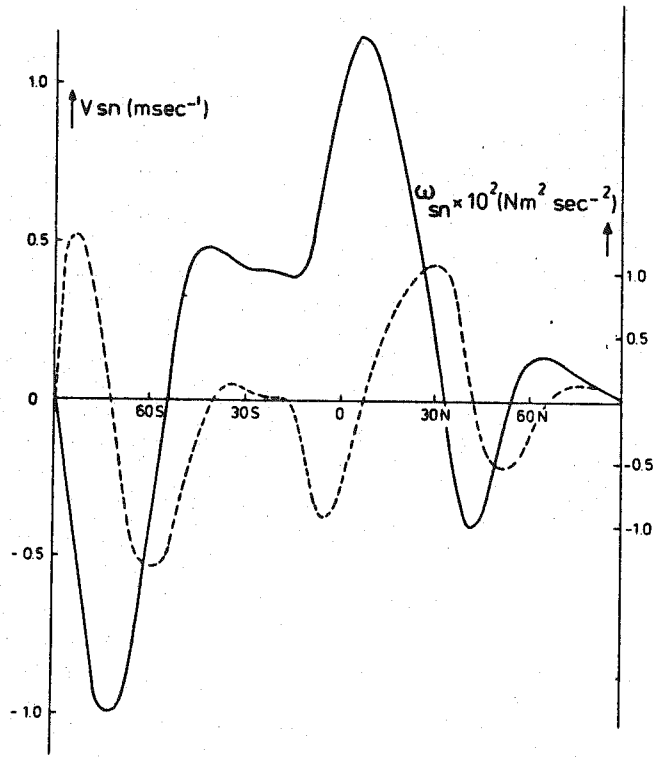

Fig. 1 The January mean zonally averaged wind at 400 mb (solid line) and at 800 mb (dashed line) as a function of latitude.

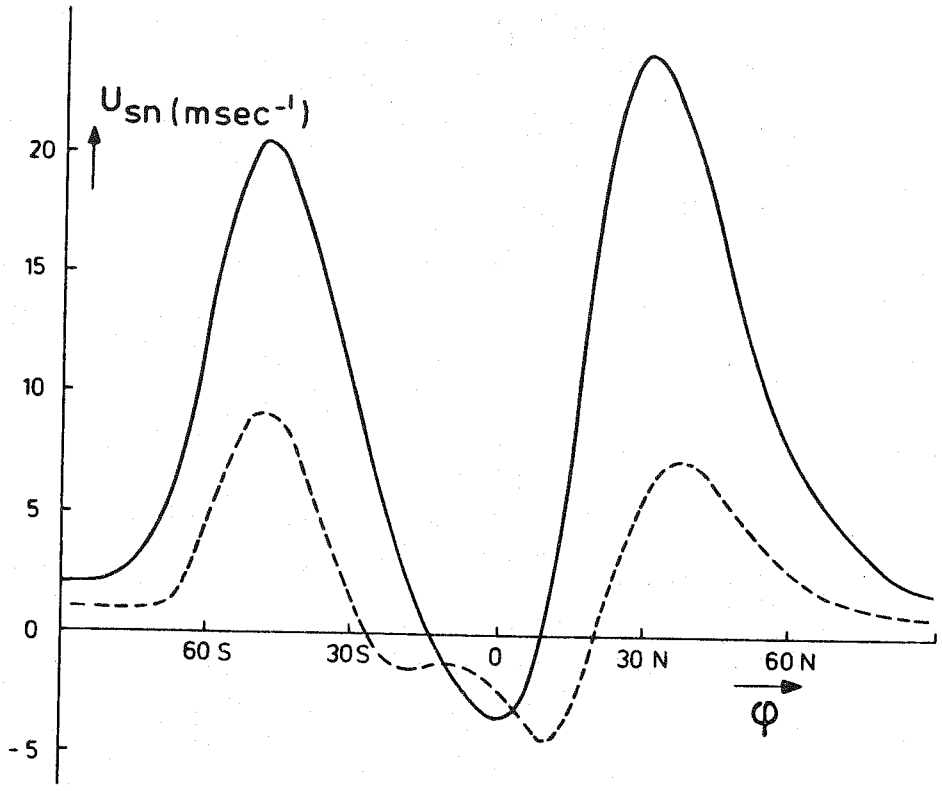

Fig. 2 January mear zonally averaged meridional circulation. The solid line gives the meridional wind at 400 mb. The vertical circulation at 400 and 800 mb is given by the dashed line.

3. Numerical Experiments

The simple idea outlined in the previous section is tested with a linear global two level steady-state primitive equation model. The essentials of the model are described in Opsteegh and Van den Dool (1980).

The influence of the MMC is described by adding the following terms to the original equations.

1. zonal momentum equation:

$$V_n \frac{\partial \hat{u}}{a\ \partial \phi} + \omega_n \frac{\partial \hat{u}}{\partial p} \tag{8}$$

2. Meridional momentum equation:

$$V_n \frac{\partial \hat{v}}{a\ \partial \phi} + \hat{v} \frac{\partial\ V_n}{a\ \partial \phi} + \omega_n \frac{\partial \hat{v}}{\partial p} + \hat{\omega} \frac{\partial\ V_n}{\partial p} \tag{9}$$

In the thermodynamic equation no terms are added because the equation is applied at 600 mb where the MMC is assumed to be negligible.

The basic state consists of observed January mean zonal, meridional and vertical winds, temperature and static stability. The data are from Oort (1982). It is the mean state for the years 1963-1973. Fig. 1 shows the zonal wind at 400 and 800 mb as a function of latitude. As the model has only two levels continuity considerations demand that the mean meridional wind at 400 mb has equal strength and is opposite to the mean wind at 800 mb. Fig. 2 shows V_n and ω_n at 400 mb. The vertical velocities of the MMC are computed from V_n with the help of the continuity equation.

In the first experiment we consider a local heat source in the Southern Hemisphere (SH). The latitudinal extent of the heat source ranges from 25 S to 42 S. In longitudinal direction it covers 45 degrees. The exact position is unimportant. The heating rate in this area is constant and 1K/day. Fig. 3 shows the amplitude of the response in zonal wavenumber 1 and 2 as a function of latitude. The solid line is with and the dashed line without inclusion of the MMC in the zonally-symmetric state. When the MMC is neglected the response in both wavenumbers is restricted to the SH, but with Hadley circulation a remote response in the NH shows up, especially in wavenumber 1. The high latitude response in the SH is much weaker when the MMC is included both for wavenumbers 1 and 2. These results suggest that the Hadley circulation has an important role to play in the spherical response to local heat sources, especially with regards to the exchange

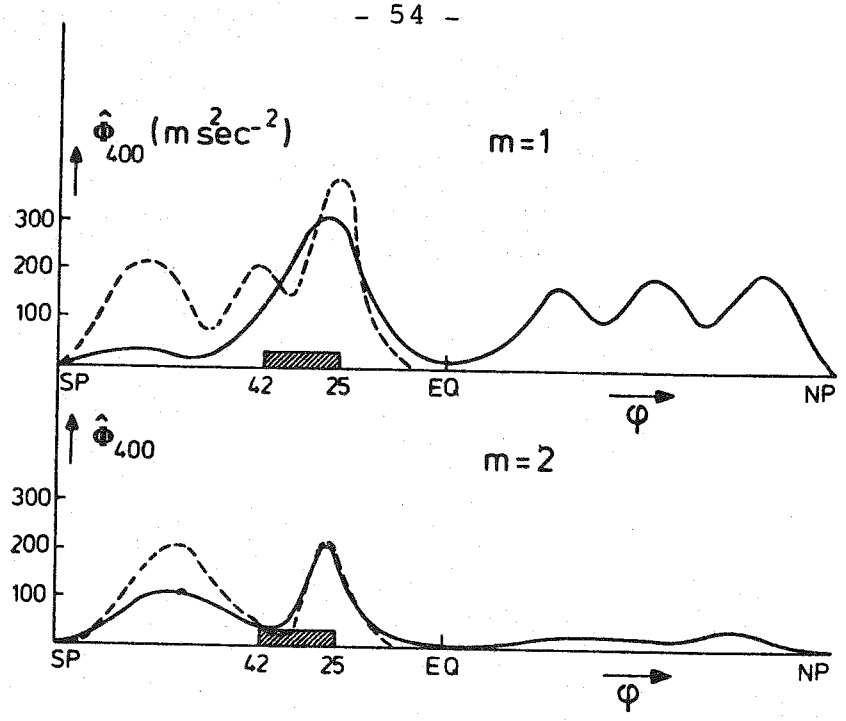

Fig. 3 Amplitude of the geopotential height response in wavenumbers 1 and 2 at 400 mb to subtropical forcing in the southern hemisphere with (solid line) and without (dashed line) MMC.

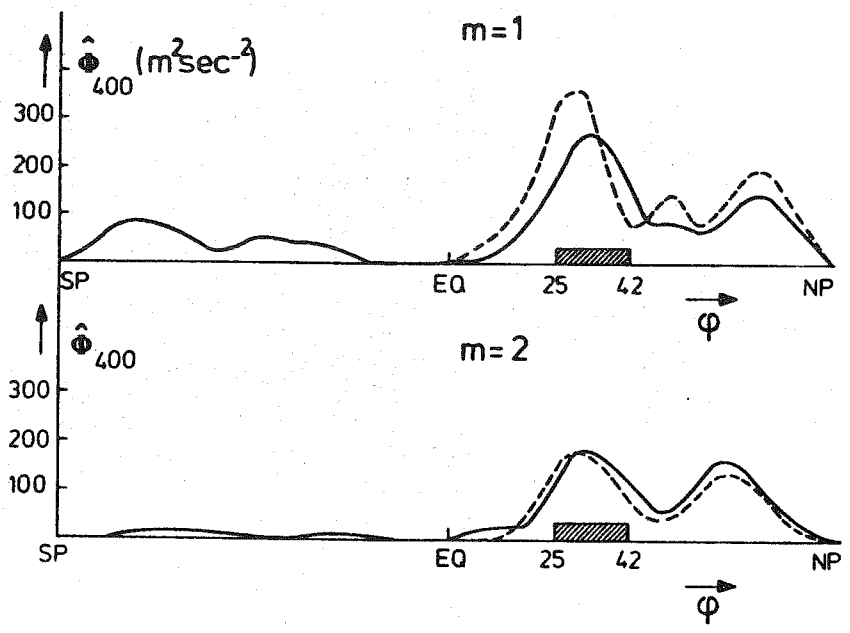

Fig. 4 Amplitude of the geopotential height response in wavenumbers 1 and 2 at 400 mb to subtropical forcing in the northern hemisphere with (solid line) and without (dashed line) MMC.

of wave energy between both hemispheres. This mechanism is important only for very long zonal waves.

In order to test the hypothesis that it is much easier to transport wave energy from the summer hemisphere to the winter hemisphere than vice versa I have done an identical experiment with the heat source in the NH (winter). The results for wavenumber 1 and 2 are shown in fig. 4. Again the dashed line gives the response when the MMC is neglected. In contrast with the previous experiment the difference between the solution with and without MMC is small for this experiment, confirming the hypothesis. So dependent on the direction of rotation the Hadley cell functions as a one way filter for stationary Rossby wave trains. This one way filtering activity may provide part of the explanation for the fact that tropically forced teleconnection patterns are so easily found in the NH winter, but less so in the NH summer (Arkin et al, 1980, Horel and Wallace, 1982).

Table 1: Un_s as a function of m^* and n^*. V_n is m sec^{-1} and β is computed at 5 degrees.

n^*	1	2	3	4	5	6	7	8	9	10
m^*										
1	182.3	50.2	18.9	6.2	-0.9	-5.6	-9.3	-12.4	-15.2	-17.7
2	114.2	44.1	20.0	9.6	3.9	0.2	2.4	-4.5	-6.2	-7.7
3	70.2	35.5	18.5	10.0	5.1	2.0	-0.2	-1.9	-3.2	-4.4
4	45.6	27.8	16.2	9.5	5.4	2.8	0.8	-0.6	-1.8	-2.8
5	31.4	21.7	13.9	8.8	5.4	3.1	1.4	0.1	-1.0	-1.8
6	22.7	17.1	11.8	7.9	5.1	3.1	1.6	0.5	-0.4	-1.2
7	17.1	13.6	10.0	7.0	4.8	3.1	1.8	0.7	-0.1	-0.8
8	13.3	11.0	8.5	6.2	4.4	2.9	1.8	0.9	0.1	-0.5
9	10.6	9.1	7.2	5.5	4.0	2.8	1.8	1.0	0.3	-0.3
10	8.7	7.5	6.2	4.8	3.6	2.6	1.7	1.0	0.4	-0.2

References

Arkin, P.A., W.Y. Chen, and E.M. Rasmussen, 1980: Fluctuations in mid and upper troposphere flow associated with the Southern Oscillation. Proceedings of the Fifth Annual Climate Diagnostic Workshop, October 22-24, 1980, US Department of Commerce, Washington D.C.

Grose, W.L. and B.J. Hoskins, 1979: On the influence of orography on large scale atmospheric flow. J. Atmos. Sci., 36, 223-245.

Horel, J.D. and J.M. Wallace, 1981: Planetary scale atmospheric phenomena associated with the interannual variability of sea surface temperature in the Equatorial Pacific. Mon. Wea. Rev., 109, 813-829.

Hoskins, B.J., A.J. Simmons and D.G. Andrews, 1977: Energy dispersion in a barotropic atmosphere. Quart. J. Roy. Met. Soc., 103, 553-567.

Oort, A.H., 1982: Global Atmospheric Circulation Statistics 1963-1973. NOAA Professional Paper, U.S. Government Printing Office, Washington D.C. (in preparation).

Opsteegh, J.D. and H.M. van den Dool, 1980: Seasonal difference in the stationary response of a linearized primitive equation model: Prospects for long range weather forecasts? J. Atmos. Sci., 37, 2169-2185.

Simmons, A.J., 1981: Tropical influences on stationary wave motion in middle and high latitudes. Technical Report of ECMWF No. 26.

Webster, P.J., 1981: Mechanisms determing the atmospheric response to sea surface temperature anomalies. J. Atmos. Sci., 38, 554-571.

PRELIMINARY RESULTS OF A CHEAP MODEL TO FORECAST THE OCEAN SURFACE TEMPERATURE ANOMALIES

Reindert Haarsma

Abstract

The changes in the spatial distribution of the monthly mean S.S.T.A. for the North Pacific and Atlantic oceans have been simulated with a mixed layer model. Of all possibly important processes we have considered here only advection of normal temperatures by anomalous winddriven currents and horizontal diffusion of the anomalies. Averaged over a year there is some skill over persistence, mainly due to the diffusion term. In one case of strong windforcing the model performed much better than persistence.

1. Introduction

Sea Surface Temperature Anomalies (S.S.T.A.) are sometimes used in steady-state models as an external forcing. With S.S.T.A. as an external forcing Opsteegh and Van den Dool (1980) have tried to simulate some of the anomalies in the monthly mean anomalous geopotential height distribution. Obviously we need a S.S.T.A. forecast to foresee the atmospheric response to external heating by the ocean.

The easiest way to make a S.S.T.A. forecast a month ahead is persistence. The autocorrelation of the S.S.T.A. distribution at a time-lag of one month ranges from 0.5 to 0.8 (Davis 1976, van den Dool, 1981). Before a more sophisticated method can be accepted it should prove to be better than persistence. In the following a simple mixed layer model will be developed in order to forecast the S.S.T.A. distributions of the Pacific and Atlantic Oceans north of 25° latitude.
Instead of testing it as a forecast model, we will first investigate its value as a simulation model.

2. The Mixed Layer

Our assumptions about the structure of the mixed layer are:

a. The mixed layer depth D is constant

The high frequency variations of D are mainly caused by the day-to-day variations in the windstress at the surface. These daily fluctuations are outside the scope of long-range weather prediction. The only variation of D that we allow for is a prescribed annual cycle. D is generally small in summer and large in winter. We account for this by chosing a constant D for each month without horizontal variation.

b. The temperature is constant in vertical direction in the mixed layer

This implies that we assume thorough mixing in the layer.

c. There is no anomalous diabatic heating at the surface: $\hat{Q} = 0$

Although the diabatic cooling in the winter months is large, the influence on the temperature of the mixed layer is small because of the great depth and thus large heat capacity of the mixed layer in these months.

d. No heat exchange at the bottom of the layer

Because of the above assumptions the model is not expected to have much potential in the summertime; in the wintertime skill can only be expected north of the tropics.

3. The Model

With these basic assumptions the thermodynamic equation for the monthly S.S.T.A. becomes an ordinary advection equation including horizontal diffusion.

$$\frac{\partial \hat{T}}{\partial t} = - \hat{\vec{U}}_H . \nabla_H T_N - \vec{U}_{H_N} . \nabla_H \hat{T} + K_H \nabla_H^2 \hat{T} \qquad (1)$$

(a) (b) (c) (d)

The time rate of change of the S.S.T.A. (a), is balanced by advection of normal Sea Surface Temperatures by anomalous currents (b), by advection of S.S.T.A. by normal currents (c) and by a horizontal diffusion term (d). We have neglected the advection of S.S.T.A. by anomalous currents. The horizontal diffusion is believed to be a crude parameterization of sub-grid state processes.

We started our investigations with processes (b) and (d). For calculations of $\hat{\vec{U}}_H$ we used only anomalous winddriven currents $\hat{\vec{U}}_H = \hat{\vec{U}}_W$, hereby neglecting the presumably small anomalous geostrophic currents. We calculated $\hat{\vec{U}}_W$ according to the expression of the total mass transport by the Ekman layer (Pedlosky 1979).

$$\hat{\vec{U}}_W = \frac{\hat{\vec{\tau}}}{\rho f D} \times \vec{k} \qquad (2)$$

D is the depth of the Ekman layer. This is the depth over which the momentum generated by the windstress is carried down. Because of our assumption of thorough mixing in the mixed layer, we will set D equal to the depth of the mixed layer. The windstress $\vec{\tau}$ is calculated from the quadratic law $\vec{\tau} = C_D |U_{10}| \vec{U}_{10}$ with $C_D = 2.10^{-3}$.

Integration of (1) gives:

$$\hat{T}(i+1) = \hat{T}(i) + \int_i^{i+1} \left[- \hat{\vec{U}}_W . \nabla_H T_N + K_H \nabla_H^2 \hat{T} \right] dt. \qquad (3)$$

where $\hat{T}(i)$ is the S.S.T.A. in month i.
Obviously the second term on the right hand side of (3) gives the extra contribution over persistence.

4. Results

We applied (3) for a grid of 25° N- 70° N and 150° E-10°E, that is the northern part of the Atlantic and Pacific oceans (fig. 1). The

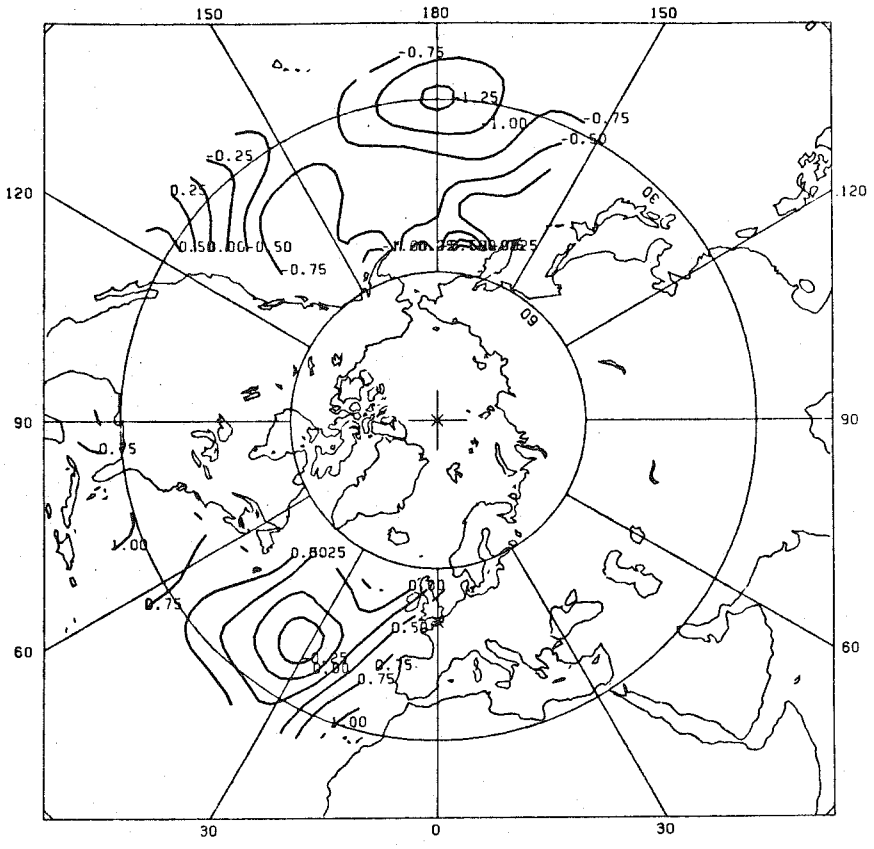

Fig. 1 : The S.S.T.A. distribution for the period half December 1977-half January 1978 (Data kindly provided by the U.K. Met. Office).

Table 1

	Pattern correlation Tendency	Pattern correlation	r.m.s. error normalised	Sign correctly predicted (percentage)
P	-	0.71	0.57	-
A	0.12	0.71	0.57	58
D	0.39	0.72	0.50	66
A + D	0.40	0.73	0.48	68

Table 1: Results of the S.S.T.A. simulation averaged over 1978. P = persistence; A = advection of normal temperature by anomalous currents; D = horizontal diffusion.

Table 2

	Pattern correlation Tendency	Pattern correlation	r.m.s. error normalised	Sign correctly predicted (percentage)
P	-	0.46	0.51	-
A	0.49	0.63	0.43	80
D	0.39	0.49	0.44	63
A + D	0.71	0.67	0.35	82

Table 2: Results of the S.S.T.A. simulation for the North Pacific, January 1978.

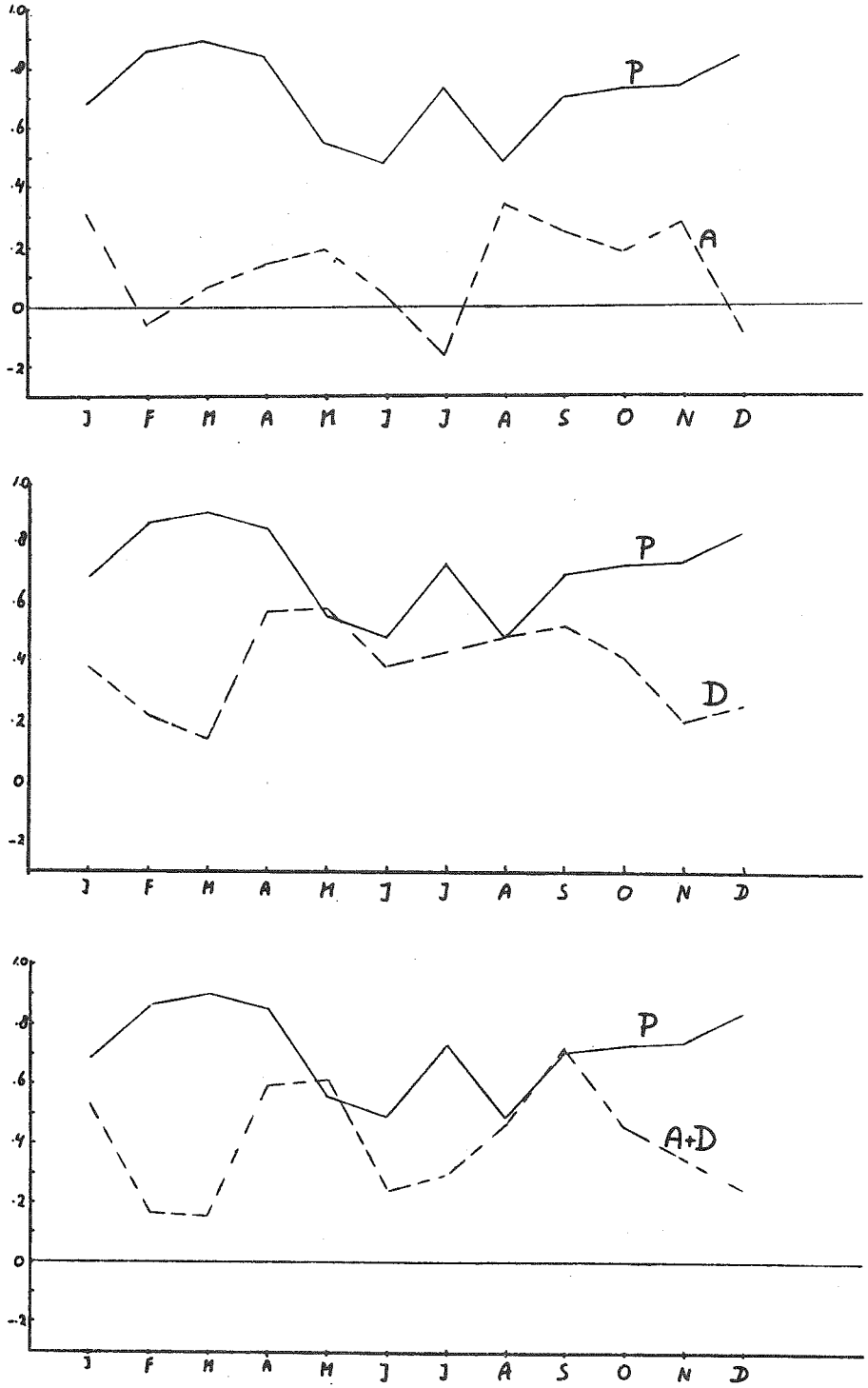

Fig. 2 : Verification of the results of some forecasting schemes.
Solid line: pattern correlation between measured S.S.T.A. and the S.S.T.A. of the foregoing month (Persistence).
Dashed line: pattern correlation of the measured change of the S.S.T.A. and the simulated changes of the S.S.T.A. (Tendencies).
a: Advection of normal temperature by anomalous currents (A).
b: Horizontal diffusion of the anomalies (D).
c: A + D.

griddistance was $\Delta\phi = \Delta\lambda = 2.5^{\circ}$. We choose the mixed layer depth D to be 100 m for the period October to March and 25 m for April to September, while $K_H = 3.10^4$ m^2/s (Adem 1970). Data of the S.S.T.A.'s were kindly provided by the UK Meteorological Office. The integration time step is 1.5 day.

In order to test the model we did a simulation experiment for the year 1978. Starting from an observed monthly mean S.S.T.A. distribution centred at the first of a month (say January), we applied the empirically obtained anomalous January mean winddriven current in order to advect T_N. Including also diffusion the integration is supposed to give a quess of the monthly mean S.S.T.A. centred at February 1.

The results were verified against observations by (1) the tendency pattern correlation coefficient (pcc) and (2) the number of correctly predicted signs in the change of the S.S.T.A.'s. The tendency pcc's for the year 1978 are shown in fig. 2, together with the pcc's of the persistence forecast. As expected a persistence forecast gives a rather high pcc (0.5-0.8), but in addition some of the observed changes could be simulated. Both the advection term and the diffusion term (fig. 2a, b) show, on the average, a positive tendency pcc. Horizontal diffusion turns out to be much more important than advection of normal temperatures by anomalous currents. That means we have mainly simulated "the back to normal" tendency of the ocean. The "back to normal" tendency of the ocean is probably not only the result of horizontal mixing, but also of diabatic heating. That is, under normal atmospheric conditions a cold spot will be heated through diabatic heating, until it has reached its normal value. The latter process can be better represented by a vertical exchange coefficient between atmosphere and ocean, or a logarithmic time decay of the anomalies, because horizontal diffusion takes only horizontal gradients into account and not vertical gradients between ocean and atmosphere. We will include this process in the near future. However, we found for the month January 1978, in which case there was a particularly strong negative sea level pressure anomaly over the North Pacific ocean, that advection was more important than diffusion. In that case the tendency pcc for the Pacific ocean for advection and diffusion were 0.49 and 0.39 respectively.

There appears to be a kind of anti-phase between the pcc of the persistence and the pcc of the tendency (see fig. 2), which indicates that the model seems to be able to capture the most important changes in

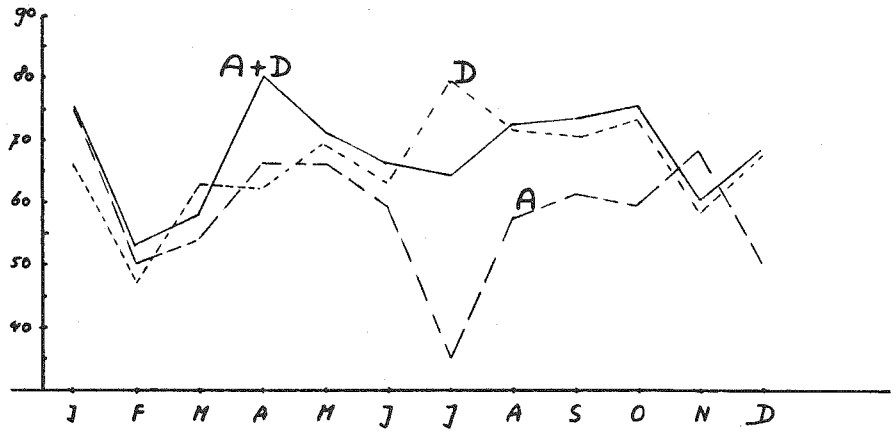

Fig. 3 : Percentage of points for which the sign of the anomaly change has been simulated correctly.
Advection: A (long dashes); diffusion: D (short dashes); advection + diffusion: A + D (solid line).

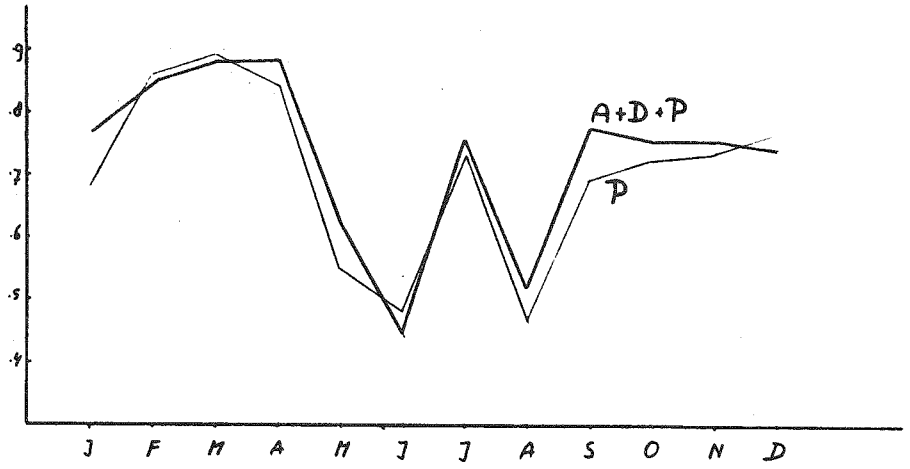

Fig. 4 : Pattern correlations: Thin line: persistence (P).
Heavy line: simulation (A + D + P).

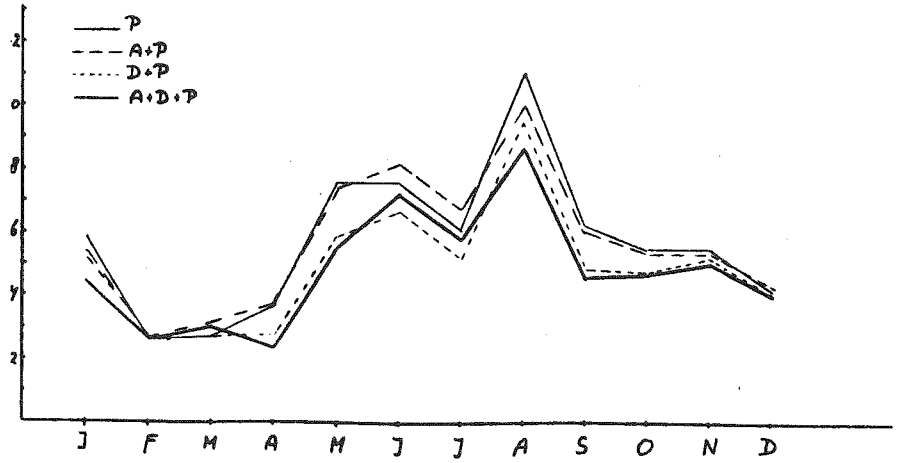

Fig. 5 : r.m.s. error of S.S.T.A. simulations normalized by the r.m.s. of the observed S.S.T.A.
Thin solid line: P: long dashed line: A + P.
Short dashed line: D + P; heavy dashed line: A + D + P.

the S.S.T.A. distribution, if there are any. The results have also been, verified by counting the percentage of points for which the sign of the anomaly changes have been simulated correct (see fig. 3). The general picture is the same as the one revealed by fig. 2.

In terms of the pcc of the simulated S.S.T.A. distribution with the measured S.S.T.A. distribution (Fig. 4), there seems to be hardly any improvement above persistence, also in the months when persistence is low. This reflects the fact that in any case the tendency pcc's, although positive, are small compared to the pcc's of the persistence. The r.m.s. error normalized by the r.m.s. error of a climatological simulation is shown in fig. 5. A value of 1.0 indicates a simulation that has an r.m.s. error equal to that of a climatological simulation (anomaly predicted to vanish). Here the improvement stands out more clearly, the most important contribution here is again from the diffusion term. The results over a year are given in table 1.

In his study of the time evolution of the S.S.T.A. Haney (1978) found that advection of normal temperatures by anomalous currents is the most important process in creating S.S.T.A.'s. He considered the winter of 76-77 for the North Pacific and simulated a period of 4 months, from September to January. In this period, especially in January there was a large negative s.l.p. anomaly over the Pacific with a minimum of -20 mb. In our case the situation over the Pacific in January 1978, with a minimum of -15 mb, more or less resembles the situation in the study of Haney. Table 2 shows clearly that in this case the advection is dominating. When averaged over a year our results come close to those of Adem (1970, 1975).

5. Conclusion

Averaged over a year there is some skill above persistence which comes mainly from the horizontal diffusion of the S.S.T.A.'s. In some cases with large wind induced currents the advection of normal temperatures by anomalous currents may be an important mechanism.

6. Prospect

In the near future the influence of the other processes will be investigated. We may think of processes such as advection of anomalous temperatures by normal currents and upwelling or the inclusion of a logarithmic time decay to parameterize the effect of diabatic heating. We can also expect that simulation over a season instead of a month gives a better skill above persistence.

References

Adem, J., 1970. On the prediction of mean monthly ocean temperatures. Tellus 27, 410-430.

Adem, J., 1975. Numerical-Thermodynamical prediction of mean monthly ocean temperatures. Tellus 27, 541-551.

Dool, H.M. van den, and Nap, J.L., 1981. An explanation of persistence in monthly mean temperatures in the Netherlands. Tellus 33, 123-131.

Haney, R.L., et al, 1978. A dynamical-numerical study of the formation and evolution of large-scale ocean anomalies. J. Phys. Oceanogr. 8, 952-969.

Haney, R.L., 1980. A numerical case study of the development of large-scale thermal anomalies in the central north Pacific ocean. J. Phys. Oceangr. 10, 541-556.

Opsteegh, J.D. and van den Dool, H.M., 1980. Seasonal differences in the stationary response of a linearized primitive equation model prospects for long-range weather forecasting. J. Atmos. Sci. 37, 2169-2185.

Pedlosky, 1979. Geophysical Fluid Dynamics 624 pp. Springer-Verlag, New York.

NONLINEAR OROGRAPHIC EFFECTS AND BIFURCATION PROPERTIES OF LOW ORDER MODELS

Erland Källén

The bifurcation properties of low order models with orographic and thermal or direct vorticity forcing are reviewed. The low order model results that multiple equilibria develop as a result of a sufficiently strong orographic forcing and that a suitably positioned wave vorticity forcing can enhance this bifurcation mechanism are verified with a high resolution, spectral model. The effects of baroclinic eddies in connection with orographic forcing is also discussed.

1. INTRODUCTION

In recent years there has been a renewed interest in the study of low-order systems to gain some insight into nonlinear mechanisms present in the atmosphere. The basic procedure used when studying a low-order system is to expand the space dependent quantities into a series of orthogonal functions and to truncate this expansion by just retaining a few components. Each component is thought of as representing a certain scale of motion and, by inserting the truncated expansion into an equation of motion, one can study the nonlinear interactions between the scales considered. One thus neglects all interactions with spectral components not taken into account. This is of course a serious limitation of low-order systems, but it is nevertheless believed that a study of such systems is one way of getting an insight into the nonlinear mechanisms present in the atmosphere. To verify results found with a low-order model one should also perform experiments with a high-resolution, fully nonlinear model. These experiments must, however, be guided by the qualitative properties of the low-order systems.

To study the effect of orographic forcing on the nonlinear energy transfer between the larger scales of motion, Charney and DeVore (1979) (hereafter called CdV) extended Lorenz's (1960) barotropic β-plane model to include orographic forcing. With a low-order system they showed that for a given forcing it was possible for the flow to arrange itself in several equilibrium states, some stable and some unstable. The multiplicity of equilibrium states is associated with the resonance occurring when the Rossby wave, generated by the zonal flow over the orography, becomes stationary. Through the nonlinear interaction between the zonal flow and the wave components of the flow and due to the orography, the components can arrange themselves in two stable equilibria, one close to resonance with a large amplitude wave and a weak zonal flow, the other with a strong zonal flow and a weaker wave component. The large amplitude wave flow may be associated with a blocked flow in the atmosphere.

This result was first derived for a β-plane, channel model with reflecting side walls, but later studies by Davey (1980, 1981) and Källén (1981) have shown that the same type of mechanism can be found with an annular or a spherical geometry. Trevisan and Buzzi (1980) also showed the same phenomenon using a different expansion method on a β-plane geometry.

The basic equation used for the models of all these studies is the quasi-geostrophic, barotropic vorticity equation with linear dissipation, a Newtonian type of vorticity forcing and orographic forcing. In a non-dimensional form this equation is

$$\frac{\partial \zeta}{\partial t} = J(\zeta+f+h,\psi) + \varepsilon\ (\zeta_E-\zeta) \qquad (1)$$

where ζ is the non-dimensional vorticity, f is the planetary vorticity, ζ_E the vorticity forcing, ψ the stream function and h is a parameter related to the orographic effects. The non-dimensional time is given by t and ε is the dissipation rate. The orographic forcing may be introduced as a forced vertical velocity of the lower boundary in an equivalent barotropic model, in which case h is related to a dimensional mountain height m via

$$h = C \cdot \frac{m}{H} \tag{2}$$

where H is the scale height of the equivalent barotropic atmosphere and C is a constant which depends on the equivalent barotropic assumption. For normal atmospheric conditions the constant C is approximately equal to one. For details of the derivation of Eq.(1) see Källén (1981).

The nonlinearity of the model is contained in the term involving the Jacobian ($J(\zeta+ f+h,\psi)$), and one way of investigating the nonlinear properties of this model is to expand the space dependent variables in a series of orthogonal functions, $F_\gamma(\underline{x})$, where $\underline{x}$ is the space vector. It is convenient to choose the F_γ's to be eigenfunctions of the Laplacian operator, because $\zeta \hat{=} \nabla^2\psi$. The exact functional form of the F_γ's of course depends on the geometry of the model and the boundary conditions.

The variables to be expanded are the vorticity (also gives the streamfunction), vorticity forcing and the orography. The expansion may be written

$$\begin{pmatrix} \zeta \\ \zeta_E \\ h \end{pmatrix} = \sum_\gamma \begin{pmatrix} \zeta_\gamma(t) \\ \zeta_{E,\gamma} \\ h_\gamma \end{pmatrix} F_\gamma(\underline{x}) \tag{3}$$

For a β-plane, channel model trigonometric functions can be used and $F_{m,n}(x,y) = e^{i(mx+ny)}$, x and y being the Cartesian coordinates (CdV). In an annular geometry, Bessel functions are involved (see Davey, 1981) and on the sphere the F_γ's may be written

$$F_{m,n}(\mu,\lambda) = P_n^m(\mu)\, e^{im\lambda} \tag{4}$$

where μ is the sine of latitude (ϕ), λ is the longitude and $P_n^m(\mu)$ are associated Legendre functions. Most of the results discussed in this paper will refer to a spherical geometry as in Källen (1981) and thus the expansion functions given by Eq.(4) are the appropriate ones.

A low-order model may be formulated by inserting the expansion Eq.(3) in the model Eq.(1) and truncating the expansion at a very low order just leaving a few components to describe the fluid motion. Each component may be thought of as describing a certain scale of motion and only the nonlinear interactions between the scales involved in the low order system are taken into account.

To study the effects of the orography on the interaction between the waves and the mean zonal flow, at least one purely zonal component and two wave components have to be included. The mathematical structure of such a minimal system is independent of the geometry and multiple equilibrium states may be found even in such a simple model, as first pointed out by CdV. When additional components are included the geometry will affect the structure of the equations, but the basic mechanism for the formation of multiple equilibrium states still remains. In the following section a minimal system will be analyzed, following the basic idea of CdV. Section 3 will deal with a combination of orographic and direct wave vorticity forcing as discussed by Källén (1981). The direct wave vorticity forcing is thought to represent the time mean effect of the small scale baroclinic eddies on the long waves in the atmosphere. In Section 4 a verification of some of the drastic assumptions made when deal with low-order models will be made and finally in Section 5 a review will be made of studies which have dealt with baroclinic effects in combination with orographic forcing.

2. WAVE-MEAN FLOW INTERACTIONS VIA THE OROGRAPHY

The simplest possible low-order model in which one may investigate the non-linear coupling between the zonal mean flow and the eddies through the effect of the orography, is a model which involves one component describing a purely zonal flow and two components describing the phase and amplitude of a wave. On the sphere the streamfunction may thus be written

$$\psi = - u_o(t)\ P_1(\mu) + (x_1(t)\ \cos \ell\lambda + y_1(t)\ \sin \ell\lambda)\ P_n^{\ell}(\mu)$$

where u_o, x_1 and y_1 are the time dependent amplitudes of each flow component. To drive the zonal flow, a vorticity forcing is introduced in the $P_1(\mu)$ component with an amplitude, u_{oE}. The orography is assumed to be present with an amplitude, h_1, in the $\cos(\ell\lambda)P_n^{\ell}(\mu)$ component. Inserting these expansions of the stream function, vorticity forcing and the orography into the barotropic

vorticity equation (1), a set of three ordinary differential equations governing the time evolution of the model is obtained,

$$\begin{aligned}
\dot{u}_o &= h_1\,\delta_1\,y_1 && + \varepsilon(u_{oE} - u_o)\\
\dot{x}_1 &= && (\beta - \alpha\,u_o)y_1 \quad - \varepsilon\,x_1\\
\dot{y}_1 &= -\,h_1\,\delta_2\,u_o \quad - (\beta - \alpha\,u_o)x_1 && - \varepsilon\,y_1
\end{aligned} \tag{5}$$

The coefficients appearing in (5) are defined

$$\alpha = \sqrt{3}\,\ell\,\left[1-2/n(n+1)\right]\ ,\ \beta = \frac{2\ell}{n(n+1)},\ \delta_1 = \frac{\sqrt{3}}{4}\,\ell\ ,\ \delta_2 = \frac{\sqrt{3}\ell}{n(n+1)}$$

These expressions for the coefficients have been derived for a spherical geometry, but in fact the structure of the equations is exactly the same for a β-plane or an annular geometry, the only difference between the different geometries lie in the expressions for and values of the coefficients. The results shown in this section, may thus equally well be applied to the other types of geometry.

To investigate the mathematical properties of the nonlinear system of equations (5), we first determine the steady-state values of u_o, x_1 and y_1. Setting the time derivatives equal to zero and solving the resulting system of equations for one of the steady-state amplitudes (u_o), we arrive at the following equation in $\bar{u}_o$ (hereafter an overbar will denote a steady-state amplitude)

$$\bar{u}_o^{\,3} - \bar{u}_o^{\,2}\,(u_{oE} + \frac{2\beta}{\alpha}) + \frac{\bar{u}_o}{\alpha^2}\,\left[\delta_1\,\delta_2\,h_1^{\,2} + \varepsilon^2 + \beta^2 + 2\beta u_{oE}\right] = u_{oE}\,\frac{(\varepsilon^2+\beta^2)}{\alpha^2} \tag{6}$$

which also may be written

$$u_{oE} = \frac{\delta_1\,\delta_2\,h_1^{\,2}\,\bar{u}_o}{\varepsilon^2 + (\beta-\alpha\bar{u}_o)^2} + \bar{u}_o \tag{7}$$

The polynomial form (6) of the steady-state equation shows that we can at the most have three steady-states for certain values of the forcing parameters.

The other form of the steady-state equation, (7), allows us to investigate by graphical methods how the number of steady-states varies with the forcing parameters. Note that on the left hand side of (7), u_{oE} is a velocity. This velocity is the purely linear response of the u_o-component when there is no orography.

The example chosen to illustrate Eq. (7) is one in which $\ell=3$ and $n=4$. This implies an orography with a zonal wavenumber three and a maximum in mid-latitudes. Fig. 1 is a plot of the curves given by Eq. (7) for some values of h_1. Both axes are given in non-dimensional and dimensional units. The dimensional units are m/s and correspond to the windspeed of the u_o component at 45^o latitude.

The curve in Fig. 1 for $h_1 = 0$ is a straight line and for increasing values of h_1 we obtain a family of curves, some having a section with a negative slope. As each point on the curves represents a steady-state of the system given by Eq.5, a negatively sloping section of a curve implies that within a certain forcing parameter (u_{oE}) interval it is possible to have three steady-states. Taking as an example the curve for $h_1 = 0.100$ it can be seen from Fig. 1 that in the interval $1.06 < u_{oE} < 1.27$ three steady-states exist. The stability properties of each steady-state are found by linearising Eq. (5) around each steady-state, and finding the eigenvalues of the linearized equations. An investigation of this kind gives stability properties as indicated by full (stable) and dashed (unstable) lines in Fig. 1. In Fig. 1 it may also be seen that the bifurcation from one to three steady-states occurs for a value of h_1 somewhere between 0.050 and 0.075.

The possibility of having two stable equilibrium states for constant values of the forcing parameters is due to the nonlinear coupling between the zonal flow and the waves. The coupling by itself, however, without the effect of the orography, does not give rise to multiple steady-states in Eq.(5). It is the influence of the orography which is crucial in creating an instability which gives the possibility of having multiple steady-states. CdV called this a form drag instability, where the form drag refers to the effect of the orography in this simple model.

One of the stable steady-states is close to a resonant flow configuration, and in this steady-state the wave component has a high amplitude. The phase

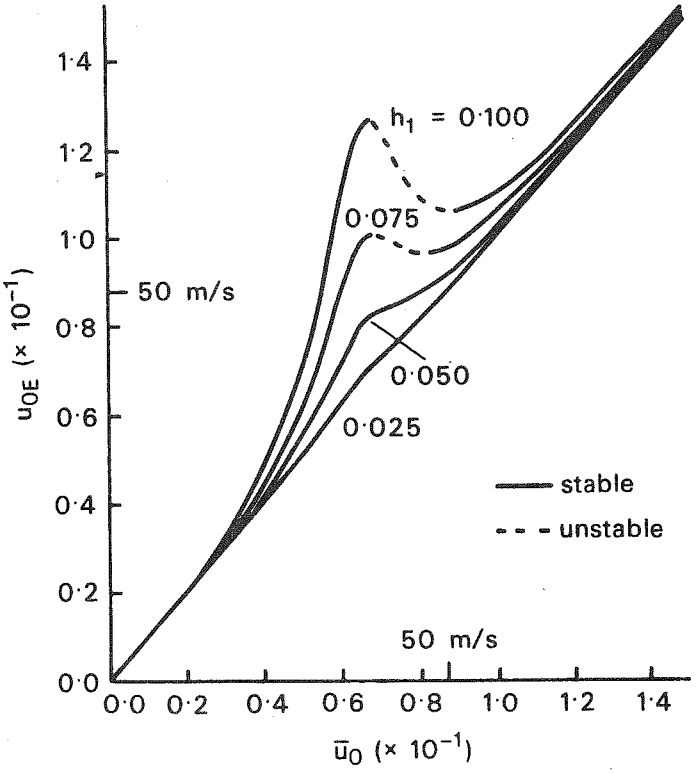

Fig. 1 Steady-state curves for the low order model of section 2 with different values of the orographic parameter. The horizontal axis gives the amplitude of the $\bar{u}_o$-component, both in non-dimensional and dimensional units. On the vertical axis the forcing is also given in both units. The dimensional units are the flow velocity at 45° latitude. Each curve corresponds to a certain value of the orographic parameter, h_1, and a numerical evaluation of the eigenvalues shows stability properties as indicated by full (stable) and dashed (unstable) lines. For further explanations, see text.
Parameter values: $\varepsilon = 0.06$, $\ell = 3$, $n_1 = 4$.

of the wave is such that there is a high drag across the orographic ridges and thus energy is transferred from the zonal forcing, via the effect of the orography, to the wave components of the flow. In Fig. 1 this type of a steady-state falls on the left hand part of the diagram where the response in the zonal component (u_o) is much less than the forcing.

The steady-states on the right hand side of the unstable region have a more intense zonal flow and a less marked wave component. In these steady-states the orographic drag is much lower, both due to the lower amplitude of the wave component and a different phase of the wave.

The steady-state with a high wave amplitude may be associated with a blocked flow in the atmosphere. The wave ridge occurs downstream of the orographic ridge, and the persistence of blocking ridges in the atmosphere may be due to the stable wave-mean flow interaction described by this simple model. The model also predicts that there may be another stable flow configuration without a high amplitude wave, but a much more pronounced zonal flow. Which one of these steady-states the flow settles into is crucially dependent on the initial state of the flow. CdV offered this feature as a possible explanation for the observed variability in the frequency of the occurrence of blocked flows.

3. A COMBINATION OF WAVE VORTICITY AND OROGRAPHIC FORCING

In the model described in the previous section, the waves of the flow are only due to the interaction between the zonal flow and the orography. In the atmosphere there are numerous other processes which generate waves and in mid-latitudes the most important one is the baroclinic instability process. Baroclinic waves have a characteristic wavelength which is shorter than the scales involved in the low order models of the previously mentioned studies, but seen as an effect on the time mean flow the energy generated by baroclinically unstable waves on the shorter scales is transported in the spectrum through nonlinear processes and thus also exports energy to the longer waves (Saltzmann, 1970 and Steinberg et al., 1971). In a barotropic model it is impossible to describe these baroclinic effects explicitly, but one may be able to take the long wave effect into account by introducing a wave vorticity forcing in the same components as the orography. The wave vorticity forcing should thus be seen as the time mean effect of cyclone waves rather than a direct diabatic heating.

A wave vorticity forcing can easily be introduced into the low order model of the previous section by adding εx_{1E} and εy_{1E} to the right hand sides of the equations for $\dot{x}_1$ and $\dot{y}_1$ of Eq.(5). The steady-states may be analyzed in the same way by writing the steady-state equation in terms of the zonal forcing (u_{oE}) as a function of the zonal response (u_o) with the orography (h_1), the amplitude ($\sqrt{x_{1E}^2 + y_{1E}^2}$) and the phase ($\tan^{-1}\frac{y_{1E}}{x_{1E}}$) of the wave vorticity forcing as parameters. In Källén (1981) this was done, but with a slightly more complicated model. Two extra wavecomponents and one extra zonal component was included to take into account some of the interactions with unforced parts of the spectrum. It is still possible to solve for the steady-states analytically in such a model according to the procedure given in Källén (1981). We will not go into any detail here regarding the solution method, but only display some of the results.

A plot of the steady-states of the system is given in Fig. 2. On the horizontal axis the steady-state response is given in terms of the amplitude of a sheared zonal component, z. The vertical axis gives the zonal momentum forcing, u_{oE}.

The orographic forcing is fixed at a value of 0.05 while the wave vorticity forcing has a varying amplitude, but the phase in relation to the orography is fixed. Multiple steady-states of the system are identified in the figure by the condition that a horizontal line should have multiple intersections with one of the steady-state curves. The forcing parameters are in a range where multiple steady states are just possible, i.e. close to the first bifurcation point. For smaller values of the forcing parameters the non-linear system behaves quasi-linearly, with just one steady state for a certain value of the forcing parameters. By linearizing the system around a steady-state and computing the eigenvalues of the matrix governing the linearized motion around each of the steady-states, stability properties are found as indicated in Fig.2. It may be noted that no Hopf-bifurcations (see Marsden and McCracken, 1979) indicating the existence of limit-cycles around the steady-states have been found in this low order model for reasonable values of the forcing parameters.

For the curve marked I in Fig. 2 the wave vorticity forcing is set to zero and the only forcing of the model is in the orography and the zonal momentum. For the orography height chosen in Fig. 2 there is only one, stable steady-state

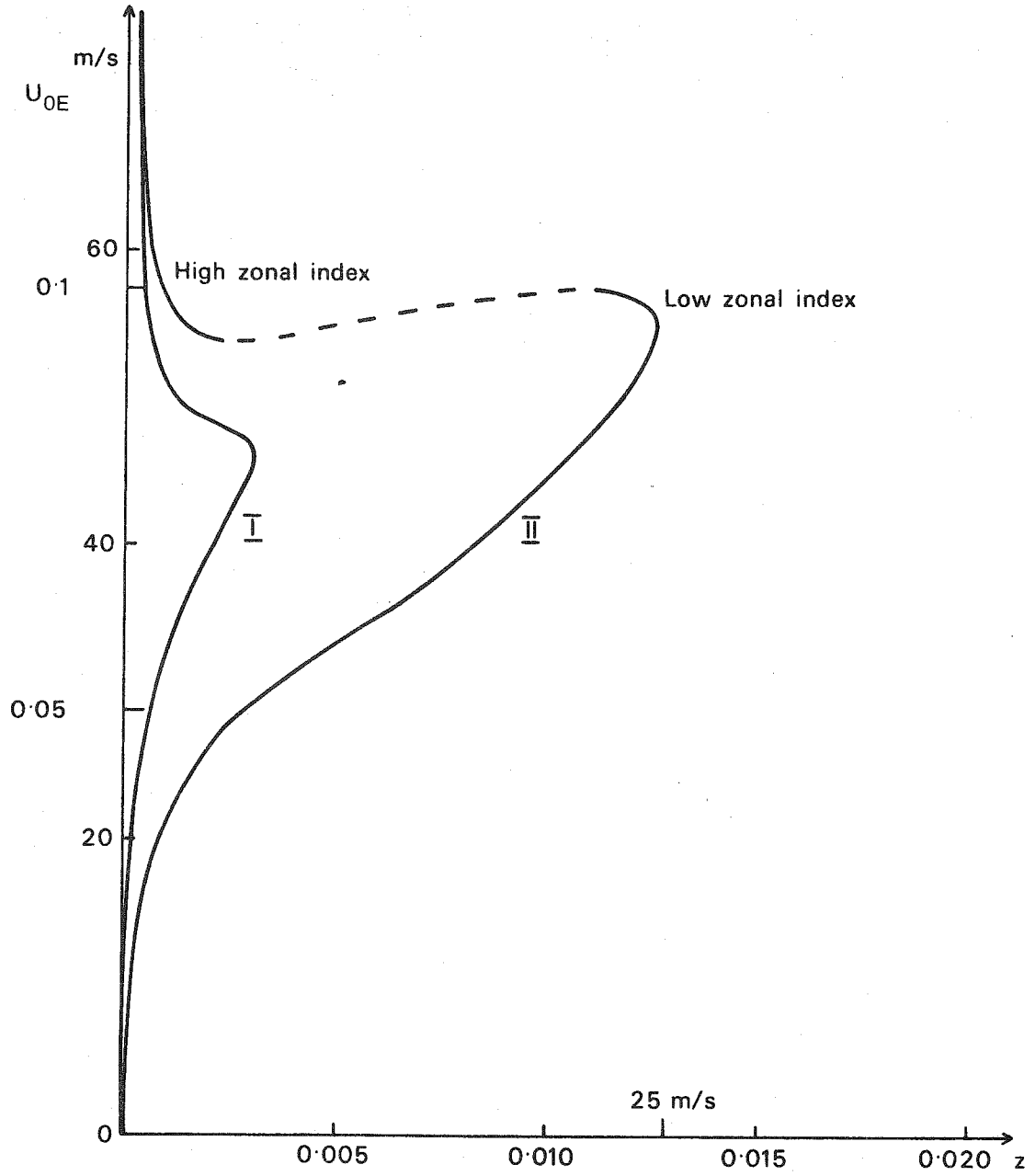

Fig. 2 Steady-state curves for the low order model of section 3. The abscissa gives the response in terms of the amplitude of one of the zonal components (z), the ordinate gives the strength of the zonal forcing (u_{oE}). Both axes are given in dimensional and non-dimensional units, the dimensional units being taken as the zonal average at 45° latitude. The height of the orography, h_1 = 0.05 and the dissipation rate, ε = 0.06. For curve I there is no wave vorticity forcing while for curve II there is a wave vorticity forcing in the same component as the orography (ℓ=3, n_1=4). The amplitude of the wave forcing of curve II is x_{1E}= 0., y_{1E}=-0.015 which corresponds to 20 m/s in terms of a zonally averaged absolute value of the meridional wind at 45° latitude and a phase angle of -90°. Stability properties as indicated by dashed (unstable) and full (stable) lines.

for all values of the zonal momentum forcing. For higher values of the orographic parameter multiple steady-states are possible within certain ranges of values of the zonal momentum forcing. Fur further details of this, see Källén (1981). Another way of obtaining a region of multiple equilibria is to include vorticity forcing in one of the wave components and this is shown with steady state curve II in Fig. 2. The phase of the wave vorticity forcing is -90^{o}, i.e. positive (cyclonic) vorticity forcing on the leeward side of the highs in the orography. In Källén 1981 it was shown that this phase angle is the most favourable one for bifurcations to occur. The characteristics of the steady-states within the region of multiple equilibria can be found in the example displayed in Fig. 3. The steady-states on the left hand, upper branch of curve II in Fig. 2 have a marked zonal flow and a rather weak wave component as the top flow of Fig. 3. The steady-states on the right-hand branch, on the other hand, have a much stronger wave component and a weaker zonal flow as the bottom flow of Fig. 3. These latter steady-states can be associated with low index atmospheric circulations, i.e. blocking periods, while the steady-states on the left hand branch have the characteristics of a high index, zonal type of circulation. Examining the energetics of these two solution types it was found in Källén (1981) that in the zonal steady-state the orographic influence on the flow was much weaker than in the blocked state. In the blocked state the orography acted to transform zonal kinetic energy into wave kinetic energy in a much more intense way than in the zonal state. Furthermore, the efficiency of the flow in picking up energy from the wave vorticity forcing was markedly different. In the blocked flow the phase difference between the forced wave and the wave forcing is very small, thus giving a high amplitude response. In the zonal steady state the trough on the leeward side of the orography is further downstream from the orographic high than in the blocked case, and the response amplitude is thus lower. The unstable steady-states on the dashed part of curve II have properties somewhere intermediate between the two stable branch steady-states. The unstable steady-states are, of course, not very interesting. Because of their instability the flow will never settle into them.

It has thus been demonstrated that a combination of orographic and wave vorticity forcing can give rise to multiple equilibrium states, even when the separate effects of the two types of forcing do not show this type of behaviour. Only a wave vorticity forcing in this model does not give rise to more than one equilibrium state. The orography can be seen to act as a triggering mechanism, directing the basically vorticity forced flow into one or the other of the stable equilibria.

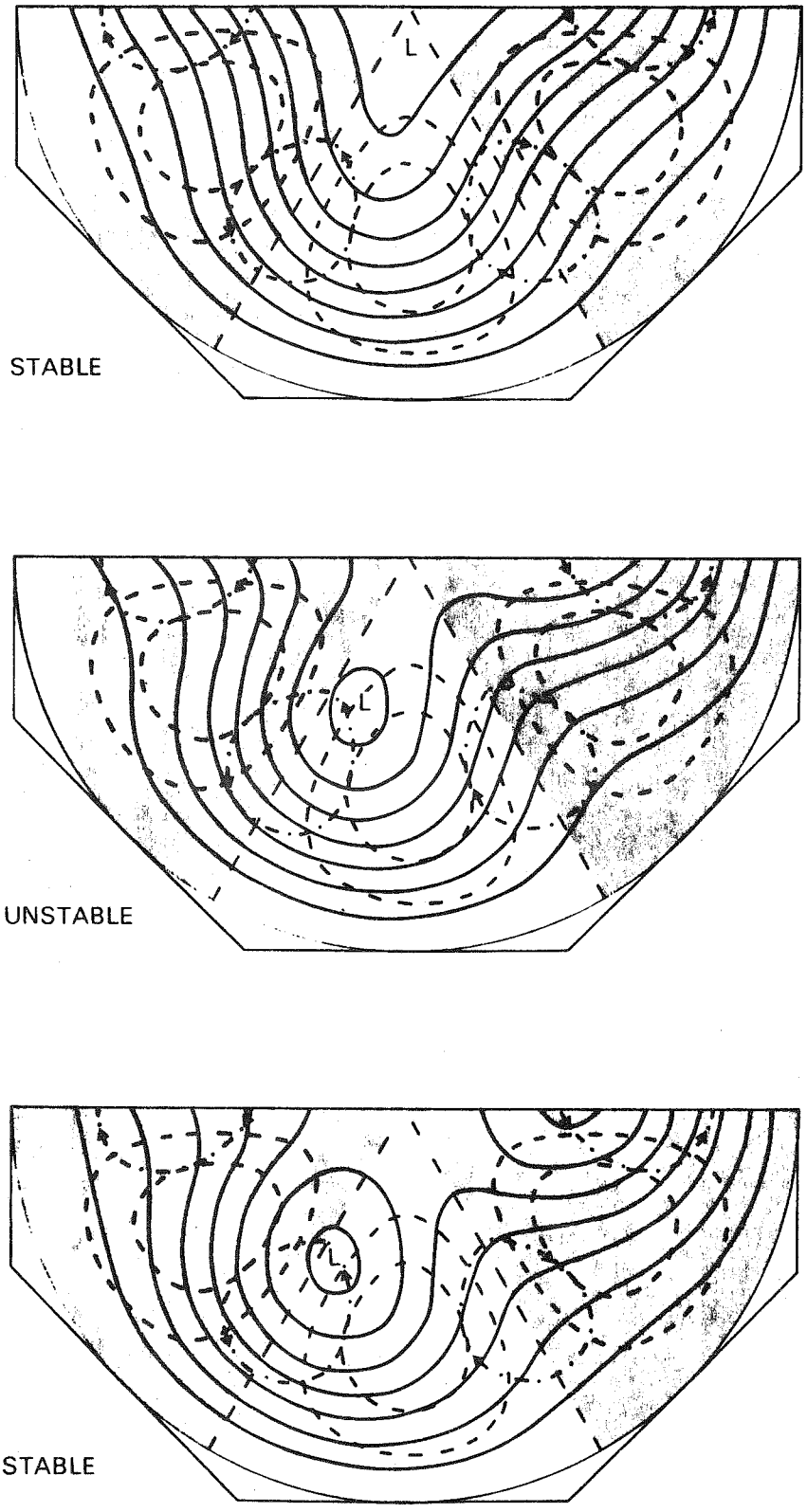

Fig. 3 Examples of stream function fields for three steady-states within the region of possible multiple equilibria of Fig. 2 (curve II). Full lines are isolines of the streamfunction while the dashed lines are isolines for the orography. Over the hatched area the orography is above its mean value ("land areas") while otherwise it is below its mean value ("ocean area"). Dash-dotted curves with arrows showing direction of circulation indicate regions with maximum cyclonic and anti-cyclonic wave vorticity forcing.

A serious shortcoming of a severely truncated low order system is of course the lack of interaction between waves of all scales. Only a few scales of motion are taken into account and the interactions with other scales are either neglected completely or included via a bulk momentum forcing. To investigate whether the bifurcation mechanism found in a low order model is sensitive to the number of waves present in the model, the results should be verified with a high resolution model. CdV showed that the multiple equilibria in their 3-plane channel model could also be found in a model with an increased resolution, while (Davey 1981) pointed out that it is possible to find the multiple equilibria in a high resolution model but they do not obtain as easily as in a low order model.

To verify the results of Källén (1981) for a spherical geometry, experiments have been performed with a high resolution, quasi-geostrophic, spectral, barotropic model (Källén, 1982). Forcing is introduced in exactly the same components as in the low-order model and the model is integrated in time to find the steady-state(s). For reasons of economy, most of the experiments were done with a T21 truncation ($k \leq 21$ and $n \leq 21$ in the Legendre ($P_n^k(\mu)$) representation). However, some integrations done with a T42 truncation showed no significant differences to the T21 experiments.

To find multiple stable steady-states the time integrations are set up in the following manner. Initially the forcing is held constant for a time period of twenty days. The model, starting from a state of rest, is allowed this time to find a steady-state. After the model has settled into a steady-state the zonal momentum forcing is slowly increased or decreased in time. The time scale of this slow increase or decrease is chosen to be significantly slower than the dissipation time scale of the model (the forcing is doubled or halved in 100 days while the dissipation time scale is around 2.5 days). In this way it is hoped that the model stays reasonably close to a stable steady-state all of the time. If, however, a bifurcation of the type pictured in Fig. 2 occurs, the model has to make a sudden jump from one stable branch of the steady-state curve to the other when a critical value in the zonal forcing is passed. In a time plot of some of the spectral coefficients this shows up as a sudden change of the amplitude and perhaps some damped oscillations when the model settles into a steady-state on the other branch.

The numerical experiments with the high resolution spectral model strongly support the results derived from the low order model of Källén (1981). There

are, however, some aspects of the low order model behaviour which are not verified by the high resolution experiments. One such behaviour is the bifurcation obtained in a low order model in the absence of orography. With a low order model it is possible to find multiple equilibria with only vorticity forcing (Wiin-Nielsen, 1979) on the longer waves. Experiments with the high resolution model have not shown this feature, even for very large values of the forcing parameters. The model behaves perfectly linearly when only momentum forcing is applied, the response to the forcing being purely in the forced components. For shorter waves this is no longer true. Hoskins (1973) has demonstrated that for zonal wavenumbers larger than five a nonlinear instability develops which is mainly due to wave-wave interactions. For the longer waves the Coriolis effect acts as a stabilizing factor which prevents this type of nonlinear instability. With orography present it thus seems that a new type of instability develops as first pointed out by CdV. An intuitive reasoning which points to a possible reason for this property of the orography can be given as follows. The governing equation of the model at a steady-state may be written,

$$J(\zeta,\psi) + J(h,\psi) - 2\frac{\partial\psi}{\partial\lambda} + \varepsilon(\zeta_E - \zeta) = 0 \qquad (8)$$

If $h=0$ (no orographic forcing) and $\zeta_E \neq 0$ it is possible to have a steady-state where the response is in the same component as the forcing and the nonlinear term $J(\zeta,\psi)$ is zero. As mentioned above, numerical experiments with reasonable values of the vorticity forcing on the longer waves have shown that such a steady-state is stable. Equation (8) is in this case linear. This also holds if the wave vorticity forcing is applied at several low wave numbers simultaneously. If an orographic forcing is introduced ($h \neq 0$) the term $J(h,\psi)$ forces energy introduced via the vorticity forcing ζ_E at a certain wavenumber to spread over the whole spectrum. It is this energy spread combined with a suitable vorticity forcing that appears to give rise to a nonlinear instability and the bifurcation leading to multiple steady-states. The experiments with the high resolution model have also confirmed that a suitably positioned vorticity forcing in a wave component enhances this bifurcation mechanism.

Another aspect of using one Fourier component to represent the orography which can be tested with a high resolution model, is to see whether multiple equilibria can be obtained with an isolated orographic ridge. Davey (1981) did an experiment of this type with an annular geometry and within a certain, rather narrow, range of the forcing parameter space, he obtained multiple steady-states. These states have the same characteristics as the blocked and zonal states

described previously. Davey (1981) also pointed out that the waves generated in the high amplitude wave state on the leeward side of the orographic ridge are almost totally dissipated when the flow reaches the upwind side of the orographic ridge. The high amplitude wave state is thus not associated with a global resonance, the phenomenon is rather local in character. The resonance occurring is instead of the type where the Rossby wave generated by the orography has a phase speed which is such that it is stationary in the zonal flow which results.

5. BAROCLINIC LOW-ORDER MODELS

To extend the original findings of CdV to a baroclinic model, Charney and Strauss (1980) developed a two-layer, channel model with the same low order truncation as the one used by CdV. This baroclinic model contained the same type of orographic instability as found in the barotropic case for moderately large values of the meridional temperature gradient forcing. For larger values of the driving force several other steady-states developed, but these new steady-states appeared to be more coupled to baroclinically unstable waves than to the basic orographic instability.

In a recent investigation, Reinhold (1981) has examined the properties of a further extended version of the Charney and Strauss (1980) model. Reinhold included a second set of modes in addition to the long wave ones used by Charney and Strauss, and this second set has a length scale close to the wavelength for maximum baroclinic instability. Through time integrations and analytical work on simplified versions of the model, he investigates the non-linear feedback between baroclinic eddies and the orographically forced long waves. Analytic investigations show that the model has up to five steady-states for reasonable values of the forcing parameters, but all of these are unstable due to the existence of short-scale baroclinic waves. In a long time integration he nevertheless finds that the model has certain preferred modes of circulation, or weather regimes, which resemble the purely orographically induced multiple equilibria. The model stays in either of these two regimes for extended periods of time, while the transition from one regime to the other is comparatively rapid. Neither the fluctuations within each regime nor the transition from one regime to the other appears to be periodic, but the two different regimes are well separated and appear to be statistically significant. A change of the zonal forcing in the model changes the characteristics of the regimes, but for a wide range of the zonal forcing parameter the regime type of behaviour is maintained.

From the five steady states mentioned above it is possible to identify the two which correspond to the original multiple equilibria found by CdV. The regime averages, however, are not very close to either of these although they fall within the same region. Parameterizing the effect of the small scale eddies on the long waves via an assumption that the total energy of the eddies is a certain fraction of the total energy of the zonal flow, Reinhold shows that multiple equilibria can be found which correspond very well to the regime averages. This type of parameterization is analogous to the zonally asymmetric momentum forcing, which was used by Källén (1981) to represent the effect of the baroclinic eddies.

The inclusion of the short scale baroclinic eddies thus has two effects on the model flow, it helps to maintain the orographically induced multiple steady states or flow regimes and it acts to transfer the flow from one regime to the other. Without the orography Reinhold's model does not have any characteristic circulation regimes and without the short scale eddies it cannot transfer between the multiple steady states established through the effect of the orography.

REFERENCES

Charney, J.G. and De Vore J.G. 1979. Multiple flow equilibria in the atmosphere and blocking. J.Atmos.Sci., 36, 1205-1216.

Charney, J.G. and Strauss, D.M. 1980. Form-drag instability, multiple equilibria and propagating planetary waves in baroclinic, orographically forced, planetary wave systems. J. Atmos. Sci., 37, 1157-1176.

Davey, M.K. 1980. A quasi-linear theory for rotating flow over topography. Part I: Steady β-plane channel. J.Fluid Mech., 99, 267-292.

Davey, M.K. 1981. A quasi-linear theory for rotating flow over topography. Part II: Beta-plane annulus. J.Fluid Mech., 103, 297-320.

Hoskins, B.J. 1973. Stability of the Rossby-Haurwits wave. Quart.J.R.Met.Soc., 99, 723-745.

Källén, E. 1981. The nonlinear effects of orographic and momentum forcing in a low-order, barotropic model. J.Atmos.Sci., 39, 2150-2163.

Källén, E. 1982. Bifurcation properties of quasi-geostrophic, barotropic models and the relation to atmospheric blocking. Tellus, in press.

Lorenz, E.N. 1960. Maximum simplification of the dynamic equations. Tellus, 12, 243-254.

Marsden, J.E. and McCracken, M. 1976. The Hopf bifurcation and its applications. Springer Verlag, New York, pp. 408.

Reinhold, B.B. 1981. Dynamics of weather regimes: quasi-stationary waves and blocking. Ph.D. thesis from Dept. of Meteorology, Massachussetts Institute of Technology, Cambridge, Mass., USA, pp. 218.

Saltzmann, B. 1970. Large-scale atmospheric energetics in wave-number domain. Rev. of Geophysics and Space Physics, 8, 289-302.

Steinberg, H.L., Wiin-Nielsen, A. and C-H. Yang. 1971. On nonlinear cascades in large-scale atmospheric flow. J. Geophys. Res., 76, 8629-8640.

Trevisan, A., and Buzzi, A. 1980. Stationary response of barotropic weakly nonlinear Rossby waves to quasi-resonant orographic forcing. J. Atmos.Sci., 37, 947-957.

Wiin-Nielsen, A.C. 1979. Steady states and stability properties of a low order barotropic system with forcing and dissipation. Tellus, 31, 375-386.

STOCHASTIC FORCING IN HIGHLY TRUNCATED GCMS

J. Egger

1. The problem

Assume for the moment that the atmosphere at midlatitudes is governed by the barotropic vorticity equation with β-plane approximation

$$\frac{\partial}{\partial t} \nabla^2\psi + J(\psi, \nabla^2\psi + f_o h/H + \beta y) = - C \nabla^2\psi + F \qquad (1.1)$$

(ψ stream function; f_o constant, midlatitude value of the Coriolisparameter; H scale height; h orography; $\beta = df/dy$, constant; C damping constant). F is a forcing term which is thought to describe the influence of heat sources or other baroclinic effects. We assume further on that the flow is restricted to a channel with walls to the north and south and periodic boundary conditions in x direction.

Suppose that we want to make a long-range forecast of this barotropic atmosphere by aid of a highly truncated GCM. To that end we expand the stream function ψ into normal modes of the channel:

$$\psi = \sum_{m,n} \psi_{mn}(t)\, e^{ik_m x} \sin l_n y - u_o y \qquad (1.2)$$

where $k_m = 2\pi\, m/L$, $l_n = n\pi/B$. $u_o(t)$ is the zonal mean flow as obtained by averaging over the channel. L is the channel's length, B is the width. Inserting (1.2) in (1.1) we obtain a forecast equation for the expansion coefficients ψ_{mn}. In particular, the forecast equation for u_o is

$$\frac{du_o}{dt} = - f_o I_m\Big(\sum_{m,n} k_m\, \psi_{mn}\, h^*_{mn}\Big)/H + F_u - Cu_o \qquad (1.3)$$

(e.g. Egger und Metz, 1981). h_{mn} are the expansion coefficients of the orography. The GCM will be based on only few modes. So we have in the model $m \leq M \lesssim 5$, $n \leq N \lesssim 5$. Correspondingly we split the stream function into a part ψ_r resolved by the model and an unresolved part ψ_u

$$\psi = \psi_r + \psi_u \qquad (1.4)$$

where

$$\psi_r = \sum_{m=o}^{M} \sum_{n=1}^{N} \psi_{mn}\, e^{ik_m x} \sin l_n y - u_o y \qquad (1.5)$$

The forecast equation of the GCM is

$$\frac{\partial}{\partial t} \nabla^2\psi_r + J(\psi_r, \nabla^2\psi_r + f_o h_r/H + \beta y) = - C \nabla^2\psi_r + F_r + P_r \qquad (1.6)$$

where the term P_r may stand for an attempt to parameterize the effect of the unresolved modes in terms of the resolved modes. The GCM would also have to include a properly truncated version of (1.3). Quite recently White and Green (1982) described a 2-parameter model of this type.

Nobody will expect that the GCM is succesful at a day by day basis. It is hoped, however, that forecasts of $\hat{\psi}_r$, say, monthly means or ensemble $< \psi_r >$ will show some skill. In this lecture we shall try to assess the forecast errors of $\hat{\psi}_r$ and/or $< \psi_r >$ caused by our ignorance of the unresolved modes. To make this assessment we have to look at the exact equation for ψ_r:

$$\begin{aligned} \frac{\partial}{\partial t} \nabla^2\psi_r + J_r(\psi_r, \nabla^2\psi_r + f_o h_r/H + \beta y) = - C \nabla^2\psi_r + F_r - J_r(\psi_r, \nabla^2\psi_u) \\ - J_r(\psi_u, \nabla^2\psi_u) - J_r(\psi_u, \nabla^2\psi_r) - J_r(\psi_u, f_o h/H) - J_r(\psi_r, f_o h_u/H) \end{aligned} \qquad (1.7)$$

The symbol J_r denotes the projection of a Jacobian on the resolved modes. Since the various Jacobians on the right hand side of (1.7) are not forecast (except for the last one) we may call them external forcing terms. They describe the impact of the unresolved modes on the flow forecast by the GCM. In the following we shall lump together the first three Jacobians on the right hand side of (1.7) and treat them as one external forcing J_e. Essential statistical characteristics of this term will be otbained through data analysis. These are used in turn to estimate the error which arises because this forcing is not known in a forecast situation. Our approach is similar to that used by Frankignoul and Hasselmann (1977) for the mixed layer of the ocean.

2. Data

Schilling (1981) took two years of daily height observations (1000 mb, 500 mb, 300 mb) and analyzed them in terms of eigenfunctions for the domain 10° N-90° N on the sphere. The data grid had a resolution $\Delta\lambda \times \Delta p = 10^\circ \times 5^\circ$. He used geostrophic balance to obtain the stream function. He then computed

the terms J_{emn} on a day by day basis where the subscripts m,n denote the contribution of J_e to the forecast equation for ψ_{mn}. Therefore we have a two-year time series of the forcing term J_e for each mode (m,n). J_{emn} is a random variable. To study the impact of this stochastic forcing on ψ_{mn} we have to evaluate the spectral characteristics of this time series. Powerspectra will turn out to be most important and we are going to discuss only these although certain cross-spectra have to be evaluated as well to represent J_{emn} properly. Since J_{emn} is a complex quantity we have to analyse the real part and the imaginary part separately. Furthermore, the mean value has to be removed. For the sake of brevity we shall omit such details in our notation. Schilling computed the autocorrelation

$$R_{mn}(\tau) = \{J_{emn}(t)\, J_{emn}(t+\tau)\} \tag{2.1}$$

and the powerspectrum

$$S_{mn}(\omega) = 2 \int_0^\infty R_{mn}(\tau)\cos\,\omega\tau d\tau \tag{2.2}$$

The symbol { } denotes a time average over the two years of data. Stationarity is assumed. Schilling's computations are based on the choice M = 5, N = 5. Schilling had a total of 12 (5) wave numbers in zonal (meridional) direction available so that the modes with $6 \leq m \leq 12$, $1 \leq n \leq 5$ are regarded as unresolved modes. To classify the spectra of the various J_{emn} by aid of a few parameters Schilling fitted the stationary Markov process

$$x_{j+1} = e^{-b}x_j + \left[(1 - e^{-2b})R_{mn}(0)\right]^{\frac{1}{2}} W(j) \tag{2.3}$$

to each time series. j is the running index in time increasing by one every day. W(j) is a white noise process with power 1. b is the parameter to be fitted which depends on m,n of course.
We find from (2.3) the autocorrelation

$$R_{mn}(\tau) = e^{-b\tau}\, R_{mn}(0) \tag{2.4}$$

and the power spectrum

$$S_{mn}(\omega) = 2\, R_{mn}(0)b/(b^2 + \omega^2) \tag{2.5}$$

According to (2.5) the powerspectra of J_{emn} are essentially red. However, the power $S_{mn}(\omega)$ is constant ($\sim R_{mn}(0)/b$) for periods $T > 2\pi/b$. It decays with increasing ω for $\omega \gtrsim b$. Fig. 1 shows the parameter b for the various

modes of the truncated GCM as evaluated from the time series of the J_{emn}. Typically b is of the order 1 day^{-1}. Roughly speaking the largest modes (m,n small) have the smallest values of b whereas the smallest modes have the largest b. Note that (2.3) is a prognostic equation for J_{emn}. It tells us that J_{emn} is essentially unpredictable beyond say, 2/b days. Therefore, no high resolution GCM would be able to predict J_{e55} (J_{e11}) for more than 1(3) day. In particular, the forcing by the unresolved modes can be viewed as essentially white and unpredictable if we are concerned with longrange predictions. Fig. 2 shows the average of all the powerspectra with $1.25 \leq b \leq 1.75$ and the average of the corresponding fitted powerspectra. We see that the power is nearly constant for $T \geq 3d$. The variances $R_{mn}(0)$ have been computed as well. They are typically of the order 50 - 100 $m^4 s^{-4}$.

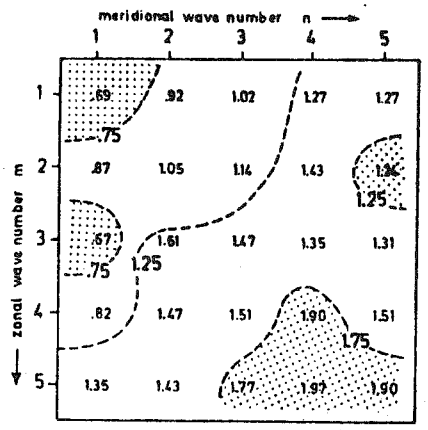

Fig. 1. Autocorrelation decay rate b of J_{emn} for the various modes of the GCM.

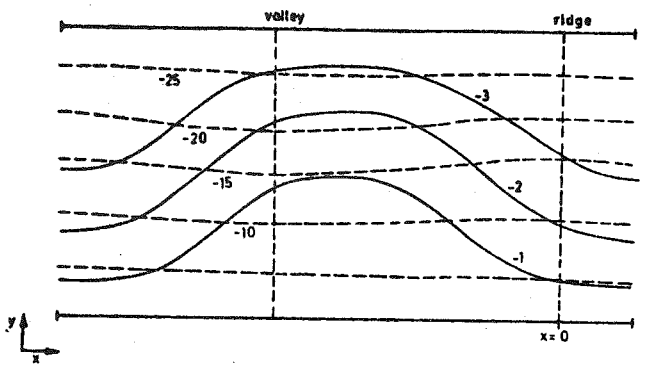

Fig. 3. Stream function $\psi(10^6 m^2 s^{-1})$ at E_1 (strong) and at E_h (dashed). L=B=3x10^6m; u_o^*=10 ms^{-1}; h_{11} = 500 m.

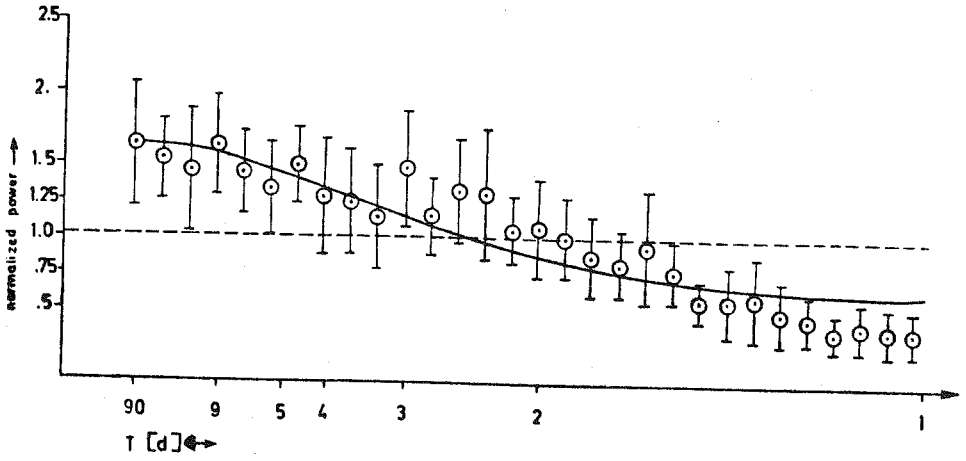

Fig. 2. Average over the power spectra of all modes with $1.25 < b < 1.75$ d^{-1} and the mean fitting curve (strong) of these modes (Schilling 1982). The power is normalized with respect to a white spectrum (dashed) for the same frequency interval.

3. Two-mode "GCM"

What is the reaction of a highly truncated GCM if the external forcing has spectral characteristics as described in the foregoing? As a first example let us look at an extremly simple model which contains only one wave mode and the mean flow u_o as variables. The stream function is then $\psi = - u_o y + \psi_{11}$. It is convenient to define the velocities $v_r = k_1 \, Re(\psi_{11})$, $v_i = k_1 Im(\psi_{11})$ and to assume that h_{11} is real so that $h = h_{11} \cos k_1 x \sin l_1 y$.
Then (1.6) and the equation for the mean flow take the form (e.g. Egger, 1982):

$$\frac{dv_r}{dt} = v_i \, \omega_r - C \, v_r + J_1 \tag{3.1}$$

$$\frac{dv_i}{dt} = - v_r \, \omega_r - C \, v_i + f_o \, u_o \, h_{11} \, k_1^2/k_{11}^2 H + J_2 \tag{3.2}$$

$$\frac{du_o}{dt} = - f_o \, v_i \, h_{11}/H - C(u_o - u_o^*) + J_3 \tag{3.3}$$

where $k_{11}^2 = k_1^2 + l_1^2$, $\omega_R = k_1 \, (u_o - \beta/k_{11}^2)$. The term $- C(u_o - u_o^*)$ represents the Newtonian forcing of the mean flow. (3.1) - (3.3) is so simple that it cannot serve as a useful forecast model. However, because of its simplicity, the model may help to understand the underlying problems. (3.1) - (3.3) with $J_i = 0$ has been studied by Charney and DeVore (1979). They found that there are two stable and one unstable equilibrium where and equilibrium is defined as a steady state solution of (3.1) - (3.3). One of the stable equilibria, let us call it E_h, resembles a high index solution with strong zonal flow and weak waves, whereas the other one, E_l, reminds us of a low index situation with weak zonal flow and a clearly visible standing wave (Fig. 3).

If we define a phase space withe the coordinates (v_r, v_i, u_o), an integration of (3.1) - (3.3) produces a trajectory in this phase space. It has been found through extensive numerical experimentation (Hart, 1979; Egger, 1982) that whatever the initial state virtually all trajectories will end in either E_h or E_l. If we include the influence of the unresolved modes by adding the stochastic forcing terms J_i on the right hand sides of (3.1) - (3.3) the J_i will kick the system out of an equilibrium situation and we may have transistions from the vicinity of one equilibrium to that of the other. With J_i included (3.1) - (3.3) is no longer deterministic and the solution can be described in probabilistic terms only. We define a probability

density $f(v_r, v_i, u_o, t)$ where $f\, dv_f\, dv_i\, du_o$ is the probability to find the system at time t in a cube with side lengths dv_r, dv_i, du_o centered at the point $\underset{\sim}{r} = (v_r, v_i, u_o)$. The evolution of f in time is governed by the Fokker-Planck equation:

$$\frac{\partial f}{\partial t} = -\frac{\partial}{\partial v_r}(f(v_i\,\omega_r - C\,v_r)) - \frac{\partial}{\partial v_i}(f(-v_r\,\omega_r - C\,v_i + f_o\,u_o\,h_{11}$$

$$k_1^2/k_{11}^2 H)) - \frac{\partial}{\partial u_o}(f(-f_o\,v_i\,k_{11}/H - C(u_o - \overset{*}{u_o})) + \qquad (3.4)$$

$$\frac{Q}{2}\left(\frac{\partial^2}{\partial v_r^2} + \frac{\partial^2}{\partial v_i^2} + \frac{\partial^2}{\partial u_o^2}\right)f$$

In writing down (3.4) we have assumed that J_i is strictly a white noise forcing. This is an oversimplification which appears, however, not to invaliditate the main conclusions to be drawn (see Egger, 1982). Q measures the intensity of the white noise forcing where we have assumed that all the J_i have the same spectral characteristics and are independent. f is normalized to have probability 1 to find the system in the phase space.

(3.4) has been integrated numerically for a large number of initial distributions of f. If we continue the integration of (3.4) beyond about 50-60 days we end up with a climatic mean distribution of f_c which does almost not change in time. Fig. 4 shows a surface of constant f_c in phase space. Obviously, the likelihood to find the system near one of the equilibria E_h or E_l is larger than to find it in between. This reminds us of the climatology of the atmosphere where certain types of circulation (Grosswetterlagen) are preferred as compared to others.

Let us now turn to our central problem. We have to deep in mind that (3.1) - (3.3) is a GCM which could be used to predict u_o and ψ_{11}. What is the predictive power of this model? To answer this question, we have conducted a large number of relative dispersion experiments where pairs of forecasts $\underset{\sim}{r}(t)$, $\underset{\sim}{r}'(t)$ with $\underset{\sim}{r}(o) = \underset{\sim}{r}'(o)$ have been made using (3.1) - (3.3) as a forecast model with J_i different in both runs. If $D(t) = |\underset{\sim}{r}(t) - \underset{\sim}{r}'(t)|$ is the distance of the trajectories in phase space and if <D> is the average over many such pairs <D(t)> may serve as a measure of predictability. Any forecast with (3.1) - (3.3) will have a mean forecast error of at least <D>.

Fig. 5 shows <D> as evaluated from more than 1000 pairs started as E_1 (dashed) and at a point E_z in between E_1 and E_h (dash-dotted). The bold curve gives the relative dispersion if all deterministic terms on the right sides of (3.1) - (3.3) are neglected, i.e. for purely random dispersion. Predictability is certainly lost if <D> crosses this random curve. Therefore, if E_z is the initial point of a forecast, there is no predictability beyond three days. There is more predictability if we start at E_1 although it is not clear what use we can make of a forecast when <D> approaches the "climatic mean" $D_c \sim 6$ ms^{-1}. Obviously predictability in our system depends on the initial state and is of the order of a week under favorable circumstances. This is a situation which is also found in numerical weather forecasting (Bengtsson, 1981).

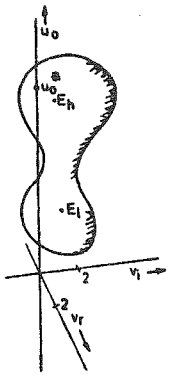

Fig. 4. Schematic presentation of a surface f_c =const. in phase space and the two stable equilibria.

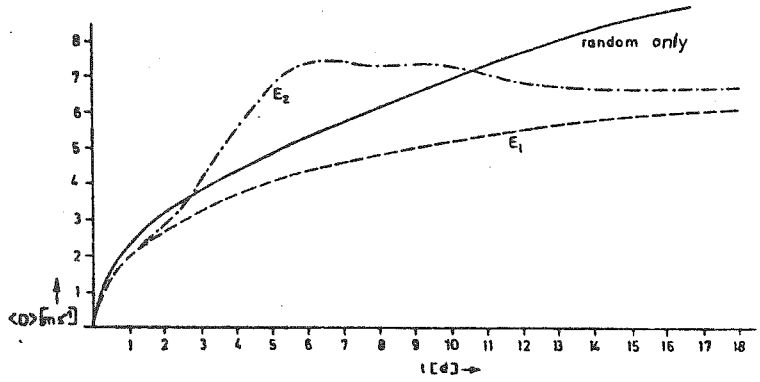

Fig. 5. Curves of relative dispersion < D > for runs started at E_1, E_z and for purely random dispersion.

Is there any possibility to make long-range forecasts with the highly truncated GCM (3.1) - (3.3)? Since the limit of predictability of the model has been found to be on the order of a week or so for single forecasts the only way to make more extended predictions is to make probability forecasts by running (3.4) instead of (3.1) - (3.3). Note that a similar approach has been taken in the so called stochastic prediction models (e.g. Epstein, 1969). Here, we shall discuss only the impact of anomalous forcing on long-range forecasts. There are processes in the atmosphere - ocean system which have larger time scales and better predictability than the atmosphere itself. If such a process acts as forcing on the atmosphere we may hope that the better predictability of the forcing will be reflected

in an increased predictability of the atmosphere. The influence of anomalies of the sea surface temperature (SST) is a wellknown example. Given a SST at t = o we may be able to forecast the SST a month ahead either by making a persistence forecast or by using a more elaborate linear statistical model (Davis, 1976). We may imitate such a situation by adding an anomalous forcing term Z_1 (Z_2) on the right hand side of (3.1), (3.2). We shall not alter Z_i in time, thus assuming that the anomalous forcing will persist throughout the forecast period.

Fig. 6 shows two 30-day forecasts of the probability density f in the planes u_o = 1 ms^{-1}, u_o = 10 ms^{-1}, respectively, for an anomalous forcing (strong) and for the control experiment with Z_i = o. The equilibrium E_1 (E_h) is close to the lower (upper) plane and is marked by a cross. The initial state in both runs has been a "cloud" of states centered at E_1. In our example, we chose $Z_1 = 2 \times 10^{-6}$ ms^{-2}; Z_2 = 0. We see, that the anomaly forecast differs considerably from the control forecast. The probability to find the system close to E_1 decreases if the forcing is included. On the other hand the probability to have a transition to the high index Grosswetterlage within 30 days is double of that in the control run.

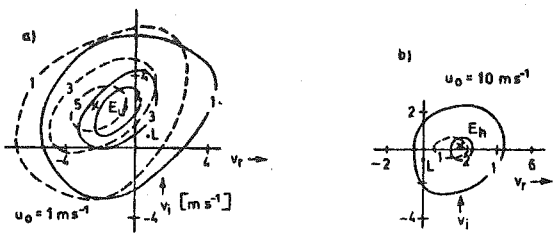

Fig. 6. Isolines of probability density f x 10^3 after 30 days for the anomalous forcing run (strong) and the control run (dashed)

Opsteegh and van den Dool (1980) proposed to use a linear steady-state model for long range forecasting. The points in Fig. 6a, b mark the linear steady-state solution of (3.1), (3.2) given the corresponding mean flows u_o. Near E_1, the linear theory says that the anomalous forcing would shift the states a bit towards higher values of v_r and v_i. This forecast appears to have some skill. The linear forecast fails completely at E_h. If, however, the initial state is a cloud centered at E_h we found virtually no difference between control and anomaly run. We have the result that there is indeed longrange predictability induced by anomalous forcing but the predictability appears to depend on the initial state.

Note that the control run does not arrive at the climatic mean state f_c (shown in Egger, 1982) after 30 days. Therefore (3.4) exhibits predictability beyond a month even without anomalous forcing.

We are lead to expect on the basis of the results obtained with the two-mode GCM that a highly truncated GCM may have long-range predictability if the probability density can be forecast. The success in anomalous forcing experiments appears to depend on the state of the model atmosphere.

4. Stochastic forcing in a GCM with 25 modes

We include now modes up to N = 5, M = 5 in the GCM (1.6) and try to assess the errors which will be caused in a long-range forecast by the external forcing J_e. In principle we could proceed by the same method as used for the two-mode system. However, a numerical integration of the Fokker-Planck equation for 25 modes is not feasible. One might consider running the GCM for a large number of cases but we shall proceed along a different and less expensive path by determining just the linear response of (1.6) to the stochastic forcing as obtained from the data. This corresponds to assuming that the nonlinear interactions in the GCM are not more important than the linear response to forcing. This assumption is corroborated by the findings of White and Green (1982). If (1.7) is linearized with respect to a zonal mean flow U_o we arrive with (1.5) at

$$\frac{d}{dt}\psi_{mn} = (-ik_m(U_o - \beta/k_{mn}^2) - C/\psi_{mn} + ik_m f_o U_o h_{mn}/k_{mn}^2 H - F_{mn}/k_{mn}^2 + J_{emn} \tag{4.1}$$

In what follows we shall exclude the mountain forcing term and the baroclinic forcing F_{mn}. Furthermore we assume a scale dependence of the damping: $C = \nu k_{mn}^2$. Note that the response in a linear system like (4.1) to various types of forcing can be obtained by superposition.

First, we perform a Fourier transformation in time where

$$P_{mn}(\omega) = \int_{-\infty}^{\infty} e^{i\omega t}\,\psi_{mn}\,dt \tag{4.2}$$

$$P(x,y,\omega) = \int_{-\infty}^{+\infty} e^{i\omega t}\,\psi(x,y,t)\,dt \tag{4.3}$$

Let $j_{mn}(\omega)$ be the Fouriertransform J_{emn}. We obtain from (4.2)

$$P_{mn}(\omega) = ij_{mn}/-1(-\omega + \omega_{Rmn} - i\nu k_{mn}^2) \tag{4.4}$$

with the Rossby frequency

$$\omega_{Rmn} = k_m(U_o - \beta/k_{mn}^2)$$

The powerspectrum of the response of a mode to the forcing is $S_{mn}(\omega) \sim P_{mn}(\omega)\, P_{mn}^*(\omega)$. Although a lot can be learned from a discussion of S_{mn} it appears to be more interesting with respect to the long-range problem to look at the power spectra of the stream function at various localities in the channel. Accordingly we switch back to physical space to find

$$P(x,y,\omega) = \frac{1}{2} \sum_{m=o}^{M} \sum_{n=1}^{N} (P_{mn}(\omega)e^{ik_m x} + P_{mn}^*(-\omega)e^{-ik_m x})\sin l_n y \tag{4.5}$$

where P_{mn}^* is obtained from the complex conjugate form of (4.1) just as P_{mn} comes from (4.1). The Powerspectrum S (x,y,ω) of the stream-function is

$$S \sim PP^* \tag{4.6}$$

As can be seen from (4.4) - (4.6) S can be computed if we know the spectra j_{mn}. Therefore we have to insert the forcing spectra as described in section 2 into (4.6) to obtain the power S (x,y,ω).

If (1.6) would be used for long-range purposes one would run the model, say, for two months, average the result, over an interval of ten days, for example, and look at this forecast of $\hat{\psi}_r$. Such an averaging corresponds to cutting out all frequencies with periods less than 10 days. Correspondingly we are only interested in S for frequencies $\omega < \omega_{10} = 2\pi/10\ d^{-1}$. A convenient way to display this low frequent variability is to compute the variance

$$\sigma_{10}^2 = \frac{2}{\pi} \int_{\omega_{10}}^{\infty} S\, d\omega \tag{4.7}$$

We display σ_{10}^2 in Fig. 7 as induced in the GCM by the unresolved modes. We note a rather high level of background power of the order $\sim 6 \times 10^{13}\ m^4\ S^{-2}$ at midlatitudes. This means that the longterm variability of the height field caused by the unresolved modes is of the order $\sim$80 m. There are maxima over the Atlantic and over the eastern USA where height errors of the order of 100 m are to be expected. Although a diagram like Fig. 7 must be viewed with caution since it depends to some degree on the choice of the damping

and of U_o we believe that a least the order of magnitude σ_{10} is correct. If that is true our chances to run a successful anomaly forecast are not bright. The variance of the stream function depicted in Fig. 7 is due to stochastic and unpredictable forcing. Therefore forecasts with the GCM where J_{emn} has to be excluded, will have an error of the order 8-10 10^6 $m^2\ S^{-1}$ in ψ_r. Note that the variance of ψ_r as found in the atmosphere is of the same order of magnitude as that shown in Fig. 7 (Blackmon, 1976). Even if the anomalous forcing like the SST field for the forecast period is known, the response to this forcing normally does not have the same order of magnitude as the error. Therefore, the skill of the long-range forecast must be low. That is not surprising, of course. On the other hand error fields like those presented in Fig. 7 enable us to make a reasonably good assessment of the skills a GCM like (1.6) can achieve. We can, for example, estimate the response to anomalous forcing by use of the linear steady-state theory and compare that to the noise level shown in Fig. 7.

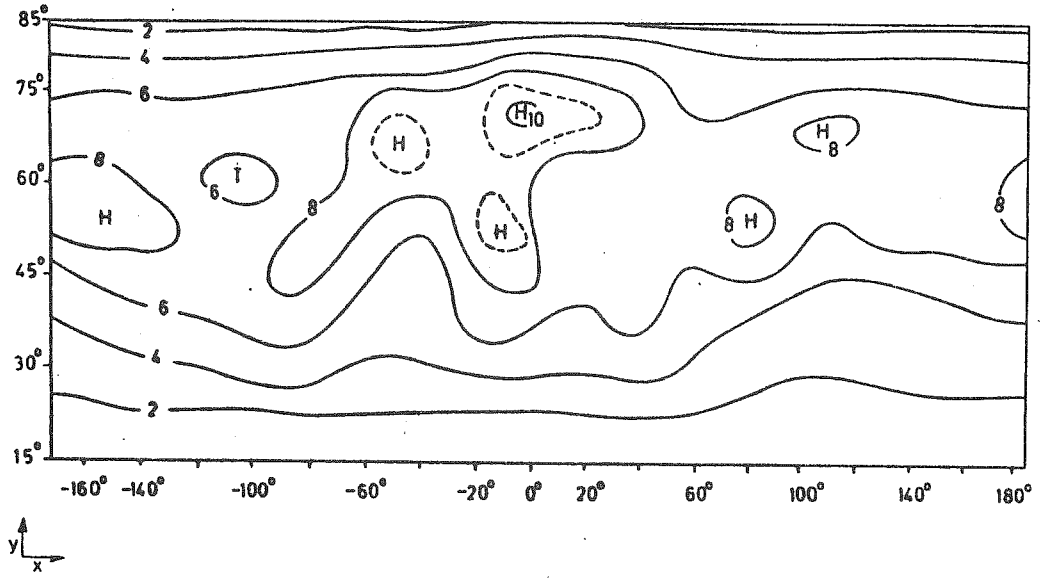

Fig. 7. Variance σ^2_{10} in $10^{13}m^4s^{-2}$ induced in the GCM with M=5,N=5 by the unresolved modes. ß-plane channel (Schilling, 1982).

At the moment we are not able to draw any firm conclusions with respect to the feasibility of long-range forecasts by aid of highly truncated GCM. It appears, however, that we can arrive at a fairly realistic assessment of the merits of this approach by using a blend of data analysis and numerical methods along the lines described here.

References

Bengtsson, L., Tellus, 33, 1981

Blackmon, M., JAS, 33, 1976

Charney, J. and J. De Vore, JAS 36, 1979

Davis, R., JPO, 6, 1976

Egger, J., JAS 39, 1982

Egger, J., and W. Metz, Q. J. Roy. Met. Soc., 167, 1981

Epstein, J., Tellus, 21, 1969

Frankignoul, C. and K. Hasselmann, Tellus, 29, 1977

Hart, J., JAS, 36, 1979

Lorenz, E., Tellus, 17, 1965

Madden, R., M.W.R. 103, 1975

Opsteegh, J., and H. van den Dool, JAS, 37, 1980

Schilling, H.D., priv. comm., 1981-82

White, A., and J. Green, Q. J. Roy. Met. Soc., 168, 1982

LOW ORDER STEADY CLIMATE MODELS

Michael Hantel

Abstract

We consider climate models after projection into phase space. The concepts applied in this field (existence of steady solutions; stability with respect to infinitesimal, finite, structural changes; sensitivity; response; numerical solution) are exemplified in terms of Riccati's differential equation for one spectral component. The pertinent analytic solution is compared with Lorenz's (1964) equivalent numerical solution. The concept of linear response is further demonstrated for the equations of the zonal mean global circulation. A 3-component version is gained by projection upon the observed climate functions (the zonal wind, mass streamfunction, temperature); climate changes are only possible through intensity changes. A 162-component version is gained by projection upon spectral expansions (3 in time, 6 in latitude, 3 in altitude) of the observed atmospheric functions. Climate changes now include structural changes. This is demonstrated for 10 % increases of the diabatic heating and the zonal wind eddies.

1. Introduction

We want to consider the behaviour of climate models once they havebeen transformed into phase space. We first ask: how to project? Let us consider the advection equation with forcing and dissipation in dimensionless form (e.g., Källén and Wiin-Nielsen, 1980):

$$\frac{\partial u}{\partial t} + u \frac{\partial u}{\partial x} = - \varepsilon u + u_E \qquad (1.1)$$

$u_E = u_E(x)$ is the forcing function, $u = u(x,t)$ the solution. The parameter ε, if positive, represents friction; if negative, we interprete it as a rudimentary form of the Coriolis parameter. We assume that a steady solution u_s exists; u_s may depend of x but not of t. The simplest possible expansion appears to be the separation:

$$u(x,t) = X(t)\ u_s(x) \tag{1.2}$$

We may think of X(t) as the climate *intensity* while $u_s(x)$ is the climate *structure*. Projection now means to multiply (1.1) with $u_s(x)$ and integrate over the space domain with the result:

$$\dot{X} + RoX^2 = -\varepsilon X + c \tag{1.3}$$

The parameter Ro is formally defined through $\int u_s^2\ \partial u_s/\partial x\ dx\ /\ \int u_s^2\ dx$. It depends upon the values of u_s at the boundaries of the x-domain; we shall assume $Ro \geq 0$. For ε we shall adopt the value $\varepsilon = -2$. The parameter c (formally defined through $\int u_s u_E dx / \int u_s^2 dx$) plays the role of a constant forcing quantity.

2. Extension to more components

The simple expansion (1.2) can also be applied if there are more than just one model equation like (1.1) and if there are more than just one space argument like x. For example, Hantel (1978) has considered 3 model equations in the zonal mean domain (one for zonal wind $\tilde{u}$, one for meridional mass streamfunction $\tilde{\psi}$, one for potential temperature $\tilde{\theta}$; $\tilde{}$ is the operator of zonal plus 1-month-time averaging); the expansion applied in analogy to (1.2) was:

$$\begin{aligned} \tilde{u}(t,q,p) &= X(T)\ \hat{u}(t,q,p) \\ \tilde{\psi}(t,q,p) &= Y(T)\ \hat{\psi}(t,q,p) \\ \tilde{\theta}(t,q,p) &= Z(T)\ \hat{\theta}(t,q,p) \end{aligned} \tag{2.1}$$

t is ordinary time, T is time scaled with a constant ($\geq$ 10 years) to make T something like climate time (scale separation; see Pedlosky,

1979), $q = a \sin\phi$ is meridional coordinate, p is pressure, $\hat{u}$, $\hat{\psi}$, $\hat{\theta}$ is the present observed zonal mean climate with annual cycle. The integration necessary to project the equations into (X,Y,Z)-space is over the entire atmosphere and over the year.

Expansions more elaborate than (1.2) for eq. (1.1) in terms of harmonic functions have been discussed, for example, by Wiin-Nielsen (1975), Källén and Wiin-Nielsen (1980), and Memmesheimer (1982).

Expansions more elaborate than (2.1) for the zonal mean climate equations in terms of orthogonal functions (Fourier in t, Legendre in q, Bessel in p) have been discussed by Hantel and Majewski (1980).

3. Riccati's differential equation

Eq. (1.3) now reads:

$$\dot{x} = f(x) \quad \text{with} \quad f(x) = - Rox^2 + 2x + c \tag{3.1}$$

We have switched from X to x to conform with the general nomenclature; note that $x = x(t)$ is a coordinate in phase space, not in physical space. (3.1) is a special case of a quadratic differential equation which has been studied, beginning with Riccati (1676-1754), by various authors in various fields, including mathematics (Liouville, 1841), cup anemometer instrumentation (Corcoran und Esau, 1964; Kondo et al., 1971), theoretical ecology (May, 1976; Wiin-Nielsen, 1977), and meteorology in general (Memmesheimer, 1982). In our case (3.1) has analytic solutions; the numerical solution for a particular case has been studied by Lorenz (1964) and will be discussed later. The steady states of (3.1) are:

$$x_s^I = \frac{1}{Ro}\left[1 + (1+Ro\ c)^{1/2}\right]$$
$$x_s^{II} = \frac{1}{Ro}\left[1 - (1+Ro\ c)^{1/2}\right] \tag{3.2}$$

(3.1) may be interpreted as model of a climate model. A steady state solution may be called climate point. We shall now demonstrate some of the concepts applied in low order climate modelling by considering (3.1) along with (3.2).

4. Existence

The existence of real solutions depends of the condition:

$$c \geq -1/Ro \tag{4.1}$$

In our case ($Ro \geq 0$) a positive forcing parameter is sufficient for (4.1).

5. Local stability

Stability of a steady solution with respect to infinitesimal disturbances is obtained by linearizing the original equation around x_s. With $x'(t) \equiv x(t)-x_s$ this yields:

$$\frac{dx'}{dt} = -\lambda x' \quad \text{with} \quad \lambda = 2(Rox_s-1) \tag{5.1}$$

Consequently, if the solutions (3.2) exist, we find:

$$\begin{aligned} x_s^I: &\quad \lambda \geq 0 \quad \rightarrow \quad x_s^I \text{ stable} \\ x_s^{II}: &\quad \lambda \leq 0 \quad \rightarrow \quad x_s^{II} \text{ unstable} \end{aligned} \tag{5.2}$$

6. Global stability

A solution stable for infinitesimal disturbances may be unstable for finite disturbances. A criterion for global stability can be gained through Liapunov's theory. We choose the potential energy as natural candidate for a Liapunov function:

$$V_{x_s}(x(t)) = [x(t)-x_s]^2/2 \tag{6.1}$$

$V_{x_s}(x)$ is called *Liapunov function* for x_s if its time derivative:

$$\dot{V}_{x_s}(x) = [x(t)-x_s]\,\dot{x}(t) = (x-x_s)(-Rox^2+2x+c) \qquad (6.2)$$

is negative definite within a finite environment of x_s. Liapunov's theory now guarantees: The climate point is globally stable if it has a Liapunov function.

In Fig. 1 we have picked the parameters c=0, Ro = 2/2.75 with the steady climate points x_s^I=2.75 (linearly stable), x_s^{II}=0 (linearly un-

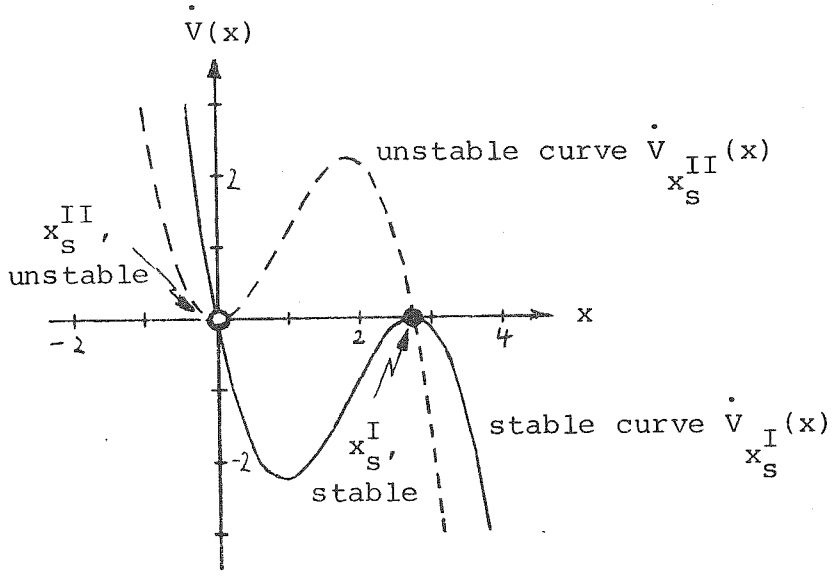

Fig. 1: Energy functions for Riccati model

stable). The x_s^I-curve (full) is negative definite around x_s^I and proves this point to be globally stable; we say that x_s^I is *attractive* within $0 \leq x < \infty$. On the other hand, x_s^{II} is *repellent* within $-\infty < x \leq 2.75$.

7. The climate hypersurface

Fig. 2 shows isolines of the steady state as function of Ro and c. The complete steady state function $x_s = x_s(Ro,c)$ constitutes what we may call the *climate hypersurface* in parameter space.

A section through the climate hypersurface for Ro = 2/2.75 is shown in Fig. 3. If for a specified parameter combination (e.g., c=2 in Fig. 3) the system is not in equilibrium, $x(t) \neq x_s$, it starts to

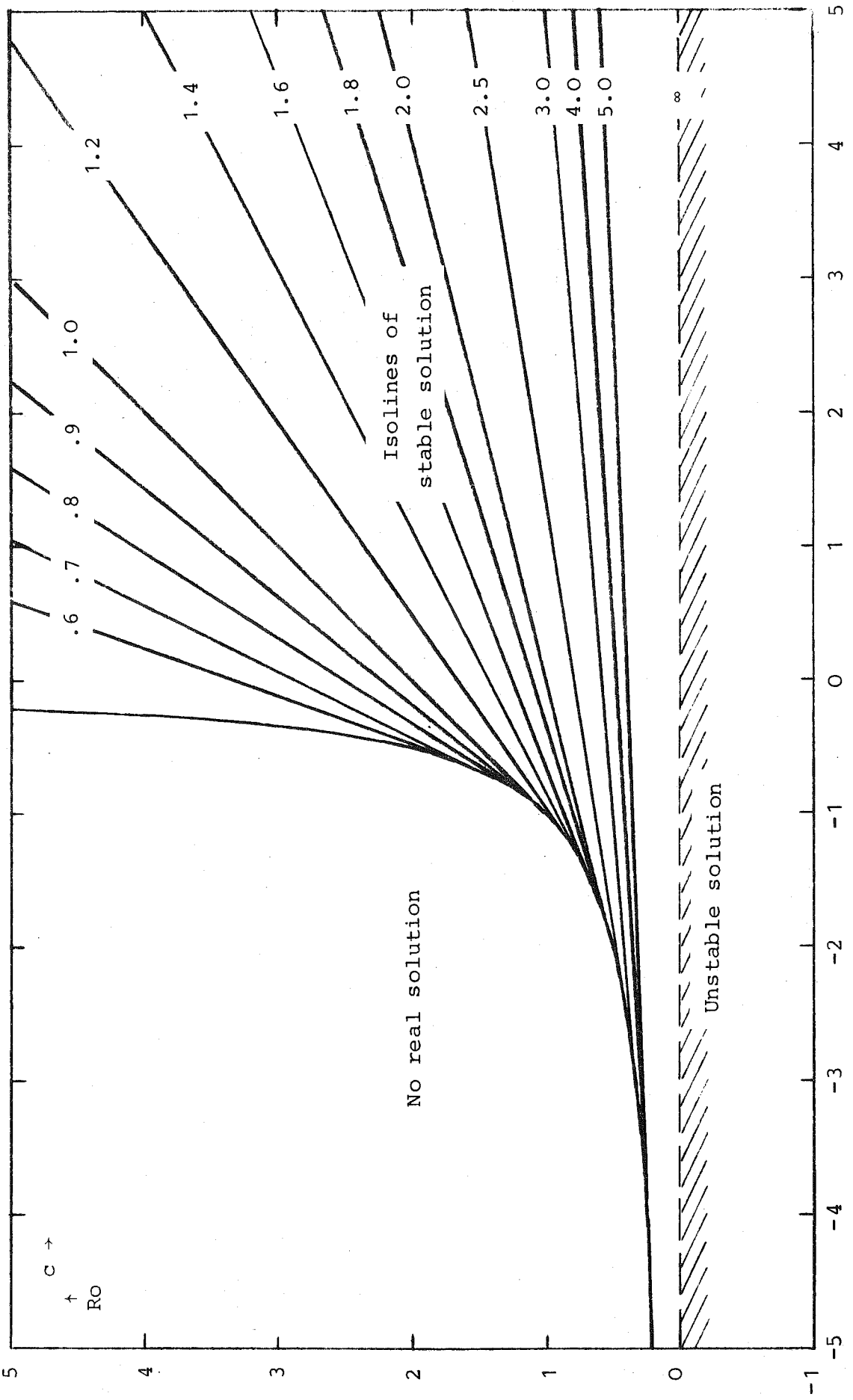

Fig. 2: Phase diagram of stable solution of Riccati differential equation.
Drawn are isolines of $x_s = \frac{1}{Ro}(1 + \sqrt{1+Ro\ c})$.

move away from the unstable and towards the stable branch; for the Riccati system the distance $x(t)-x_s$ decays exponentially to zero. In more complicated cases the distance may oscillate around the stable steady state.

In the two-component model of Källén and Wiin Nielsen (1980) the stable branch turns back towards smaller c and reaches a new stable branch. This is the case of a catastrophe (two different stable states for the same argument vector in phase space). For

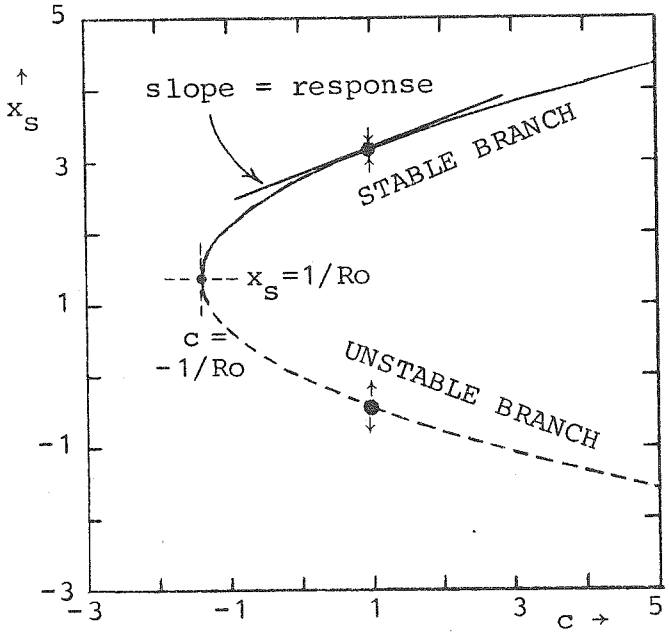

Fig. 3:
$x_s(Ro,c)$ for Ro = 2/2.75 as function of c.

this reason the climate hypersurface is often called *catastrophe surface*. Catastrophes for Budyko-Sellers-type models have been discussed by Held and Suarez (1974) and Fraedrich (1978).

8. Response and sensitivity

The state of a real system will never be exactly on but at most close to the climate hypersurface. It may nevertheless be of value to ask for the change of the climate point if the forcing is changed. We define the linear and relative (logarithmic) response:

$$R_c^{x_s} \equiv \partial x_s/\partial c; \qquad r_c^{x_s} \equiv \frac{\partial \log x_s}{\partial \log c} = \frac{c}{x_s} R_c^{x_s} \tag{8.1}$$

The linear response is the slope of the climate hypersurface for fixed Ro. The equivalent quantity when c is replaced by Ro may be referred to as *sensitivity* (with respect to parameter changes).

The response of the Riccati system is the following function of c:

$$R_c^{x_s^I} = 0.5(1+\mathrm{Ro}\ c)^{-1/2} \tag{8.2}$$

It starts from $+\infty$ at the catastrophe point $c = -1/\mathrm{Ro}$ and is positive everywhere on the stable branch.

The responses of more complex climate models are the solutions of a set of linear equations, even if the corresponding steady state is given through a set of nonlinearly coupled equations. As an example, let us consider again Källén and Wiin-Nielsen's (1980) model. Its steady states are defined through:

$$\frac{1}{2}\,xy - x + x_E = 0; \qquad -\frac{1}{2}\,x^2 - y + y_E = 0 \tag{8.3}$$

Be x_s, y_s the solutions. Then (8.3) defines a climate hypersurface in (x_s, y_s, x_E, y_E)-space. The tangential surface has 4 slope components which are given by the response matrix:

$$\begin{pmatrix} R_{x_E}^{x_s} & R_{y_E}^{x_s} \\ R_{x_E}^{y_s} & R_{y_E}^{y_s} \end{pmatrix} = \frac{1}{x_s^2/2 - y_s/2 + 1} \begin{pmatrix} 1 & x_s/2 \\ -x_s & 1-y_s/2 \end{pmatrix} \tag{8.4}$$

The response matrix is identical to the Jacobian $\partial(x_s,y_s)/\partial(x_E/y_E)$; (8.4) has been gained as the linearized version of (8.3). In realistic models the concept of response allows to estimate the trend towards other climates from the observed climate without explicitly knowing other climate states.

9. Response of a 3-component model

The model studied by Hantel (1978) has a 3x3 response matrix because there are 3 response intensities and 3 independent forcing parameters. We restrict ourselves to one example. R_A^Y describes the response of the streamfunction $\tilde{\psi}$ intensity (Y) with respect to the zonal mean eddy flux convergence intensity (A). The numerical value of this matrix component for today's climate is:

$$R_A^Y = 0.95 \tag{9.1}$$

This reproduces the near balance $f\,\tilde{v} \simeq \partial\,\widetilde{u^e v^e}/\partial y$, a parameterization familiar in zonal mean climate modelling (Schneider and Dickinson, 1974; upper index e is deviation from $\tilde{}$).

10. Response of a 162-component model

The above-mentioned more elaborate model of Hantel and Majewski (1980) has 3x6x3 = 54 expansion coefficients for the three zonal mean functions $\tilde{u}$, $\tilde{\psi}$, $\tilde{\theta}$. Models of this type may yield a complex response, including structural changes of the observed mean circulation. We restrict ourselves to one example (Fig. 4). It shows in the upper part the pertinent zonal mean observed $\tilde{\theta}$ for July. In the middle part the change $\Delta\tilde{\theta}$ is plotted which appears in response to a 10 % increase of the diabatic heating. This causes warming in the entire atmosphere (>3 K in northern tropics) with the only exception of a small area north of 70°N with cooling. The lower part of Fig. 4 shows $\Delta\tilde{\theta}$ for a 10 % increase of the zonal eddies. This causes cooling in most of the northern atmosphere and heating in most of the southern atmosphere, both on the order of 1 K.

11. Numerical solution

As a rule, nonlinearly coupled ordinary differential equations cannot be solved analytically. When numerical methods are applied in more complex models, the problem of truncation error arises.

Riccati's equation (3.1) has, for all constant values of Ro, c, analytic time-dependent solutions. Thus an objective comparison is possible. We consider the case c=0, with the solution:

$$x(t) = \frac{2\, e^{2t}}{2/x_o + Ro(e^{2t}-1)} \qquad \rightarrow \quad x_s = 2/Ro \tag{11.1}$$

The initial value x_o is restricted, according to Fig. 1, to the globally stable interval $0 < x_o < \infty$.

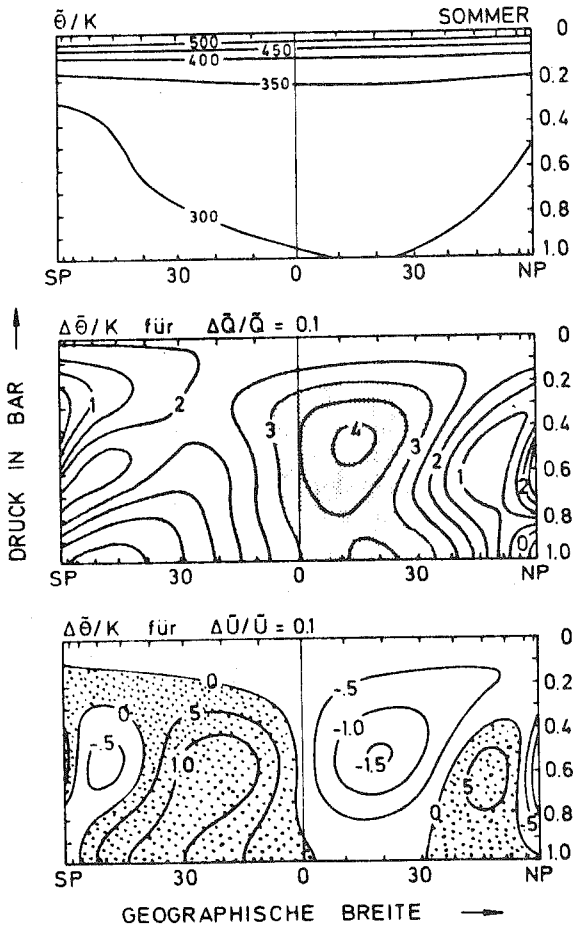

Fig. 4:
Observed zonal mean potential temperature $\tilde{\theta}$ in northern summer for global atmosphere (upper picture). Change of $\tilde{\theta}$ when diabatic heating is increased by 10% (middle). Change of $\tilde{\theta}$ when zonal wind eddies are increased by 10% (lower picture). Representation with 54 spectral components.

A numerical solution of (3.1) may be obtained by a forward integration in time through

$$x_{n+1} = (1+2\Delta t)x_n - Ro\ \Delta t\ x_n^2, \qquad n = 0,\ 1,\ 2,\ \ldots \tag{11.2}$$

where $x_n \equiv x(n\Delta t)$. For $Ro\Delta t = 1$ this is identical to Lorenz's (1964) quadratic equation. We note first that the steady solution of (11.2) is identical to (11.1) and further that the scheme (11.2) is linearly stable under the condition

$$2\ \Delta t < 2\ Ro\ \Delta t\ x_s \quad \rightarrow \quad 1/Ro < x_s \tag{11.3}$$

which is fulfilled independent of Δt. Thus the predictability problem considered by Lorenz is closely related to a numerically stable approximation of Riccati's differential equation for $Ro\Delta t = 1$.

On the other hand the numerical solution does not converge towards the steady state (11.1). Fig. 5 is drawn from Tab. 1 of Lorenz

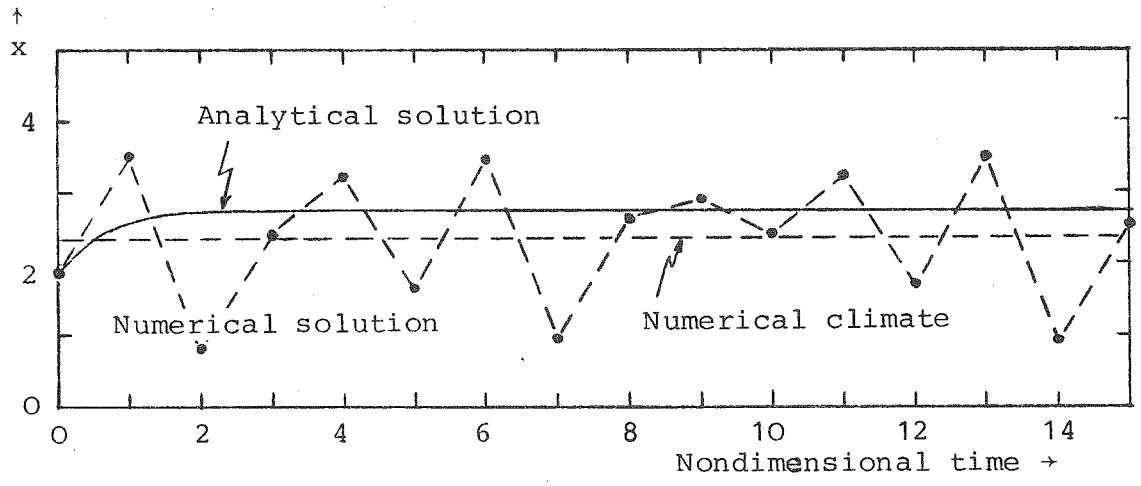

Fig. 5: Analytical solution of Riccati's differential equation (c=0, Ro=2/2.75) compared with Lorenz's equivalent numerical solution ($Ro\Delta t$=1).

for $a = 1 + 2/Ro = 3.75 \rightarrow Ro = 2/2.75$, $x_s = 2.75$; these parameters have also been chosen in the previous figures. We see that Lorenz's mean value $x_s^* \simeq 2.4$ (determined graphically from his Fig. 3) is not equal to x_s. The numerical solution, although numerically stable, does not converge to the analytical climate.

This is the effect of the truncation error. It may be reduced by reducing Δt. This would, however, alter Lorenz's parameters. At this point the relationship between Riccati's and Lorenz's equations ends. If, however, a numerical calculation like Lorenz's is to be a relevant

approximation to the path of a real system in phase space, one has to investigate not only its numerical stability but also its truncation errors; in our example, Lorenz's numerical solution would have to be repeated for smaller time steps. We cannot rule out the possibility that erratic oscillations like the ones of Fig. 5 remain to appear in numerical approximations even if the truncation error is much less severe than in the present case.

12. Conclusions

Riccati's one-component differential equation has served for a broad classification of the methods applied in low order climate modelling. Following the method of projection we have discussed various techniques applied in phase space. The special choice $\varepsilon = -2$ has been made in order to be consistent with Lorenz's numerical solution. Further, a negative ε makes Riccati's equation linearly unstable for $Ro = 0$; so this may serve as an example that stability is through the nonlinear term. The general behaviour of Riccati's equation, however, does not depend on the specific choice of ε.

What cannot be modelled with such a simple system is the nonlinear interaction between different components (Källén and Wiin-Nielsen). This interaction may force the atmosphere to jump, from time to time, over unstable branches of the climate hypersurface. There is hope, however, that these branches, due to the many scales involved, are sufficiently close together so that climate catastrophes like boiling oceans or a white earth are sufficiently far from reality. It is for this reason that the concept of response (slope of climate surface for infinitesimal changes of forcing parameters) may prove fruitful for a quantitative estimate of future climate trends from today's data.

13. Acknowledgments

The ideas presented draw extensively from earlier discussions with U. Callies, D. Majewski and M. Memmesheimer. Mrs. C. Frese took care of the manuscript.

14. References

Corcoran, J.W., and D.L. Esau, 1964: Comparison of a theoretical model for anemometer cups with experimental data. Backmare & Whitley, Inc., San Carlos, California, Met. 9, 21 pp.

Fraedrich, K., 1978: Structural and stochastic analysis of a zero-dimensional climate system. Quart.J.Roy.Met.Soc., 104, 461-474.

Hantel, M., 1978: A three-component global climate model. Proceedings, International Conference: Evolution of Planetary Atmospheres and Climatology of the Earth, Nizza, 16-20 Oct. 1978; Centre Nationale d'Etudes Spatiales, Toulouse, pp. 481-492.

Hantel, M., and D. Majewski, 1980: Ein neues, einfaches Klimamodell für die globale Atmosphäre. Annalen der Meteorologie, N.F., Nr. 15, 83-86.

Held, I.M., and M.J. Suarez, 1974: Simple albedo feedback models of the icecaps. Tellus, 26, 613-629.

Källén, E., and A.C. Wiin-Nielsen, 1980: Non-linear, low order interactions. Tellus, 32, 393-409.

Kondo, J., G.-i. Naito and Y. Fujinawa, 1971: Response of cup anemometer in turbulence. J.Met.Soc.Japan, 49, 63-74.

Liouville, J., 1841 (publication in: J.de Math.pures et appl., 6).

Lorenz, E.N., 1964: The problem of deducing the climate from the governing equations. Tellus, XVI, 1-11.

May, R., 1976: Theoretical Ecology.

Memmesheimer, M., 1982: Die Verzweigungsstrukturen stationärer Lösungen bei einfachen nichtlinearen spektralen Modellen und ihre Bedeutung für die Theorie der Klimaschwankungen. Bonner Meteorologische Abhandlungen, 28, in print.

Pedlosky, J., 1979: Geophysical Fluid Dynamics. Springer-Verlag, New York, Berlin, Heidelberg, 624 pp.

Schneider, St.H., and R.E. Dickinson, 1974: Climate Modeling. Rev. Geoph.Space Phys., 12, 447-493.

Wiin-Nielsen, A.C., 1975: Predictability and climate variation illustrated by a low-order system. Proceedings of Seminars on Scientific Foundation of Medium Range Weather Forecasts, 258-306.

Wiin-Nielsen, A.C., 1977: On the asymptotic behaviour of simple stochastic-dynamic systems. European Center for Medium Range Weather Forecasts. Technical Report No. 8.

ON THE INTERACTION BETWEEN LONG WAVE MOTION AND SYNOPTIC EDDIES

Brian J. Hoskins

In recent years many studies have shown the interesting and, in some cases, quite realistic results that may be obtained from linearized, steady-state models. Both from budget analyses of observational data and the realism of such results arises the question whether the synoptic time-scale eddies play any crucial role in the low frequency motions of the atmosphere. The investigations described in this paper are the start of an effort where aim is to address this question.

The budget analyses of Lau (1979) and others suggest very strongly that the mean long-term effect of the horizontal heat flux by synoptic eddies is such as to weaken not only the zonally averaged temperature gradient but also the mean longitudinal temperature wave. The e-folding time for this latter damping effect is of the order of seven days. Studies at the U. of Reading using ECMWF data suggest that this is qualitatively the case even when the mean is over as short a period as 15 days. The vertical flux of heat by the transient eddies results in a heating at upper tropospheric levels and cooling at lower levels in the storm-track region of the order of 1 K day^{-1}. This effect is important in maintaining the static stability against the destabilising effects of the diabatic processes. One of these processes is the release of latent heat in the storm-tracks associated with large-scale precipitation which is, of course, another effect of the transient synoptic eddies. Their influence on the radiative budget and boundary layer fluxes of heat, moisture and momentum could also be important.

Transient eddy terms were found by Blackmon et al. (1977) to be negligible in the x-momentum balance in jet entrance and exit regions. The y-momentum equation however has the large eddy momentum flux convergence $(\overline{v'^2})_y$. An approach via the vorticity equation should allow the total effect of the eddy momentum flux to be evaluated. Papers by Lau (1979), Holopainen (1978) and Holopainen and Oort (1981) have suggested that in the upper troposphere the transient eddy vorticity flux convergence is generally rather smaller than the absolute vorticity advection by the mean flow but that in a vertical average the eddy term is important. Thus transient eddy vorticity

fluxes do play a role in balancing the curl of the surface stress.

Since transient eddy vorticity fluxes are not easy to visualize, it is worth reconsidering them in terms of quantities associated with the velocity correlation tensor $\overline{v_i'v_j'}$. The isotropic part of this tensor is the kinetic energy $K = \frac{1}{2}\overline{u'^2+v'^2}$. It is easily shown that the dominant transient eddy term in the balance equation is $\nabla^2 K$. Since the balance equation may be thought of as an equation for $f\xi_{ageost}$, this implies anticyclonic ageostrophic circulation around a storm-track with its associated maximum in K. However in a quasi-geostrophic atmosphere the eddy vorticity flux convergence is the important "mechanical" quantity and this may be expressed in terms of the components of the anisotropic part of $\overline{v_i'v_j'}$:

$$\nabla.\overline{\underset{\sim}{v}'\xi'} = 2M_{xy} - N_{xx} + N_{yy} \qquad (1)$$

where $M = \frac{1}{2}\overline{u'^2-v'^2}$, $N = \overline{u'v'}$

and $\sim$ denotes a vector

The principal axes of the tensor give the local orientation of the eddies.

The form (1) can easily be used to estimate the vorticity flux divergence due to transient eddies. However, an approximation allows a great simplification to be made. Since N is generally much smaller in magnitude than M and the x-length scale is generally much larger than the y-length scale, the term N_{xx} in (1) may be neglected. Then

$$\nabla.\overline{\underset{\sim}{v}'\xi'} = \partial/\partial y\ \{\nabla.(2M,N)\} \qquad (2)$$

$$= \partial/\partial y\ \{\nabla.(\overline{u'^2-v'^2}\ ,\ \overline{u'v'})\}$$

The term in brackets denoted by $\underset{\sim}{P}$, may be thought of as the effective westerly momentum flux though its real meaning is in terms of a mean vor-

ticity source. For example, the distribution of $\underset{\sim}{P}$ for the high pass transient eddies in a storm-track is qualitatively as shown in Fig. 1. For these eddies $\overline{v'^2} > \overline{u'^2}$ i.e. they are elongated meridionally. Also $\overline{u'v'}$ tends to be positive to the south of the track and negative to the north. The convergence of $\underset{\sim}{P}$ and the forcing of the mean horizontal circulation are also indicated in Fig. 1.

The distribution of $\underset{\sim}{P}$ for high pass eddies over shorter periods can be very different. Two specific 15 day periods in the months Dec. 1981 - Feb. 1982 with significant blocks in the NE Atlantic-European sector showed eddies with $\underset{\sim}{P}$ pointing away from the blocks downstream as well as upstream. This indicates that for these periods the synoptic eddies were acting in the sense of maintaining the blocked situation of weak westerly winds as sketched in Fig. 2.

It is easily shown that for the high pass eddies the principal axis of the tensor $\overline{v_i'v_j'}$ corresponding to the smallest scale of the eddies is approximately in the direction of $\underset{\sim}{P}$ so that a map of the latter indicates the orientation of the eddies.

The situation is very different for the low-pass eddies. For these it is mostly found that $\overline{u'^2}$ is greater than $\overline{v'^2}$. Thus the $\underset{\sim}{P}$ arrows point eastwards and are approximately in the direction of the principal axis of the tensor corresponding to the largest scale of the eddies.

It may also be shown that the anisotropic components of the velocity correlation tensor determine the direction of propagation of the eddies. In the limit of a slowly varying mean flow $\underset{\sim}{\bar{u}}$ which is a function of x as well as y, the group velocity may be written

$$\underset{\sim}{c}_g = \underset{\sim}{\bar{u}} - \frac{|\nabla\bar{\xi}|}{\frac{1}{2}\overline{\xi'^2}} \quad (M,N) \tag{3}$$

where ξ is the absolute vorticity and M and N are the anisotropic tensor components relative to axes along and normal to the mean absolute vorticity contours. In the absence of eddy dissipation, the potential enstrophy $\frac{1}{2}\overline{\xi'^2}$ is conserved along a ray.

The above ideas are suggestive of possible parametrisation schemes

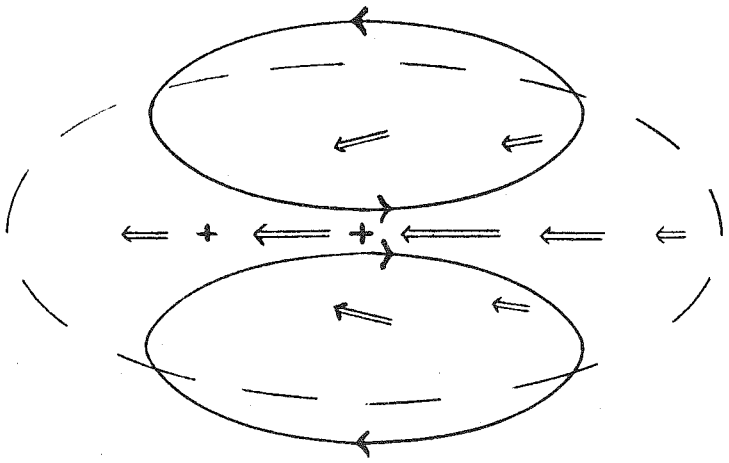

Figure 1. An idealised Northern Hemisphere storm-track, indicated by dashed lines, with its associated vectors $\underset{\sim}{P} = (\overline{u'^2 - v'^2}, \overline{u'v'})$. Their convergence is indicated by the plus signs and the resultant forcing of the mean horizontal circulation by continuous contours.

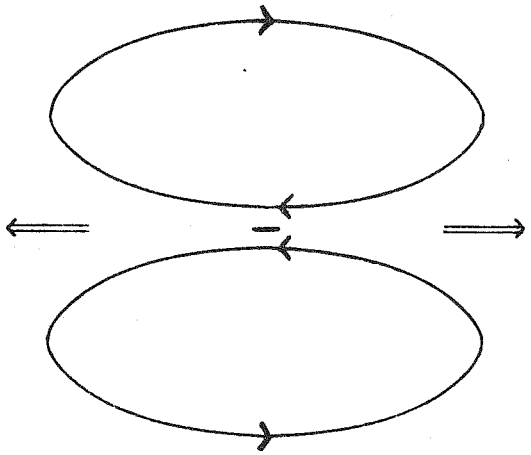

Figure 2. An idealized distribution $\underset{\sim}{P}$ in a blocking region with its divergence indicated by a minus sign.
The resultant forcing of the mean horizontal circulation acts to maintain the block.

for the synoptic time-scale eddies but, in order to provide a firmer foundation for such schemes, a programme of numerical experimentation has been initiated at the U. of Reading. It involves the use of a five layer spectral (T42) primitive equation model using ∇^6 internal dissipation. Current experiments have included only stationary wave forcing so that the baroclinic waves that develop continually erode the zonally-averaged mid-latitude baroclinity. However they already indicate the importance of the interaction between the synoptic time-scale baroclinic waves and the larger space- and time-scale motion. A realistic representation of this interaction will eventually be essential in a long-term forecast model.

References

Blackmon, M.L., J.M. Wallace, N.-C. Lau and S.L. Mullen, 1977: An observational study of the Northern Hemisphere winter-time circulation. J. Atmos. Sci., 34, 1040-1053.

Holopainen, E.O., 1978: On the dynamic forcing of the long-term mean flow by the large-scale Reynolds stresses in the atmosphere. J. Atmos. Sci., 35, 1596-1604.

Holopainen, E.O. and A.H. Oort, 1981: On the role of the large-scale transient eddies in the maintenance of the vorticity and enstrophy of the time-mean atmospheric flow. J. Atmos. Sci., 38, 270-280.

Lau, N.-C., 1979: The observed structure of tropospheric stationary waves and the local balances of vorticity and heat. J. Atmos. Sci., 36, 996-1016.

ON THE RELATIONSHIPS BETWEEN MEAN FLOW AND TRANSIENT EDDY ENERGY FLUX DIVERGENCES, COMPUTED ON MONTHLY BASIS

Mikko Alestalo

Abstract

A 96-month time series of monthly means and covariances of temperature and geopotential height and wind components at different atmospheric levels and stations in Europe have been used for the computation of the monthly mean values of vertically integrated flux divergences of sensible heat and potential energy. The total flux divergence has been partitioned into contributions due to transient flow systems and the monthly mean flow. It is found that the individual monthly anomalies of these two contributions have a tendency to partly cancel each other. The year-to-year variability of these terms is large. In the budget equation of sensible heat the rate of time change of energy storage appears to be a small residual between atmospheric large-scale net transports and diabatic effects, which act opposite to each other. The effect of transient eddies on temperature anomalies is found to be a dissipative one.

1. Introduction

In this study the relative roles of the mean monthly flow and transient eddies, defined on a monthly basis, in maintaining the vertically and area averaged monthly mean sensible heat will be investigated. The procedure followed involves the computation of vertically integrated flux divergences of temperature and geopotential height entering the budget equation for sensible heat, the fluxes being computed using original radio sonde data from Europe between July 1969 and June 1977. The individual monthly values for the eight years give additional information about the year-to-year variability of the atmospheric budget factors.

Following Newell et al. (1974), the equation for sensible heat ($c_p T$) and kinetic energy (k) per mass unit of air can be combined to give, when integrated over the mass of the atmosphere in a column with an unit cross sectional area,

$$\int_o^{p_s} \frac{\partial}{\partial t} (c_p T + k) \frac{dp}{g} = - \int_o^{p_s} \nabla.(c_p T + \Phi + k) v_H \frac{dp}{g} + R_a + LP + H_o \tag{1}$$

where c_p is the specific heat at constant pressure, T is temperature, Φ is potential energy, v_H is the horizontal wind vector, p_s surface pressure, g acceleration due to gravity, R_a atmospheric net radiation and H_o the turbulent heat transfer into the atmosphere.

For the following analysis the time averaged flux divergence can be expanded, considering an arbitrary quantity s, as follows

$$\begin{aligned} \nabla.\overline{sv_H} &= \nabla \cdot \overline{s'v_H'} + \nabla \cdot \bar{s}\,\bar{v}_H \\ &= \nabla \cdot \overline{s'v_H'} + \bar{v}_H \cdot \nabla\bar{s} + \bar{s}\,\nabla \cdot \bar{v}_H \end{aligned} \tag{2}$$

The bar denotes a time average and the prime a deviation from it. In eq. (2) the total divergence is partitioned into contributions arising due to transient eddies and a mean flow effect. The latter is still split into two parts related with advection by the mean flow and the mean mass divergence. Being interested in this study in the individual monthly values of the terms of eq. (2) we choose a wavy overbar for a one month average and a double prime for a deviation from that, i.e.

$$\nabla \cdot \widetilde{sv_H} = \nabla \cdot \widetilde{s''v_H''} + \tilde{v}_H \cdot \nabla\tilde{s} + \tilde{s}\,\nabla \cdot \tilde{v}_H \tag{3}$$

The bar will be reserved for an ensemble mean monthly value (over several Januaries for example) so that

$$\nabla \cdot \overline{\widetilde{s}\widetilde{v}_H} = \nabla \cdot \overline{\widetilde{s''v_H''}} + \overline{\widetilde{v}_H \cdot \nabla \widetilde{s}} + \overline{\widetilde{s}\, \nabla \cdot \widetilde{v}_H} \qquad (4)$$

It may be noted that the l.h.s. terms of eq. (2) and (4) are equal but the respective r.h.s. terms do not correspond to each other. Specifically, in eq. (2) the transient eddy term includes the effect of inter-annual variability whereas the similar term in eq. (4) contains only the effect of fluctuations with periods less than about 30 days (plus that of the trend which arises from the seasonal variation of daily observations).

Substituting eq. (3) into eq. (1), dropping the terms including kinetic energy and $\nabla \cdot \overline{\widetilde{\Phi''v_H''}}$ and $\widetilde{v}_H \cdot \nabla \widetilde{\Phi}$ as small, we get

$$\int_0^{p_s} \frac{\partial}{\partial t} c_p \widetilde{T} \frac{dp}{g} = - \int_0^{p_s} \nabla \cdot c_p \overline{\widetilde{T''v_H''}} \frac{dp}{g} - \int_0^{p_s} \widetilde{v}_H \cdot \nabla c_p \widetilde{T} \frac{dp}{g}$$

$$- \int_0^{p_s} (c_p \widetilde{T} + \widetilde{\Phi}) \nabla \cdot \widetilde{v}_H \frac{dp}{g} + R_a + \widetilde{LP} + \widetilde{H}_o \qquad (5)$$

According to eq. (5), the monthly mean vertically integrated sensible heat is, on one hand, determined by net atmospheric transports of sensible heat and potential energy and, on the other hand, by diabatic effects due to radiation, net condensation and turbulent heat flux. The division of the atmospheric net transport into transient eddy and mean flow parts facilitates the study of their relative roles in the maintenance of temperature. The partitioning of the mean flow part into advection and mass divergence related parts allows to isolate the divergence term, which is considered as the most unreliable of the r.h.s. terms of eq. (3) or (4).

In the following the mean annual cycles of the atmospheric terms of eq. (5) will be shown together with individual monthly values as an indication of the interannual variability of these terms. At the end of the paper correlations between the monthly anomalies of the various terms of eq. (5) will be shown.

2. Results

The area (polygon) for which the divergences are computed, is shown in Fig. 1. It is composed of 24 stations at the boundary and 35 stations inside the area. The method of computation of divergences is described in Alestalo (1981a).

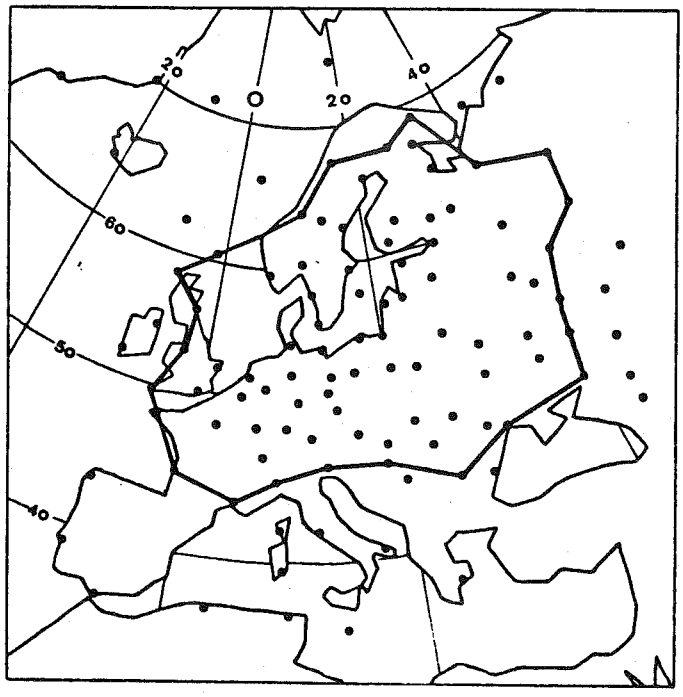

Fig. 1. The network of aerological stations in Europe (dots) and the region for divergence computations.

The individual monthly values of the vertically integrated terms $\nabla \cdot c_p \widetilde{T''v_H''}$, $\tilde{v}_H \cdot \nabla c_p \tilde{T}$ and $c_p \tilde{T} \nabla \cdot \tilde{v}_H$ are shown in Fig. 2 as circles for the period July 1969 - June 1977 (values for Novembers 1969 and 1970 have been dropped due to the poor data availability during these months). Also shown are the ensemble mean monthly values (solid lines).

Considering first the transient eddy flux divergence (Fig. 2a), the individual monthly values exhibit a very large inter-annual variability with very small amplitude for the mean annual cycle. Actually the mean multi-annual values do not significantly differ from zero in many months. The occurence of the mean values close to zero (implying rather small heating/cooling due to transient eddies) arises from the choice of the study area, which happens to be situated near the zero line for $\nabla \cdot \overline{T'v_H'}$ as evident in Lau (1979) for wintertime circulation at 1000 and 700 mb levels. The shift of the polygon, say, westward towards the Atlantic Ocean would lead to more negative values.

Turning to mean flow advection (Fig. 2b), a rather clear annual cycle is found with small cooling effect during summer and warming in other seasons, especially around January. The year-to-year variability is larger than in the case of transient eddies but not so large as to obscure the seasonal cycle of ensemble mean values. The inter-annual variability is larger during winter than summer; the range of individual monthly values is roughly three times larger in winter than in summer both in 2a and 2b.

In computing the divergence term (Fig. 2c) the conservation of the atmospheric mass has been required similarly as in Alestalo (1981a) but as some ambiguity is involved in doing that the divergence term is considered as the most unreliable among the three terms presented in Fig. 2. It shows a tendency to a stronger cooling during winter compared to summer conditions. This is related to the dominance of upper tropospheric conditions in this quantity, as $c_p \tilde{T} + \tilde{\Phi}$ increases monotonously with height, together with the observed annual cycle of the upper tropospheric mean mass divergence (stronger divergence during winter).

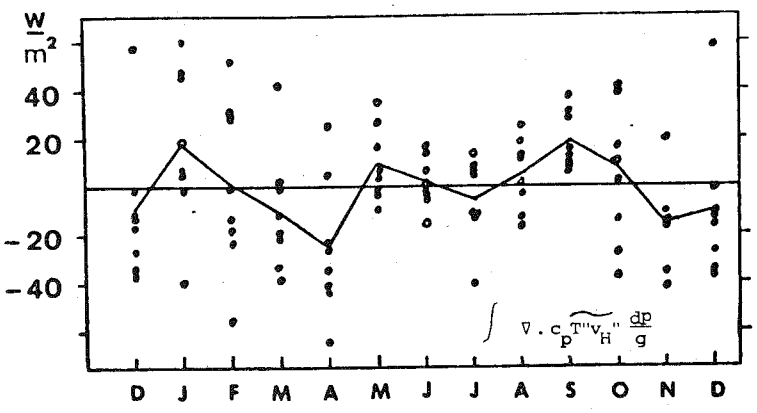

Fig. 2a. The monthly values of the vertically integrated transient eddy flux divergences for each month between July 1969 and July 1977 (circles) and their average values for each calendar month (solid line).

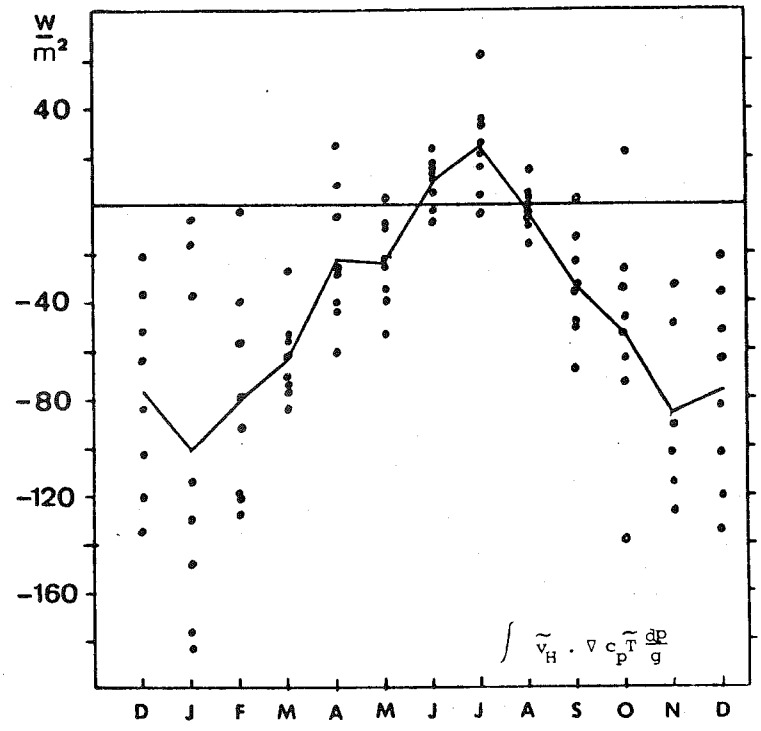

Fig. 2b. As in fig. 2a but for mean flow advection of sensible heat.

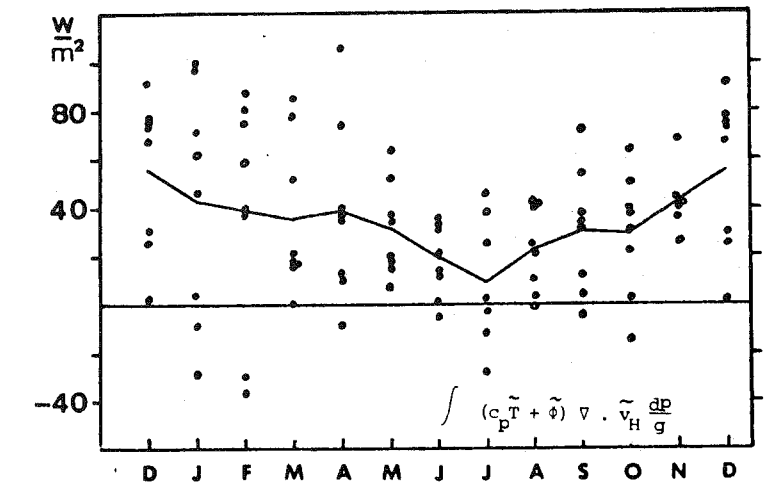

Fig. 2c. As in fig. 2a but for the divergence term (see eq. (5)).

In Fig. 3 the total flux divergence $\int \nabla.\widetilde{(c_p T + \Phi) v_H} \frac{dp}{g}$ is shown together with individual monthly values. The annual course arises mainly from the advection term. The variability of the monthly values is evidently not so large as might be expected on the basis of the three components. This implies a partial cancellation among the three components.

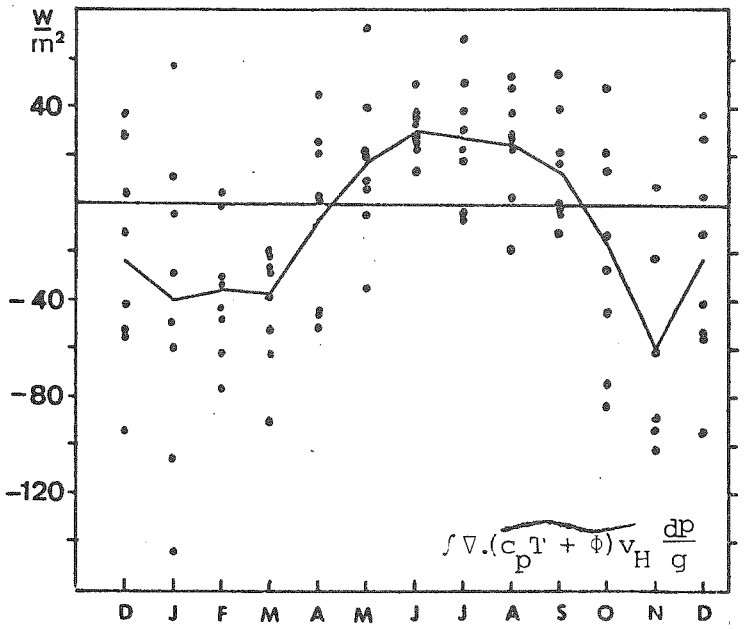

Fig. 3. The monthly values of the vertically integrated total flux divergence of the sum of sensible heat and potential energy for each month from July 1969 - June 1977 (circles) and their average values for each calendar month (solid line).

The correlations between the monthly anomalies of $\nabla \cdot c_p \widetilde{T''v_H''}$ and $\tilde{v}_H \cdot \nabla c_p \tilde{T}$ for vertical integrals and 850, 700, 500 and 300 mb levels are given in Table 1 for each calendar month and for the whole data material.

The 95 and 99% confidence limits are 0.71/0.20 and 0.83/0.26 for cases with N=8/N=96, respectively.

It is seen that, especially in the lower troposphere over Europe, these two different atmospheric transport mechanisms tend individually to vary more than their net effect. It is interesting to note that the magnitude of the corresponding correlations in the case of latent heat instead of sensible heat were higher than those in Table 1 (Alestalo, 1981b).

Table 1.

Correlation coefficient between monthly anomalies of $\nabla \cdot \widetilde{T''v_H''}$ and $\tilde{v}_H \cdot \nabla \tilde{T}$ for the region shown in Fig. 1 for the eight year period July 1969 - June 1977. Number of cases is 8 for each calendar month and 96 for the whole sample.

level (mb)	I	II	III	IV	V	VI	VII	VIII	IX	X	XI	XII	whole sample
300	-.58	.22	.11	.27	-.28	-.28	-.10	.54	-.12	-.21	-.20	-.28	-.18
500	-.70	-.39	-.82	-.69	-.34	-.57	-.77	-.67	-.36	-.70	.40	-.19	-.48
700	-.55	-.46	-.58	-.37	-.46	-.66	-.80	-.91	-.72	-.65	-.62	-.33	-.48
850	-.39	-.33	-.23	-.17	-.70	-.42	-.92	-.80	-.42	-.76	-.68	-.60	-.45
vert. int.	-.50	.35	.18	.10	-.64	-.60	-.79	-.85	-.35	-.56	-.33	-.53	-.28

Earlier indications about corresponding relationships between transient eddy and mean flow effects based on monthly data can be found in Savijärvi (1977) where a spatial negative correlation appears between vertically integrated fields of $\nabla \cdot \widetilde{T''v_H''}$ and $\tilde{v}_H \cdot \nabla \tilde{T}$ north of 20°N. Van Loon (1979) reported negative correlations between wintertime zonally averaged transient eddy and standing (mean) eddy transports of sensible heat for latitudes 55 - 65 °N at 700 mb during a time period of 29 winters.

The annual cycle of the vertically integrated monthly mean temperature implied by the total divergence alone would exhibit maximum temperatures around April and minimum temperatures near October with an annual range roughly four times larger than the observed one. The actual monthly mean temperatures thus result as a relatively small residual from a quasi-balance between atmospheric net transports and diabatic effects (see eq. (1)).

Another interesting topic is the behaviour of anomalies of monthly temperatures. For this purpose the effect of the vertically integrated transient eddy flux divergence and mean flow advection on temperature anomalies was studied by computing for these quantities corresponding correlation coefficients as above in Table 1. These are given in Table 2 for the 850 mb level. The sign of the correlation coefficients indicates that, over Europe warmer than normal months tend to be associated with a enhanced divergence of transient eddy fluxes and with a stronger than normal warming due to advection, and that colder than normal months are associated with a reduced divergence of transient eddy fluxes and with a weaker than normal warming due to advection.

Table 2.

Correlation coefficient (r) of monthly anomalies of $\tilde{T}$ against monthly anomalies of $\nabla \cdot \widetilde{T''v_H''}$ (= eddy) and $\tilde{v}_H \cdot \nabla\tilde{T}$ (= adv) at the 850 mb level for the period July 1969 - June 1977.

	I	II	III	IV	V	VI	VII	VIII	IX	X	XI	XII	whole sample
r(T,eddy)	.54	.46	.32	-.22	.84	.40	.74	.29	.37	.81	.50	.92	.50
r(T,adv)	-.81	-.61	-.14	-.10	-.71	-.53	-.87	-.74	-.47	-.50	-.54	-.69	-.55

This suggests that the effect on temperature anomalies of transient eddies would be a dissipative one. The time scale of this dissipative effect, defined as the ratio of the variance of the monthly mean tempera-

tures (i.e. $\frac{1}{2}\overline{\tilde{T}'^2}$) to the covariance between $\tilde{T}$ and $\nabla.\widetilde{T''v_H''}$ (i.e. $\overline{\tilde{T}'\ (\nabla.\widetilde{T''v_H''})'}$) was computed to be generally about four days for the 850 mb level, and varying between 2 and 9 days amoung the various calendar months. The corresponding time scale associated with the mean flow advection in producing temperature anomalies was generally slightly shorter, about three days.

3. Summary

In this study a 96-month time series of monthly mean values of vertically integrated divergence of sensible heat and potential energy, divided into the transient eddy and mean flow parts, have been used to study the maintenance of the monthly mean temperature over Europe. Considering the relative roles of the transient eddy and mean flow (emphasis on advection) contributions, the monthly anomalies of these quantities were found to be generally of different sign which means that their total effect varies less than the components separately. Specifically, warmer than normal months tend to be associated with stronger than normal warm air advection by the mean flow and larger than normal transient eddy flux divergence.

On the basis of the above analysis it seems that the transient eddies would act so as to smooth out the temperature anomalies brought about by the mean circulation.

References

Alestalo, M., 1981a: The energy budget of the earth-atmosphere system in Europe. Tellus, 33, 360-371.

Alestalo, M., 1981b: On the maintenance of the atmospheric water vapor budget over Europe. Report No. 18, Department of Meteorology, University of Helsinki, 24 pp.

Iau, N-C., 1979: The observed structure of the tropospheric stationary waves and the local balances of vorticity and heat. J. Atmos. Sci., 36, 996-1016.

Newell, R.E., Kidson, J.W., Vincent, D.G. and Boer, G.J., 1974: The general circulation of the tropical atmosphere and interactions with extratropical latitudes. Vol. 2. The MIT Press, Cambridge, Mass., 371 pp.

Savijärvi, H., 1977: The interaction of the monthly mean flow and large-scale transient eddies in two different circulation types. Part II. Vorticity and temperature balance. Geophysica, 14, 207-229.

Van Loon, H., 1979: The association between latitudinal temperature gradient and eddy transport. Part I: Transport of sensible heat in winter. Mon. Wea. Rev., 107, 525-534.